Comparison of Interior Permanent Magnet Synchronous Machines for a High-Speed Application

Prepared by:

Mohamedreza Kalyan

KLYMOH001

Department of Electrical Engineering

University of Cape Town

Prepared for:

Professor Azeem Khan

SUBMITTED TO THE UNIVERSITY OF CAPE TOWN

In fulfilment of the requirements for the degree

MSc in Electrical Engineering

October 2018

Department of Electrical Engineering

Faculty of Engineering & the Built Environment

University of Cape Town

Declaration

I, **Mohamedreza Kalyan**, hereby declare that I know the meaning of plagiarism and declare that all the work in the document, save for that which is properly acknowledged, is my own. This thesis/dissertation has been submitted to the Turnitin module (or equivalent similarity and originality checking software) and I confirm that my supervisor has seen my report and any concerns revealed by such have been resolved with my supervisor.

Signature: Signed by candidate Date: …22 October 2018….

Terms of Reference

TITLE:

COMPARISON OF INTERIOR PERMANENT MAGNET SYNCHRONOUS MACHINES FOR A HIGH-SPEED APPLICATION

DESCRIPTION:

Permanent magnet machines are increasingly used in high-speed applications due to their advantages over other machine topologies. This dissertation discusses the design, analysis, and comparison of two high-speed interior permanent magnet machines for a high-speed application. The machines are designed for a required output of 10kW and 30,000 rpm and have been analysed using analytical and finite element analysis simulations.

DELIVERABLES:

The scope and requirements from this thesis are as follows:

- Conduct a thorough literature review of the different high-speed machines designed and used in various applications
- Conduct a thorough assessment of the various permanent magnet machine topologies and their use in high-speed applications in the literature
- Detailed analysis on how to size permanent magnet machines using analytical equations
- Thorough sizing, analytical design, and comparison of the two interior permanent magnet machines
- Thorough finite element analysis on the two interior permanent magnet machines including comparisons between the two topologies
- Development of a high-speed test rig in order to conduct experimental results on the machines as part of a future additional scope of work. The same test rig must be able to be used for both machines. In this thesis, only one IPM machine will be prototyped in order to test the validity of the rig, with any additional detail experimental tests recorded as part of future work in this field
- Conclusions and recommendations based from the analysis

Acknowledgements

In the name of the Almighty, the Most Gracious, the Most Merciful.

I would like to thank the Almighty for giving me the strength, knowledge, and patience required to complete this dissertation successfully.

This dissertation is dedicated to my dearest mother, whose love, understanding, support, and sacrifices could not be surpassed. May she rest in peace and may the Almighty grant her a very high place in paradise.

I would like to thank my father and my family for their continuous support and encouragement not only throughout the duration of this dissertation, but also through the paths of my life that have led me to this juncture.

I would like to acknowledge and sincerely thank my supervisor, Professor Azeem Khan, for his continued support, assistance, and advice throughout the dissertation. This project would not be possible without his input and advice.

I would like to sincerely thank Mr Chris Wozniack (former Chief Lab Technician at the University of Cape Town) for all his support and advice throughout the design and prototyping process of the dissertation. I would also like to thank the entire team of laboratory technicians who were always willing to assist me in matters relating to the design, prototyping, and testing involved in this dissertation.

Lastly, I would like to thank my friends for supporting and encouraging me throughout the duration of this dissertation especially Hossein Dehnavifard and my fellow Master's colleagues.

This project would not be complete without the help, encouragement and advice of the people mentioned above.

Abstract

Permanent Magnet machines have been increasingly used in high-speed applications due to the advantages they offer such as higher efficiency, output torque and, output power. This dissertation discusses the electrical and magnetic design of permanent magnet machines and the design and analysis of two 10 kW, 30000 rpm Interior Permanent Magnet (IPM) machines.

This dissertation consists of two parts: the first part discusses high-speed machine topologies, and in particular the permanent magnet machine. Trends, advantages, disadvantages, recent developments, etc. are discussed and conclusions are made. The second part presents the design, analysis and testing of interior permanent magnet machines for a high-speed application. The machines are designed from first principles and are simulated using Ansys Maxwell software to understand the finite element analysis.

In order to obtain a fair comparison between the machines, the required output criteria was used as the judging criteria (10kW, 30000 rpm). As a result, the rotor diameter, stator diameter, airgap length, and stack length were kept the same for both machines. The winding configuration was set as distributed windings, however the number of turns and other details were kept flexible in order to be able to obtain the best design for each machine. Similarly, the magnet volume was kept flexible as this could be used as a comparison criteria relating to the cost of the machines.

The two IPM topologies are compared with respect to their torque, magnetic field, airgap flux, core loss, efficiency, and cost. The radial IPM produces a smoother torque output, with lower torque ripple, and has lower losses compared to the circumferential IPM which produces a higher torque and power output. Furthermore, the circumferential IPM also experiences much higher torque ripple and core losses, both of which are highly undesirable characteristics for high-speed machines. In addition, the circumferential IPM has a much more complex manufacturing process compared to the radial IPM which would significantly increase the cost of prototyping the machine, thus the radial IPM was selected for prototyping and brief experimental analysis.

The radial IPM has been experimentally tested under no-load conditions. These results were successfully compared to the simulated and analytical results to show correlation between the design and experimental process.

Potential areas of further work may include conducting detailed loss analysis to understand the effects that changing various design parameters has on the core loss and overall performance. Detailed thermal and mechanical analysis of the machines may also result in interesting conclusions that would alter the design of the machine to make it more efficient.

Table of Contents

List of Figures

List of Tables

List of Abbreviations

FEA	Finite element analysis
HS	High-speed
IM	Induction machine
IPM	Interior permanent magnet
LCM	Least common multiple
PM	Permanent magnet
PMASynRel	Permanent magnet assisted synchronous reluctance
SPM	Surface permanent magnet
SRM	Switched reluctance machine
SynRel	Synchronous reluctance

List of Symbols

A	Cross-sectional area of the winding
A_c	Cross-sectional area of the conductor
A_{mg}	Magnet area
A_m	Electric loading
A_s	Slot area
B	Peak flux density
B_g	Airgap flux density
B_{mg}	Magnetic loading
B_r	Remnant flux density
B_s	Saturation flux density
$cos\theta$	Rated power factor
C_ϕ	Flux concentration factor
D_r	Rotor diameter
D_s	Stator bore diameter
D_{si}	Stator inner diameter
E_a	Peak back-EMF
E_f	Excitation voltage
f	Frequency
g_e	Effective airgap
h_m	Height of the magnet
h_s	Slot height
h_{sy}	Stator yoke height
H_g	Magnetic field strength in the area
H_m	Magnetic field strength in the magnet
HCF	Highest common factor
i_d	d-axis current
i_q	q-axis current
I_a	Armature current
I_{rms}	RMS phase current
J	Current density
k_a	Excess loss factor
k_d	Distribution factor
k_e	Eddy current constant
k_{gn}	Magnetic gap factor
k_h	Hysteresis constant
k_p	Pitch factor

k_{sn}	Skew factor
k_w	Winding factor
k_{w1}	Fundamental winding factor
K_c	Carter's coefficient
K_l	Leakage flux factor
K_r	Reluctance factor
K_s	Stacking factor
l_b	Length of the bridge
l_c	Length of the conductor
l_g	Airgap length
l_m	Length of the magnet
L_d	d-axis inductance
L_q	q-axis inductance
L_{stk}	Stack length
m	Number of phases
n	Rotational speed
n_h	Harmonic number
n_s	Synchronous speed (rev/s)
N_c	Number of turns per coil
N_{coil}	Number of coils
N_{cph}	Number of coils per phase
N_p	Number of rotor poles
N_{period}	Period of cogging torque waveform
N_s	Number of slots
p	Number of pole pairs
P	Power rating
P_a	Excess loss
P_c	Core loss
P_e	Eddy current loss
P_{gen}	Electrical power
P_h	Hysteresis loss
PC	Permeance coefficient
q	Slots/pole/phase
R_a	Phase resistance
R_g	Airgap reluctance
$R_{l,bottom}$	Reluctance in the bottom bridge
$R_{l,top}$	Reluctance in the top bridge
R_m	Permanent magnet reluctance
R_{rot}	Rotor radius

S_{elm}	Electromagnetic power
t_b	Thickness of the bridge
$t_{b,bottom}$	Thickness of the bottom bridge
$t_{b,top}$	Thickness of the top bridge
T	Electromagnetic torque
$T_{cogging}$	Cogging torque
T_{ph}	Turns per phase
V_a	Armature voltage
V_{LL}	Line-to-line voltage
V_n	Peak phase back-EMF
w_s	Slot width
w_t	Tooth width
α	Pole pitch
β	Steinmetz constant
γ	Coil electric angle
ε	Ratio of excitation voltage to terminal voltage
θ	Angular position
θ_m	Magnet angle (rad)
θ_{skew}	Skew angle
θ_{ph}	Phase difference
λ	Flux linkage
λ_{PM}	Permanent magnet flux linkage
λ_s	Slot fill factor
μ_0	Permeability of air
μ_{rec}	Recoil permeability
ξ	Saliency ratio
σ	Winding conductivity
τ_t	Tooth pitch
τ_s	Slot pitch
ϕ	Angle of rotation
ϕ_g	Magnetic flux
ϕ_{pp}	Flux per pole
ω_0	Angular frequency (rad/s)
Φ_g	Airgap flux
Φ_l	Leakage flux
$\Phi_{l,bottom}$	Leakage flux in the bottom bridge
$\Phi_{l,top}$	Leakage flux in the top bridge
Φ_r	Permanent magnet flux
Φ_r'	Modified permanent flux

1. Introduction

1.1 Background to the study

High-speed (HS) machines have been developed and used over the last few decades and are now considered reliable for use in a various of HS engineering applications as shown in figure 1.1 [1]. These machines have been implemented in various industries ranging from the simplest of applications like machine tools to the most complicated ones such as generators and turbines. The constant development and research into these machines mean that they will be used in even more applications in future.

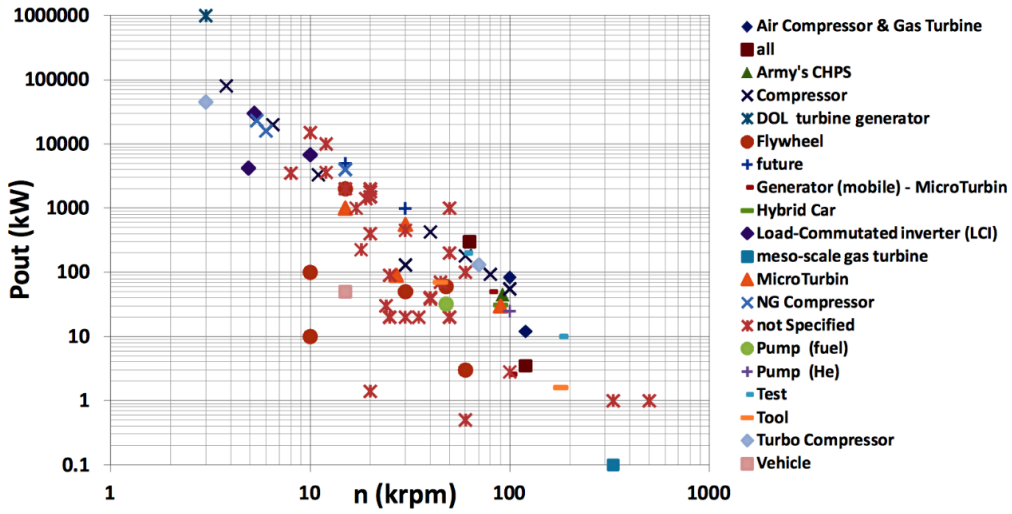

Fig. 1.1 Applications of high-speed machines [1]

1.1.1 Advantages of high-speed machines

HS machines have numerous advantages such as higher power density, smaller size, and increased reliability compared to conventional machines [2]. HS machines are more compact than conventional machines as the gearbox is often eliminated and thus for an equal power rating, a HS machine will be smaller in size compared to a conventional machine.

1.1.2 The different high-speed machine topologies

There are four most commonly used topologies in HS applications: Induction machines (IM), Permanent magnet (PM) machines, Switched reluctance machines (SRM) and Synchronous homopolar machines. IMs, PM machines, and SRMs have also been used in very HS applications, up to 600,000 rpm.

1.1.3 The permanent magnet machine for high-speed applications

The permanent magnet (PM) machine is the most commonly used machine in HS applications. There are two main PM topologies that are considered in HS applications – surface mounted permanent magnet

machines (SPM) and Interior Permanent magnet (IPM) machines. The magnets are placed on the surface of the rotor in the SPM while they are embedded inside the rotor in the IPM as shown in figure 1.2 [3].

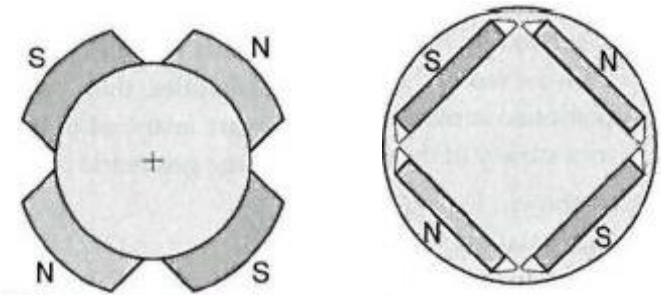

Fig. 1.2 SPM (left) and IPM (right) rotor layouts [3]

1.1.4 The interior permanent magnet machine

IPMs have been increasingly used in electric vehicle applications with the use of different IPM topologies. There are six main topologies for IPM machines as shown in figure 1.3 [2]. Given the various topologies and applications for IPMs, it is interesting to compare the IPM topologies and evaluate their performance. This dissertation will compare the circumferential and radial topology for a HS application.

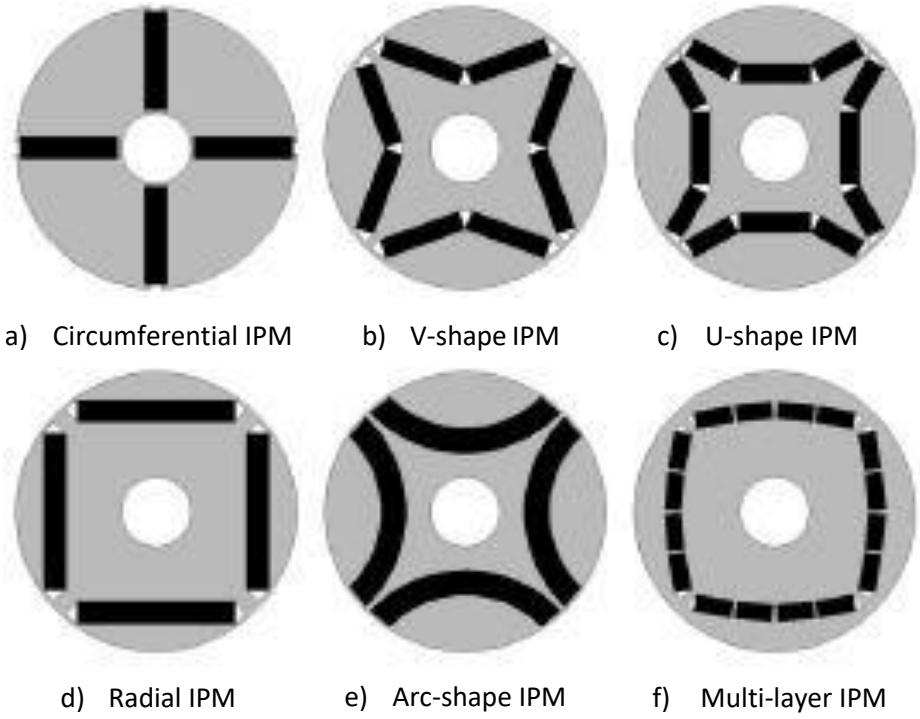

a) Circumferential IPM b) V-shape IPM c) U-shape IPM

d) Radial IPM e) Arc-shape IPM f) Multi-layer IPM

Fig. 1.3 IPM topologies used in the literature [2]

1.1.5 Factors and challenges associated with designing high-speed machines

There are several key design factors that must be considered when designing a HS machine. Some of these are the rotor and stator configuration, winding design, material selection, thermal and bearing selection,

lubrication systems, etc. Each of these has a significant effect on the performance of the machine and careful attention must be paid when designing these.

1.2 Objectives of this study

1.2.1 Problems to be investigated

The aim of this dissertation is to design, analyse, and compare HS interior permanent magnet synchronous machines for a HS application. The chosen topologies were arrived at by answering the main questions that directed the dissertation. These are as follows:

- Which HS PM machine topology is best suited to this particular application?
- What process needs to be undertaken to design this machine appropriately?
- What are the key design considerations that need to be carefully selected during the design process?
- How can the designed machines be compared to each other using finite element analysis?

1.2.2 Purpose of the study

The demand for HS machines has been increasing in recent times and there is a concerted effort in investigating the existing machine topologies for various HS applications. This project investigates the use of permanent magnet machines in an application that requires HS and high-power as well. The main objectives are to design and compare such a machine and evaluate it using finite element analysis to determine if it meets the specified speed and power requirements. Furthermore, it will also highlight the key design considerations that are critical to the performance of the machine and how changing these design factors will influence the performance.

1.3 Scope and Limitations

This dissertation compares two IPMs for a HS application and highlights the key design considerations that influence the parameters chosen and the effect these have on the performance. The two machines are also compared and analysed to determine the performance of the machines. The performance of the machines is measured by whether or not the machines meet the specifications of the project. For this project, the requirements were an output power of 10kW at 30,000 rpm. The design considerations made throughout the dissertation are to ensure that the machines meet the output power specifications while experiencing minimal losses and other undesirable effects such as torque ripple and cogging torque. Since this machines will operate at a considerably HS, the mechanical aspects such as cooling, lubrication, bearings, etc. are very sensitive and critical. As a result, these were selected after advice and direction from a professional mechanical engineer, and where the parts required design and manufacturing, these were undertaken by an

mechanical engineer and the design of these are not included as part of this dissertation. Furthermore, the development of the test rig needed to test this machine has been undertaken and a complete description of the components chosen are detailed in the relevant chapter. However, since the scope of the dissertation only included the finite element analysis of the machines and did not include the experimental testing of the machine, the test rig was only developed as an additional item not included in the scope of this dissertation. There are numerous challenges that have to be overcome in order for the test rig to operate at the design speed of 30,000 rpm, such as the cost and complexity of the equipment required to run at the specified speed. The development of a full specification, 30,000 rpm test rig is viewed as a complete dissertation on its own and as such for this dissertation, the test rig developed to test the machine at a maximum speed of 10000 rpm only. As such, the performance of the machine at 30,000 rpm has not been evaluated at this point.

1.4 Plan of development

This thesis has been structured into three main parts. The first part is a background to HS machines and their use in the industry. The second part consists of the main design aspect of the project and presents the design and analysis of the permanent magnet machine. The design equations, and finite element analysis results are also discussed in this section. The final section consists of the discussion and comparison of the machines and relevant conclusions and recommendations are made. This layout has been summarised as shown in figure 1.4.

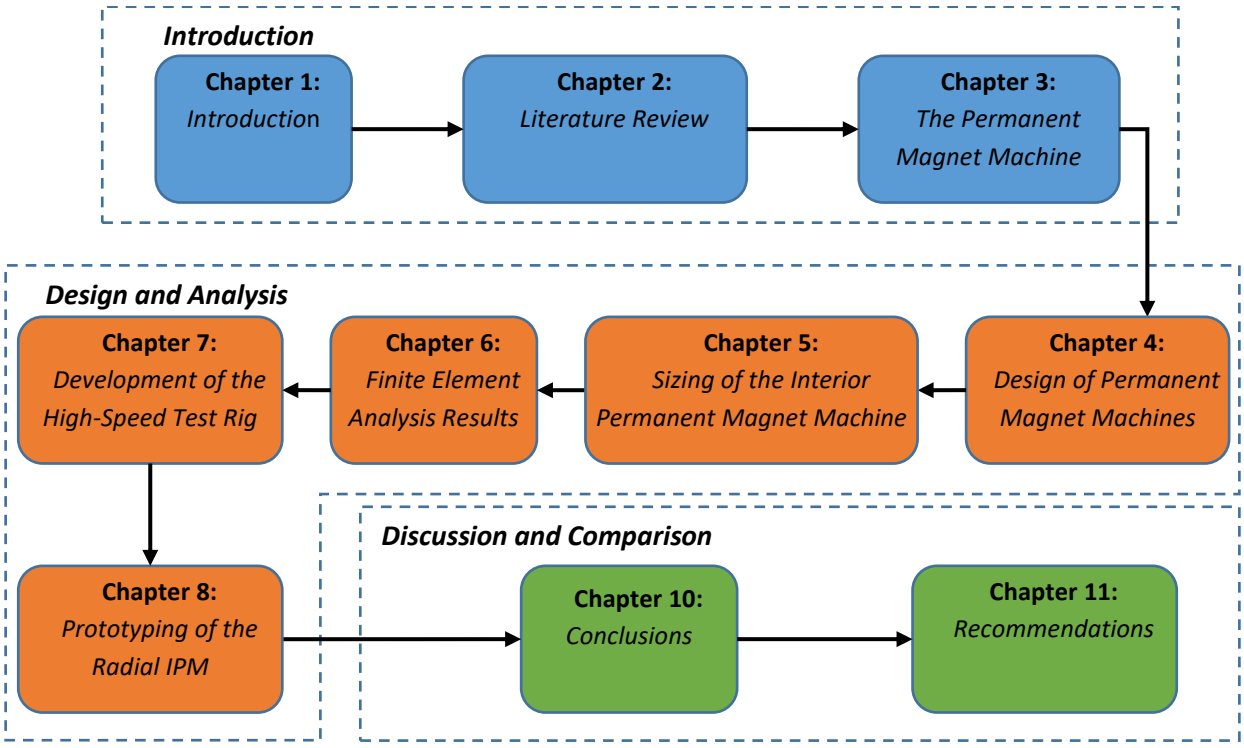

Fig. 1.4 Outline of this thesis

The layout of each chapter is as follows:

Chapter 2 presents a review of the relevant literature regarding HS machines and their applications. Different topologies are discussed and their advantages and disadvantages are also highlighted. Thereafter, the key factors that influence the performance of these machines are then discussed. Lastly, the PM machine is then looked at in detail and some of its applications in the industry are mentioned and discussed.

Chapter 3 discusses the PM machine in more detail. The different topologies are highlighted and compared to each other with references from literature. The topology that will be designed in this dissertation is then discussed.

Chapter 4 discusses the general design of PM machines. First principle equations are used to design the rotor and stator. The design and selection of the bearings, lubrication, cooling, lamination materials, etc. are all discussed in this chapter and key design considerations are highlighted. Finally, the key design equations to calculate the emf, windings, losses, etc. are presented.

Chapter 5 presents the design of the IPM machines in detail. The rotor, stator, and windings are designed and the equivalent circuits for the IPMs are presented.

Chapter 6 presents the finite element analysis results. These are used to critically analyse the IPMs and compare the topologies to determine which topology performs better

Chapter 7 presents the development of the test rig. Being a HS test rig, there are key components that must be selected to assemble the test rig and the selection of these is discussed and the final assemble test rig is presented.

Chapter 8 discusses the prototyping process for the IPM. Thereafter, no-load experimental results are presented.

Chapters 8 and 9 conclude the findings obtained and make suitable recommendations for improvements in this project.

2. Literature Review

In order to understand the development in HS machines, it is important to have an in-depth background understanding of the trends that these machines have experienced in the last few decades. This chapter will give a detailed background on HS machines, the trends experienced, applications of such machines, and finally discuss the different topologies of HS machines.

2.1 Introduction

The demand for HS machines has been increasing over the last few decades because of the widespread use of these machines. HS machines are increasingly favoured as they have a high efficiency, which means they use less energy and produce lower pollution, high power density, and improve reliability [4]. Furthermore, not only are HS smaller in size, and thus lighter, than low-speed machines, but they achieve a higher output power for the same size of machine compared to low-speed machines [5]. Interest in HS machines is essentially aimed at removing the mechanical gear and reducing the size of the machine. The increase of speed yields higher power with a comparatively small torque.

2.2 Applications, Trends and Development of High-Speed Machine

HS machines have been extensively researched over the last few years, as is evident with the increase in national and international funded programs in this area [6]. HS machines have been designed and implemented in a variety of engineering applications such as aerospace, automotive, turbo systems, and spindle systems with typical operational speeds in excess of 10,000 rpm [7].

HS machines are typically used in two ways: they either completely replace the mechanical systems or they work alongside the existing systems [6]. This section describes some of the applications of HS machines and highlights the wide implementations of these machines in the industry.

2.2.1 Automotive/Power generation

Figure 2.2 describes the application of HS electric machines in an automotive concept [6]. The figure shows the layout of four HS machines (M1-M4) around an automotive engine. The machine is used as a motor and a generator depending on the scenario the system is operating in. When the system requires to increase the speed of the compressor, the machine operates as a motor, while the machine operates as a generator to prevent the shaft over-speeding when there is excess energy [6].

2.2.2 Flywheel systems

Flywheels operate by mechanically storing energy in a rotating flywheel and typically have large diameters, rotate slowly, and have low power and energy densities. However, newer technology flywheels can operate

at higher speeds and higher power densities. HS flywheel storage systems are more compact, efficient, reliable, and have a larger operating range compared to battery technologies [8].

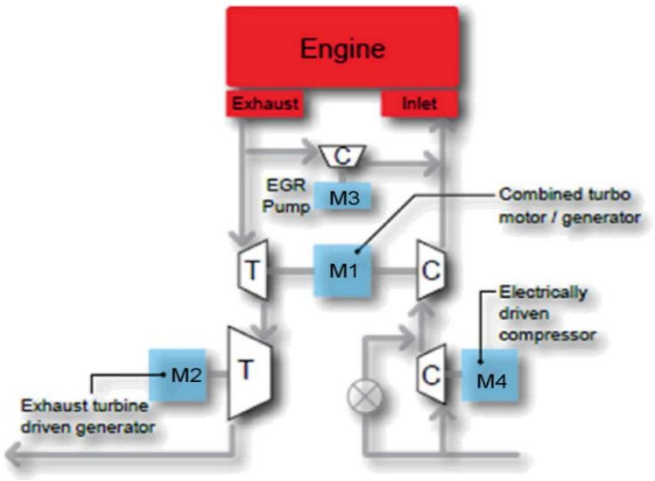

Fig. 2.1 Use of high-speed machines in automotive applications [6]

2.2.3 High-speed spindles

Another area where HS machines are fast growing is the machine tool industry. The main drawback with the traditional low-cost HS spindles is the maximum speed they can achieve. Thus, the increased demands for faster, more powerful spindles, and more reliable spindles have led to the increased use of HS machines for spindle applications. The speed and power range for spindle use varies widely from 9,000 rpm to 180,000 rpm with a corresponding power of 24kW to 1kW. Table 2.1 shows typical milling applications and their corresponding speeds [6].

Table 2.1 Speeds of different milling applications [6]

Applications	**Speed (rpm)**
Metal	4500 – 12000
Stones	8000 – 12000
Glass/Marble	8000 – 14000
Wood	18000 – 25000
Aluminium	30000 - 40000

2.2.4 Gas compressors

Gas compressors are commonly used in chemical, oil, and gas factories where HS machines are used to increase reliability and reduce the impact on the environment. The use of HS machines in these applications replaces the need for a gearbox which means the system is more reliable, efficient, and safe. [6].

2.2.5 Industrial air compressors and air blowers

There has been a significant increase in the use of HS, motor-driven compressors and blowers in the last

decade. These motors provide higher reliability, lower noise, lower pollution and, larger energy savings compared to conventional blowers [9].

2.2.6 Microturbines

Microturbines are small combustion turbines with typical outputs of 30 – 400kW and operate using a different range of fuels such as natural gas, biogas, propane, butane, diesel, and kerosene. They are used for generation applications where space is limited and therefore HS machines are attractive in this case due to their reduced size and high output.

2.2.7 Aerospace

A common use of HS machines in the aerospace industry is in aircraft applications where the aim is to replace the external gearboxes and other mechanical components [10]. The overall system would include a HS machine linking with the electrically driven control surface actuators and landing gear. A variety of HS machines have been used in aerospace applications with speeds ranging from 1000 rpm to more than 100,000 rpm. Figure 2.2 shows the use of HS machines in the aerospace industry [11].

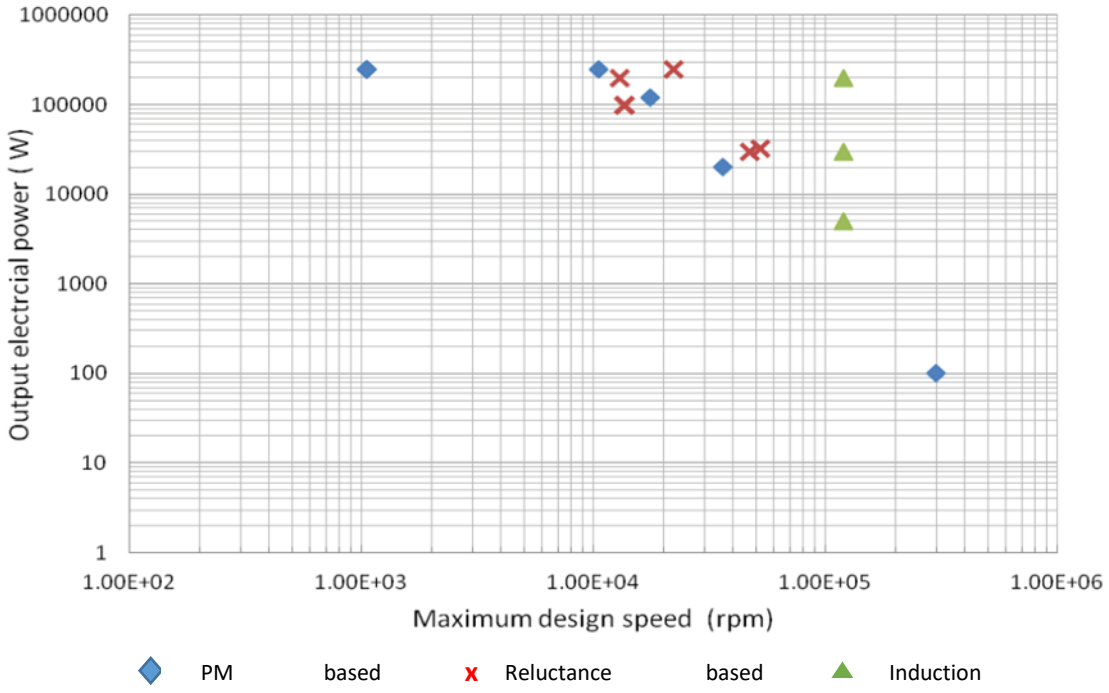

Fig. 2.2 Use of high-speed machines in aerospace applications [11]

2.2.8 Marine

Scope for HS machines in the marine industry is mainly through the use of these machines in military purposes [11]. Typically a gas turbine coupled to either a permanent magnet or field weakened synchronous motor (FWSM) machine provides the generation for the application [12]. Lower power PM machines with powers of up to 5MW were reported in [12].

2.3 Materials used in HS machines

The materials used in the design of HS machines play an important role in the performance and output of these machines. Materials used typically depend on the application of the machine and the requirements from it. This section describes some of the materials commonly used in HS machines.

2.3.1 Electrical Steels

Rotor and stator laminations are typically made from silicon–iron (SiFe) and cobalt–iron (CoFe). CoFe has a higher saturation magnetization (20% higher than SiFe) which means higher power densities can be achieved. Due to the better performance capability of CoFe, it is the preferred lamination material.

An important characteristic when selecting the lamination material for HS machines is the core loss generated in the lamination due to the high fundamental and switching frequencies. Core loss is mainly influenced by the lamination thickness and the thinner the laminations, the lower the core losses. The saturation flux density and resistivity of the steel should be considered as well, as this contributes to the eddy current loss in the machine.

In order to keep up with the demand for steel, there has been considerable research undertaken to identify other materials that could be used and produce better performance. The JNEX10-Core is a 0.1-mm-thick SiFe grade material with around 50% of the loss compared to other high-frequency thin-steel grades, which allows higher fundamental frequencies in the stator without increasing the core losses [13].

2.3.2 Permanent magnets

At HS, magnets suffer from extreme mechanical stresses and internally generated losses. There are two types of magnetic materials used in electric machines: ferrite magnets and rare earth magnets. Ferrite magnets are made from iron oxide and barium carbonate. These materials are easily available which makes them cheap and thus are commonly used in machines. However, ferrite magnets are very brittle, which makes them undesirable in HS applications which require stronger magnets. An alternative would be to use alnico magnets, but these are much more expensive than ferrite magnets. HS machines predominantly use samarium cobalt (SmCo) or neodymium iron boron (NdFeB) magnets. These are known as rare earth magnets as the materials used to make these magnets are difficult to find, and as a result these magnets are often very expensive. NdFeB magnets have the highest energy product compared to the other magnets and as a result are the preferred choice of magnets. NdFeB is made using dysprosium, which is a rare material and one whose demand is exceeding its supply [14]. As a result, the price of NdFeB magnets has been increasing and in recent years. SmCo magnets can replace NdFeB magnets, however they can only operate to about 50% of the temperature NdFeB can operate to.

2.3.3 Other materials used for the stator and rotor

With the constant increase in demand for HS machines, there needs to be an ever-increasing availability

and advancement in new materials that meet the required design necessities. New materials mainly concentrate on a higher mechanical strength, so as to meet HS requirements, and at the same time trying to improve their electromagnetic characteristics. Typically, electric machines are made from the materials described in table 2.2 [11].

Table 2.2 Different materials used in high-speed machines [11]

Material Class	**Location**	**Properties of interest**
Soft magnetic	Rotor and Stator	• Saturation flux density • Yield and tensile strengths • Ductility and Brittleness • Low iron loss behaviour over a wide frequency range
Hard magnetic	Rotor and Stator	• Coercivity • Reminiscent flux • Yield and tensile strengths • Operating temperature • Temperature variation • Low electrical conductivity
Conductors	Rotor and Stator	• Conductivity • Mechanical strength
Electrical insulation systems	Rotor and Stator	• Maximum operating temperature • Method of application • Ageing mechanism • Thermal conductivity
Retention systems	Rotor	• Yield strength • Magnetic properties • Electrical conductivity • Thermal conductivity

2.3.4 Conductors

Most HS applications currently use copper litz wires in the windings to reduce the AC copper losses. In the past, due to its lighter weight, aluminium was commonly used. However, despite being much lighter than copper, aluminium has a higher resistivity and difficulty in jointing with other metals is still a challenge. To reduce these challenges and keep the lighter weight advantage, a conductor which has a copper surface and

aluminium core made from a combination of copper and aluminium has been researched [15].

2.3.5 Electrical insulation systems

Insulation systems in HS machines are needed to offer good temperature stability and thermal conductivity, and protect from voltage overshoots, pulse repetition and other electrical faults. The electrical insulation system in any machine can be subdivided into four main functions: Strand insulation, Turn insulation, Groundwall insulation and Impregnation systems [11].

2.3.6 Structural materials

Three high yield strength retention materials are commonly used in HS applications: Inconel 718, Ti6Al4V (titanic alloy), and CFRP or Carbon fibre composites [11]. Inconel 718 has a good mass density and thermal conductivity and thus is used in highly corrosive environments. Ti6Al4V is much lighter than inconel and thus is preferred in weight sensitive applications. Carbon fibre composites exhibit impressive tensile strengths often required in flywheel applications.

2.4 Cooling Methods

The cooling mechanism selected for the HS design is responsible for the maximum attainable current density. Cooling techniques are typically split into two categories: direct cooling or indirect cooling. Direct cooling methods include oil mist cooling, oil-filled hollow section conductors, forced rotor cooling through the designed air or oil ducts, and pumped/working fluid cooling [16]. Indirect cooling methods primarily refer to all outer stator cooling methods.

2.5 Advantages and Disadvantages of High-speed Machines

HS machines have been increasingly implemented in the last few decades due to their advantages, which include higher power density, smaller size, and increased reliability in comparison with conventional machines [2]. Since a frequency converter often controls the speed and power of a HS machine, the machine is directly attached to the shaft and the gearbox can be eliminated. The elimination of the gearbox increases reliability, reduces the cost of maintenance, allows for an oil-free performance of the drive, increases the mechanical stiffness, produces lower noise, reduces wear, and offers increased compactness, lightweight, and maintenance-free operation [17], [18].

As the gearbox is eliminated, HS machines are more compact than low-speed machines. The main factor that determines the size of a machine is the torque rating. For an equal power rating, a more compact machine is obtained with a HS machine [19]. This is an advantage when the system includes a mechanical load that needs to be connected to the machine. Furthermore, the cost of a HS machine may be lower than the cost of a low-speed machine which would require a gearbox.

HS machines also have several technical advantages such as the smaller size of the compressor, pump and

gas-turbine rotor dimensions for the same power rating, improved cutting and milling performance due to raised cutting speed, reduced cutting time and increased stored energy in flywheels [17].

Despite their numerous advantages, HS machines have several disadvantages. The maximum operating range of electrical machines are determined by several parameters but can be typically grouped into three: mechanical limits, thermal limits and electromagnetic limits. The maximum speed of a machine is limited by the centrifugal force and by elastic instabilities related to critical speeds [19]. The permitted temperature rise of the stator and rotor controls the maximum power of the machine. HS generally also means high voltages and fluxes, which have to be accounted for in the electromagnetic and electrical design.

The mechanical limits of HS machines include the bearing selection which must be able to handle the speed and operation of the machine effectively. Part of the structure comes too close to the elasticity/plasticity limit, which makes material choice essential and difficult since most strong materials are non-magnetic [19]. Another limitation of HS machines is accurately determining the critical speeds as electromagnetic forces may introduce additional elasticity during operation which may affect the critical speed. This limitation can be overcome by ensuring the machine is not designed to stabilise close to the critical speed.

The thermal limit of a HS machine is the maximum temperature that can be handled by the machine before its performance is affected. Exceeding the thermal limit may reduce the lifetime of the insulation and the core, made of stacked iron, may get damaged. Permanent magnets may get irreversibly demagnetized at a higher temperature and mechanical material failures, e.g. broken conductors, are also more likely to occur.

One of the most important factor to consider when designing a HS machine is the cooling system required. Most standard machines are air-cooled, with external cooling fins, often by a ventilator mounted on the shaft. However, at HS this increases the noise produced and may affect the torque output of the machine, thus independent cooling is required. The cooling of the rotating parts is always very difficult and hard to quantify as it has to be accomplished by the airflow in the air gap and in the end-winding region [19].

Finally, HS machines would typically produce higher induced voltage with extra stress on the insulation. Furthermore, the magnetic permeability and electrical conductivity decrease with temperature, affecting the characteristics and the operation within a drive. Permanent magnets are sensitive to temperature and the conductive types will develop internal eddy currents, thus a higher risk of demagnetization arises.

The limitations in HS machines are often discussed with respect to the HS-index. This is the product of the machine's nominal power and nominal speed ($n \times P_{out}$). Figure 2.3 highlights some of the limitations of HS machines according to the HS-index and nominal speed [1]. Three different regions, A, B and C, are distinguishable based on the behaviour of the HS-index for different speeds, n. Region A consists of high power machines, typically induction machines and permanent magnet machines. The main challenges with these machines are the complex mechanical and cooling designs required. Region B consists of high power machines at a higher speed than those in Region A. Region C consists of lower power, higher speed machines in which the main challenge is the temperature of the machines during operation.

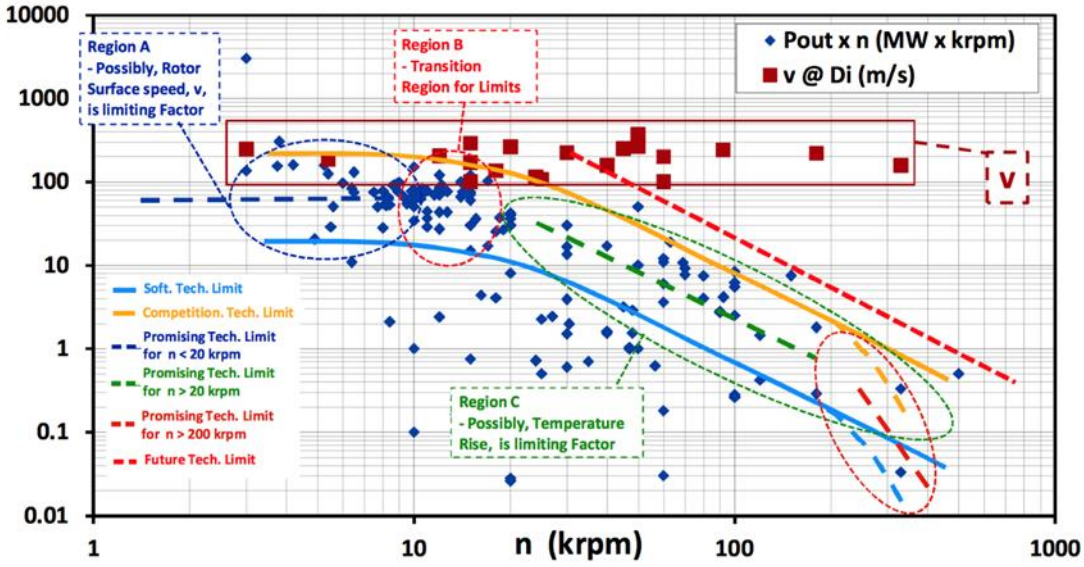

Fig. 2.3 Problems associated with different operating regions in high-speed machines[1]

2.6 Typical Design Considerations of High-speed Machines

HS machines are designed according to the requirements from the application the machine will be used in and therefore there is no general design concept for HS machines. Depending on the application, operating speed, and power range and the available finances, different HS machines can be designed for the same application. This section describes some general design considerations for HS machines.

2.6.1 Electromagnetic Utilization

When considering the electromagnetic and mechanical factors in the design of a HS machine, three major criteria are considered: copper losses in the stator winding due to eddy currents, iron losses in the iron material due to high frequency variation of the flux density, and friction losses [1]. Increase in copper and iron losses appear due to the high frequency of the fundamental supply current in the HS machine and these losses should be compensated by the reduction of current density in the winding, and the flux density in the iron, respectively.

2.6.2 Bearing system

Bearings are one of the most critical components of HS machines. Careful attention must be given to the choice of bearing selected during the design stage as this affects various aspects of the machine such as reliability and performance. Figure 2.4 outlines the distribution of various bearing solutions with respect to machine characteristics for cases reported in the literature [18]–[21].

In HS machines, the bearings experience significant challenges such as mechanical strength, friction loss, and reliability [12]. A common issue between bearing system and thermal limits relates to the axial extension of the machine due to losses and high rotor temperature, as discussed in [19]. Thus, the selection and design

of the bearing for HS machines is a critical component in HS machine design. Factors that need to be considered when selecting a bearing include: natural bending frequency of the rotor, bearing lifetime, applications, maximum speed, axial and radial stiffness, shaft size, and the number of bearings to be used [20]. Typically, four types of HS bearings are commonly used in HS machines: oil bearing, ball bearing, air bearing, and magnetic bearing. In addition, a novel hybrid bearing concept was recently proposed in [21]. Table 2.3 gives a summary and comparison of the different bearings used in HS machines obtained from literature [22].

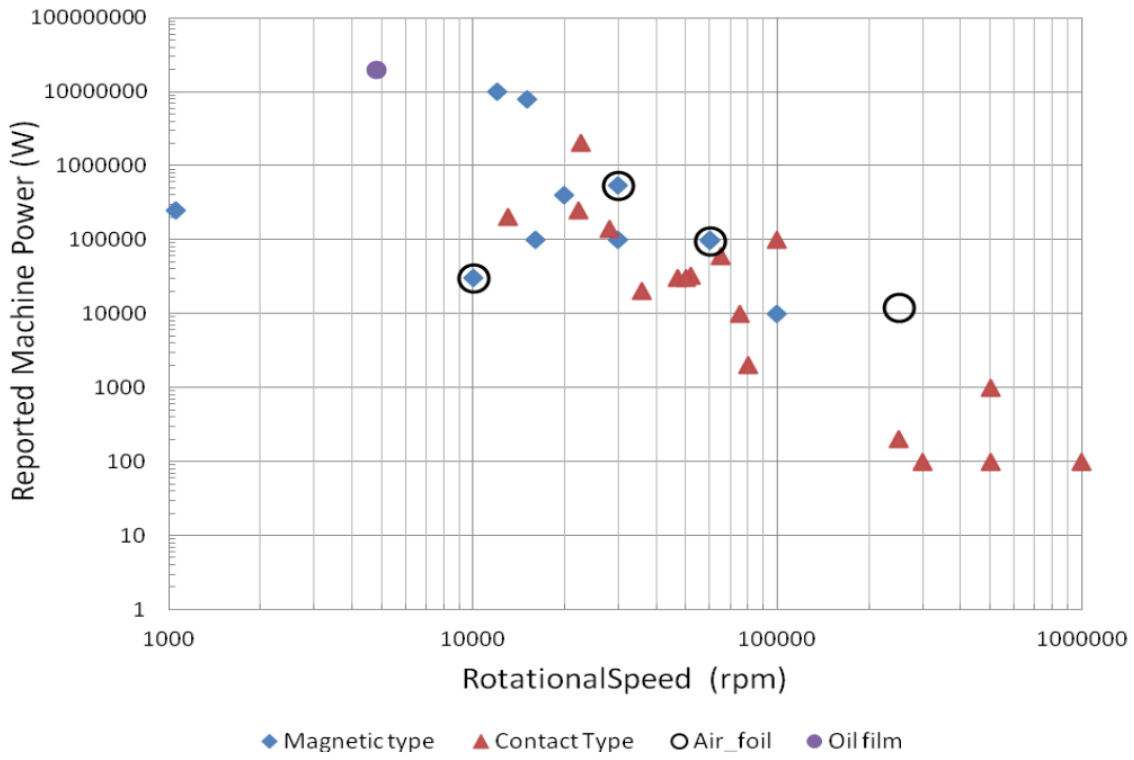

Fig. 2.4 Different bearing types used in high-speed machines [17]

The ball bearing is the most widely implemented bearing system due to its simple and small design, and high robustness [21]. On the other hand, ball bearings are of the contact type and therefore require maintenance. They are also dependent on load and speed and have a limited operating temperature. There has been a recent development from SKF with bearings “lubricated for life”, which employ the use of seals and a special type of grease [23].

An air bearing uses pressure to hold the rotor shaft in position without direct contact. The air pressure can be generated either by the rotor or by an external supply. Since there is no direct contact, air bearings have a low friction loss and a long lifetime. However, air bearings often have poor dynamic stability.

Magnetic bearings have been widely used in research in recent times [24], [25]. A magnetic bearing uses magnetic force to levitate the rotor and shaft. It has similar advantages to the air bearing, however the magnetic bearing requires complex auxiliary control systems which include sensors, actuators, and control circuitry [26]. The use of control systems inevitably increases the cost, complexity, and size of the bearing. In

addition, due to the complexity of these bearings, failsafe bearings are usually needed as a backup.

Table 2.3 Different bearings and their characteristics [22]

	Oil Bearing	**Ball Bearing**	**Air Bearing**	**Magnetic Bearing**	**Hybrid Bearing**
Max. Operating speed (m/s)	75 – 105	50 – 60	150 – 225	180 – 200	150 – 225
Load Capacity	Very high	Moderate	Low	Low	Low
Short Term Overload Capacity	Substantial	Good	Limited	Limited	N/A
Operating Temp. Range (°C)	30 – 90	-30 – 230	650+	-180 – 540	Wide range
Oil Free	No	No	Yes	Yes	Yes
Misalignment Capability	Moderate	Very low	Low	Moderate	Moderate
Complexity	Low	Low	Moderate	High	Very high
Weight	Substantial	Light	Lightest	Moderate	Moderate
Stiffness	Moderate	High	Low	Tuning dependent	Tuning dependent
Shock Tolerance	Very good	Moderate	Good	Poor	Good
Cost	Low	Low	Moderate	High	Very high

A novel hybrid-bearing concept has been proposed to overcome the disadvantages of magnetic and air bearings [21]. The proposed method combines a gas bearing with a small-sized active magnetic damper. As a consequence, the hybrid bearing does not only have the high stiffness of a gas bearing but also acquires high dynamic stability at very HS operation [22].

Alternatively, active magnetic suspension could be implemented in the design. This is usually implemented as a combination of one axial and two radial magnetic bearings [27]. Bearing-less technology has been used with most machine designs including IM, SR machines and PM machines. In all applications with magnetic bearings, auxiliary ball bearings with a rotor gap are necessary as a back-up in case of electric faults.

2.6.3 Thermal and cooling considerations

As mentioned earlier, the cooling system for HS machines is a key challenge and must be carefully selected as it has an impact on the machine's performance and structure. Therefore, a trade-off needs to be made between cooling design and machine structure. The cooling design selected is typically determined by performance requirement and the application of the HS machine. The most common cooling designs are air-cooling and liquid cooling (water/oil), or a combination of both. A comparison of different cooling methods is given in [28] and table 2.4. In addition, different cooling systems can be used for the stator and rotor, for example, fins and heat sinks, water or oil jacket, direct liquid cooling and hollow conductors, spray oil cooled end turns of the rotor winding, and liquid cooled wedges [29].

Table 2.4 Cooling techniques used in high-speed machines [28]

Cooling Medium	Characteristics of cooling medium
Oil	• Direct cooling of stator and rotor • Gravity-fed system has limited flow • Flow velocity and dynamic force impacts • Magnet temperature distribution hot-spots (for PM)
Water/ Ethylene Glycol	• Challenge to remove heat from the rotor • Heat from rotor can impact bearing durability • Magnet temperature distribution hot-spots (for PM) • May require overdesign of the magnet or machine to ensure operation within thermal limits (for PM)
Air	• Can enable rotor and stator cooling • Low cost • Lower heat transfer capacity per volume • Particulate filtering

2.7 Losses Associated with High-Speed Machines

The fundamental frequency for HS machines is much higher than for low-speed machines, which leads to many design challenges. As HS are usually more compact, all the losses generated by the machine will be realised in a smaller volume, which increases their impact on the performance of the machine. There are three main components to the overall losses experienced by a HS machine: core losses, copper losses, and windage losses.

2.7.1 Copper Losses

Copper losses are caused due to skin and proximity effects in the windings high-frequency excitation can lead to proximity losses in the stator windings [30]. The use of litz wire reduces the copper losses, however these are very expensive. Alternatively transposed wire bundles could also be used as a cheaper option to litz [31].

Figure 2.5 shows the effect of using different winding materials on the copper losses in a HS machine [32]. At low frequencies, the effect of copper losses is almost the same regardless of the type of wire used in the windings. However, at high frequencies the copper losses in the windings increase significantly if un-transposed wires are used. Thus, HS machines with high-frequency excitations typically use litz or transposed wires in order to reduce the effect of copper losses.

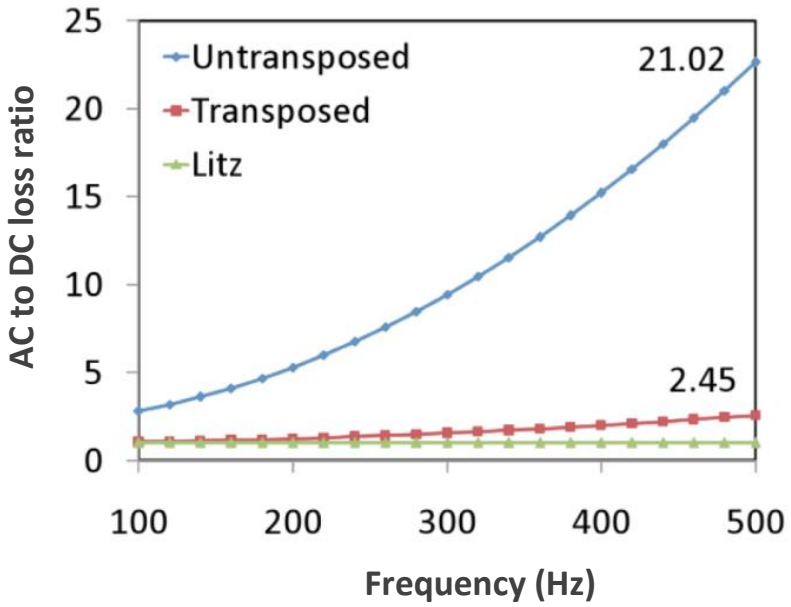

Fig. 2.5 Copper losses for different winding wires [32]

2.7.2 Core losses

Core losses are the main component of the losses experienced in HS machines. Due to the complexities associated with HS machines, accurately predicting the core losses is a challenging task, hence different methods are used to estimate the core losses during the design stage. The most common method to predict the core losses is using Steinmetz equations or finite element analysis. There have been a large number of studies in literature to investigate different methods and techniques to reduce the core losses in HS machines such as optimising the rotor and stator designs [33], using thinner laminations, and using better core materials [34], amongst others.

2.7.3 Windage losses:

There are various factors that affect the windage losses experienced by electrical machines such as the size of the rotor, rotational speed, temperature, etc. [22]. Importantly, windage losses increase with the speed of the rotor, and thus the faster the rotor spins, the higher the windage losses experienced. Therefore, rotor designs in HS machines are important to reduce the effects of windage losses.

2.7.4 Sleeve losses

Sleeves are usually employed when the HS machine consists of surface mounted permanent magnets. In SPMs, the magnets are placed on the surface of the rotor and when used in HS applications, the rotor spins at HS which means that there is a risk of the magnets flying off the rotor and causing damage. The high rotational speeds lead to a high centrifugal force and therefore the rotor sleeve ensures the mechanical integrity of the rotor and protects the magnets from flying of the rotor. Some commonly used sleeve

materials include Inconel, carbon fibre, stainless steel, titanium, copper iron alloy, and copper. Regardless of the sleeve material used, the sleeve will raise further challenges that will have to be overcome such as increased losses, cooling technique, effect on efficiency, etc. Table 2.5 shows the sleeve losses for different materials designed for a 117kW, 60 rpm PM synchronous machine [35]. In order to accurately determine the effect of different sleeve materials in [35], the rotor sleeve was divided into three parts for analysis. The upper part experienced the largest loss regardless of material, while the middle and lower parts had very low losses regardless of material as well. In total, the copper-iron alloy sleeve experienced the largest losses when compared to the other sleeve materials. Thus, it can be observed that the sleeve material plays an important role in the total losses associated with the machine and if not carefully chosen, the losses in the rotor will increase.

Table 2.5 Sleeve losses with different sleeve materials [35]

	Stainless steel	**Carbon fibre**	**Copper-iron alloy**	**Copper**
Upper Sleeve Losses (W)	245	42.4	456.4	166.1
Middle Sleeve Losses (W)	98.6	19.4	3.7	1.9
Lower Sleeve Losses (W)	41.7	8.7	0.8	0.4

2.8 Types of High-Speed Machine Topologies

The selection of the HS machine topology depends on the requirements and application of the machine. This section discusses the four most commonly used topologies in HS machines: Induction machines (IM), Permanent magnet (PM) machines, Switched reluctance machines (SRM), and Synchronous homopolar machines. Figure 2.6 shows the widespread use of machines for different speed and power combinations [6]. An important concept in HS machines is the $r/\min\sqrt{kW}$ factor that provides a tool to assess different speed-power combinations and the likeliness of dynamic challenges occurring for these combinations [6]. In general, for machines that operate below $1 \times 10^5\ rpm\sqrt{kW}$ the likeliness of dynamic challenges arising are low, while for machines that operate between $5 \times 10^5\ rpm\sqrt{kW}$ and $1 \times 10^6\ rpm\sqrt{kW}$ some dynamic challenges may be experienced. Above this rating, the prediction of dynamic challenges becomes difficult and inaccurate [6]. As noted from figure 2.6, only solid rotor IM can achieve the highest $r/\min\sqrt{kW}$ and these machines typically have peripheral speeds in excess of 400m/s. PMs are usually limited to speeds of 300m/s, however they are common in super HS machines with strong retention materials used to protect the integrity of the rotor. SRMs are commonly used in applications with peripheral speeds of around 200m/s.

2.8.1 Induction Machines

Induction machines are one of the most robust HS machines and are commonly used in HS applications such as compressors, turbo chargers, and even electric vehicles in some cases. Table 2.6 lists out a few of the HS IM used in the literature [36]. Figure 2.7 shows the different types of rotor topologies used in IMs [6].

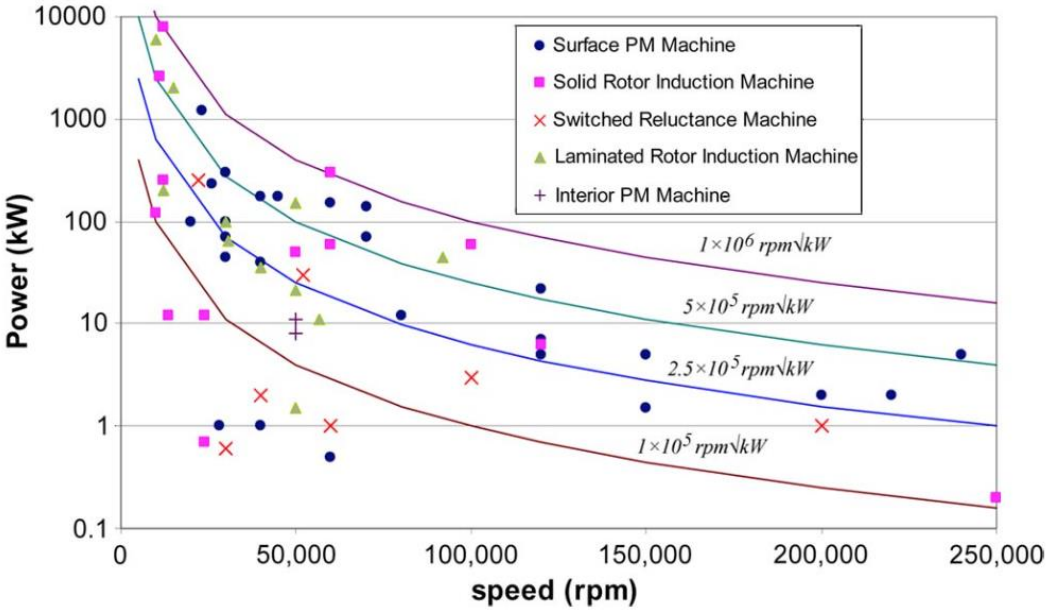

Fig. 2.6 Use of high-speed machines and their speed and power range [6]

Table 2.6 Use of Induction machines in high-speed applications [36]

V_c (m/s)	Rotor Diameter (mm)	Rotor Type	Power (kW)	Speed (rpm)	V_c (m/s)	Rotor Diameter (mm)	Rotor Type	Power (kW)	Speed (rpm)
367	70	Solid coated	60	100000	168	80	Solid coated	35	40000
342	109	Solid coated	300	60000	144	90	Solid coated	65	30600
290	-	Laminated	2000	15000	138	47	Laminated	11	56500
283	90	Solid coated	60	60000	134	51	Laminated	21	50000
250	-	Laminated	8000	12000	126	200	Laminated	200	12000
236	90	Solid caged	50	50000	126	200	Solid slitted	250	12000
204	325	Solid caged	8000	12000	124	99	Solid coated	12	24000
193	330	Solid caged	2610	11160	120	46	Laminated	1.5	50000
185	118	Laminated	100	30000	102	195	Solid slitted	120	10000
182	348	Laminated	6000	10000	63	50	Solid coated	0.7	24000
180	39	Laminated	10	90000	62	88	Solid slitted	12	13500
177	28	Solid	6.3	120000	60	25	Laminated	0.075	45000

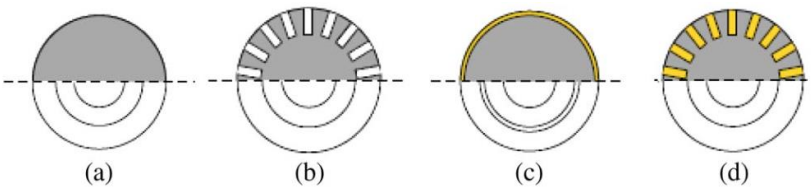

Fig. 2.7 Different rotor topologies for Induction machines [6]

The simplest rotor topology for HS IMs is the solid-rotor topology shown in figure 2.7(a). This rotor is very robust and reliable at HS due to its strong structure. However, the design produces a poor efficiency when in operation due to the lack of a high-conductivity path for the induced rotor currents [37].

Figure 2.7(b) shows an axially slitted solid rotor. By slitting the rotor, the fundamental flux component is guided into the rotor while presenting a higher impedance path to the eddy currents travelling on the rotor surface [38]. However, the robustness of the rotor is reduced as a result of the slitting and the topology typically experiences an increased airgap friction loss.

Figure 2.7(c) shows a coated solid rotor where the rotor is coated with a copper layer, thus introducing electromagnetic anisotropy [39]. This topology is much more efficient and robust compared to the solid rotor and slitter rotor topologies. This topology is often used in the high-end part of table 2.6 (highest speeds). However, by coating the rotor, the airgap is increased which leads to a poor power factor.

Figure 2.7(d) shows a solid rotor with a squirrel cage where the robustness of a solid rotor and the electromagnetic performance of a squirrel cage rotor are combined [36].

From all the possible IM rotor topologies, it is widely reported that a laminated rotor is the best performing topology, as is evident with the research and experiments carried out over the past decade for use of this topology in HS applications.

In [20], a HS laminated rotor IM is investigated and its design process is analysed. Key design challenges relating to the electromagnetic, thermal, and mechanical designs including bearing selection, lubrication,, and balancing are highlighted. In [40] a comparison is made between materials for rotor laminations by using SiFe and CoFe laminations. CoFe has a higher saturation magnetization which results in a higher magnetic loading machine and thus a higher efficiency.

Drop-shaped bars are usually used to improve the power density of IMs and in [41] the use of drop-shaped bars in place of the traditional round rotor bars is analysed. Using the drop-shaped bars allow the current density in the rotor cage to be tailored to the desired maximum rotor temperature. However, the impact of using drop-shaped bars is the increase in the forces experienced in the laminations, and hence the use of a coupled multi-domain design environment is essential [6].

2.8.2 Permanent magnet machines

PM machines typically have higher efficiency levels compared to IMs and are therefore more commonly used in HS applications. Table 2.7 lists the use of PM machines in HS applications found in the literature [6]. The table highlights some instances of PM machines used in super HS applications with speeds in excess of 200,000 rpm. These are usually SPM machines with a retaining sleeve used to protect the rotor.

An application for PM HS machines which is gaining traction is the sensorless control of HS machines. In [42] two different rotor topologies are considered for a 22kW 120,000 rpm PM machine. The conventional parallel-magnetized hollow ring magnet was compared to a design with two parallel-magnetized segments per pole. The efficiency and overall performance of the machine was improved by segmenting the rotor.

The use of PM machines in super HS applications is also another area which is gaining traction. In [43] the design, analysis and testing of a super HS, 100W, 500,000 rpm PM generator was presented, while a 5kW, 150,000 rpm PM machine for a machine tool application was presented in [44]. For this case, a large airgap was used to reduce the slot ripples and losses experienced by the PM machine. In [45] an analytical formulation for designing a carbon fibre retention system for a 40kW, 40,000 rpm interior permanent magnet (IPM) machine is provided.

The surface mounted permanent magnet (SPM) machine is typically the chosen rotor topology for PM HS machines [46], [47]. Due to the HS they operate at, these machines would require a sleeve to be placed over the rotor to protect the integrity of the machine. Titanium, Inconel, carbon fibre, or glass fibre is almost exclusively used as sleeve materials in this case.

SPMs have a poor field weakening capability and a relatively large effective air gap which limits their ability to operate in conditions requiring a wide operating speed range. In order to achieve a wider speed range, such machines are designed for a higher knee-point voltage, leading to an over-sizing of the converter VA rating and hence increased cost of the power electronics [11].

The concentrated-wound SPM topology is another potential option for HS applications [48]. The field weakening capability is improved as a result of the use of concentrated windings. Furthermore, these machines have a high inductance which limits the short circuit currents and makes fault-tolerance/fail-safe easier to achieve.

Table 2.7 Use of Permanent Magnet machines in high-speed applications [6]

V_c (m/s)	**Rotor D (mm)**	**Rotor Type**	**Sleeve**	**Power (kW)**	**Speed (rpm)**	**V_c (m/s)**	**Rotor D (mm)**	**Rotor Type**	**Sleeve**	**Power (kW)**	**Speed (rpm)**
294	47	SPM	Titanium	22	120000	188	80	SPM	Inconel	35	120000
288	25	SPM	Carbon fibre	2	220000	175	90	SPM	Carbon fibre	65	40000
261	10	SPM	Titanium	1	500000	172	47	SPM	Titanium	11	200000
233	89.4	IPM	SiFe	11	50000	161	51	SPM	Carbon fibre	21	40000
230	22	SPM	Titanium	2	200000	157	200	SPM	Titanium	200	500000
201	16	SPM	Inconel	5	240000	92	200	SPM	Carbon fibre	250	60000
200	24.5	SPM	Carbon fibre	1.5	150000	77	99	IPM	SiFe	12	40000
200	-	SPM	Carbon fibre	1100	30000	52	46	SPM	-	1.5	40000
192	24.5	SPM	Glass fibre	1.5	150000	51	195	SPM	Inconel	120	28000

2.8.3 Switched reluctance machines

Switched reluctance machines (SRM) are the most robust machines used in HS applications. The ideal

application for SRMs are high temperature, difficult to access locations such as aero engine integration. However, SRMs are not implemented as widely as IM and PM machines and are mostly simple four-slot, two pole configurations. Table 2.8 shows some of the SRMs implemented [6]:

Table 2.8 Use of Synchronous Reluctance Machines in high-speed applications [6]

Speed (rpm)	**Power (kW)**	**Rpm/kW (x^5)**
22200	250	35.1
52000	30	28.5
60000	1	6.00
48000	1	4.80
30000	0.6	2.32

2.8.4 Synchronous homopolar machines

Synchronous homopolar machines are similar in principle to wound-field synchronous machines. The main difference in the design is that the field winding is fixed to the stator rather than rotor. This allows a simple robust rotor structure that can be constructed from a single piece of high-strength steel and is suitable for HS operation [6]. The homopolar machine has been mainly used in HS flywheel energy storage systems [8].

2.9 Examples of Permanent Magnet machines designed in literature

PM machines are the most commonly used machines in HS applications and it would be impossible to describe every design in detail. This section provides a few examples of PM machines designed to date and discusses their designs.

In [45], two 40kW, 40000 rpm rotors for a magnetically levitated PMSM are designed with surface mounted Sm_2Co_{17} magnets. Issues such as mechanical stress and overheating caused multiple failures of the rotors designed.

In [49], the influence of the magnetisation pattern on the rotor losses are analysed. PM machines are often contained within a retaining sleeve when used in HS applications. However, the sleeve and magnets are exposed to high-order flux harmonics, which cause parasitic eddy current losses [50]. Rotor loss analysis showed that the Halbach magnetized rotor has a lower total rotor loss density than the parallel magnetized rotor. Hence, the Halbach design is a better rotor topology in terms of minimising the rotor losses.

In [27], two HS bearingless PMSMs are designed in which the magnetic bearings are integrated into the active motor part. The motors were designed for 40kW, 40,000 rpm and 500W, 60,000 rpm. An advantage of using a bearingless design is that the rotor losses are lower than those experienced in more conventional magnetic bearing designs. As a result of lower rotor losses, the rotor temperature is kept lower in bearingless machines. A lower temperature means there is a lower chance of rotor demagnetisation and the overall mechanical life of the machine is increased.

A 3kW 150,000 rpm radial PMSM was designed for operation in super high-speed applications [5]. There are major electrical and mechanical design challenges that arise when designing a super HS machine. Proper design of the stator lamination, rotor and stator design, effective air gap, etc. must be considered. At high frequency, proximity effect and skin effect becomes significant, and litz wires are chosen for this design to minimise these effects.

Two Spoke-type IPMs with ferrite magnets were designed in [51] for use in electric vehicles. The spoke IPM design has a larger magnet surface area and is effective for generating a larger field flux from the magnets than other IPM topologies. Furthermore, since this design uses ferrite magnets rather than the stronger neodymium magnets, the spoke design allows the use of reluctance torque more efficiently.

A new segmented IPM has been designed in [52] where the rotor is segmented using iron bridges between the magnets. Segmenting the magnets provides a flux-weakening capability to the IPM. The segmented IPM was compared to a non-segmented IPM where the same stator was used in both machines. The flux-weakening capability is extended by improving the saliency ratio of the machine to make use of the reluctance torque during field weakening. However, an issue with this method is that due to q-axis saturation, a constant ratio of L_q to L_d cannot be maintained, and thus the flux-weakening capability reduces.

Comparison between SPMs and IPMs have become very common in recent times[53]. In [54], a comparison between a distributed and fractional-slot concentrated winding SPM and two distributed winding IPMs was carried out for a wide constant-power speed range. In [55] a comparison is made with regards to fractional slot concentrated windings (FSCW) and their opportunities and challenges are discussed in detail and various parameters are analysed (power density, fault tolerance, single and double layer windings, rotor losses, etc.).

A comparison of five PM rotor topologies was conducted in [56] for use in a hybrid electric vehicle. The machines included an SPM and four IPMs (radial, segmented, V-shape and W-shape). The performance metrics included the back-electromotive force, magnet mass, iron loss and torque ripple. The results showed that the W-shape IPM is the best option for an electric vehicle application due to excellent flux weakening capability and high efficiency over a wide speed range.

2.10 Conclusion

A general overview of HS machines and their applications has been discussed in the preceding sections. The advantages of HS machines over other conventional machines were discussed. Some of these include smaller size, better performance, reliability, etc. However, HS machines also have several disadvantages, especially in the design stage. Careful attention must be paid to the design of the rotor, stator, air gap, sleeves, and other mechanical parts. The losses experienced at high-speeds also affect the performance of the machines.

Four machine types are most commonly used in HS applications: Induction machines, Permanent magnet machines, switched reluctance machines and homopolar machines. Each of these was discussed separately and the advancement in these machines was briefly discussed. The PM machine was found to be the best -

suited machine to the HS application relating to this project and therefore more research was done to understand the wide use of these types of machines. The findings from this research were also discussed briefly.

3. The Permanent Magnet Machine

Based on the literature review presented in the previous chapter, the PM topology was selected to be investigated further for this project. This chapter will give a brief overview of PM machines and will discuss the different topologies within the PM family.

3.1 Types of Permanent Magnet Machines

There are numerous layout possibilities for PM machines and only the most common layouts will be discussed in this section. PM machines are generally grouped into two categories: axial flux and radial flux.

3.1.1 Axial Flux Machines

In axial flux machines, the windings are arranged along the axial direction, and the flux flows in the radial direction. Figure 3.1 shows an axial flux motor configuration [57], where one rotor is sandwiched between two stators. These machines are mostly used when space is a constraint and due to their increased manufacturing time and cost, have not been widely used in industry.

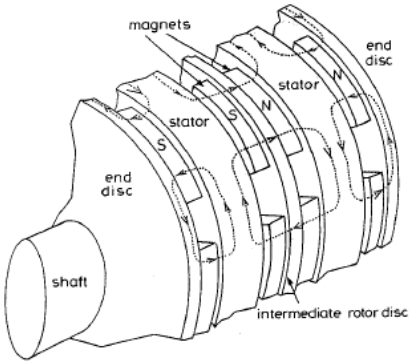

Fig. 3.1 Axial Flux motor [58]

3.1.2 Radial Flux Machines

In the radial flux topology, flux crosses from the rotor to the stator in the radial direction [58]. Radial flux machines are further designed in two categories: inner rotor or outer rotor. The vast majority of these machines consist of inner rotors and outer stators. Figure 3.2 shows various inner rotor PM machines. The motors are shown in figure 3.2a and 3.2b are surface mounted PM motors, while motors in figure 3.2c and 3.2d are interior PM motors.

Stator layouts for inner rotor motors can be either slotted or slotless as shown in figure 3.3a, and figure 3.3b respectively. The stator in figure 3.3c has no slot openings – the stator teeth are connected by bridges at the inner radius and end at the outer stator yoke [58].

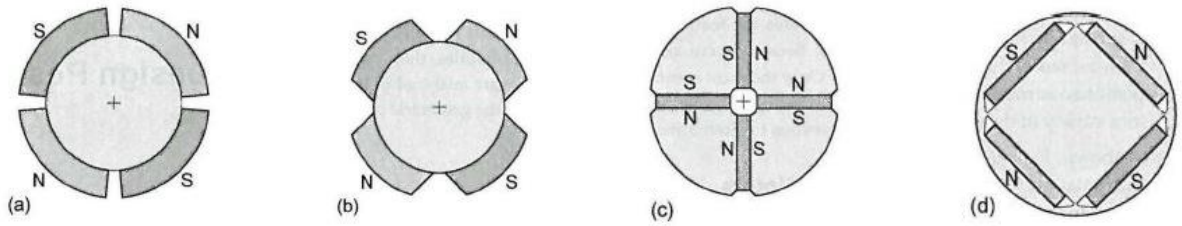

Fig. 3.2 Inner rotor layouts [58]

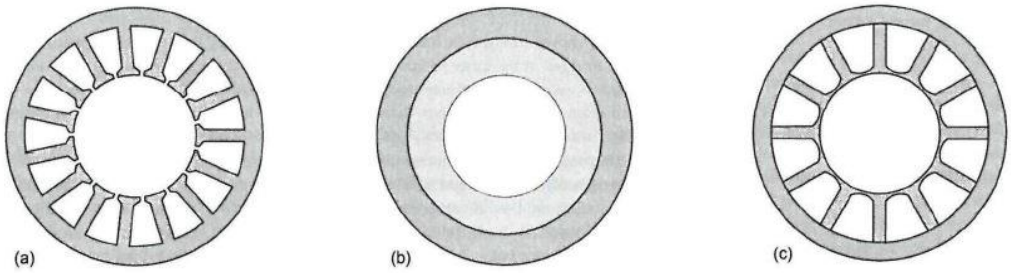

Fig. 3.3 Stator layouts for inner rotor motors [58]

The inner rotor machine has a better torque and power capability with good heat conduction and cooling properties making it ideal for HS applications [59]. The advantages of the axial flux configuration are its low-cost, flat shape and smooth rotation. However, the construction of these motors is a drawback as it must be laminated circumferentially which increases manufacturing time and cost. Furthermore, if they are operated at high-speeds (above 1000 rpm), eddy current losses and heating become excessive [59]. Overall, because of its advantages in performance capability and ease of manufacturing, the inner rotor radial flux configuration is the preferred choice for HS PM machines.

3.2 Permanent Magnet Topologies

There are various PM machine topologies that have been designed in literature, however, they all are part of the three main topologies which are the Surface Mounted Permanent Magnet machine (SPM), Interior Permanent Magnet machine (IPM) and Synchronous Reluctance machine (SynRel).

3.2.1 Surface Mounted Permanent Magnet Machine

The SPM machine is an inner rotor radial flux machine with magnets placed on the surface of the rotor as shown in figure 3.2a and 3.2b. Figure 3.2a shows the traditional radial arc magnet layout. Figure 3.2b is similar, but the sides of the magnets are parallel, rather than radial.

3.2.2 Interior permanent magnet machine

The IPM machine is an inner rotor radial flux machine with magnets embedded inside the rotor as shown in figure 3.2c and 3.2d. There are various IPM topologies available in literature and these were shown in

chapter 1 in figure 1.3. The main difference between the SPM and IPM is the saliency the IPMs experience due to the orientation of the magnets inside the rotors.

3.2.3 Synchronous Reluctance Machine

The SynRel machine is similar to the IPM machine with the exception being that conventional SynRels do not have magnets in the barriers. SynRels with magnets embedded in the barriers are known as permanent magnet assisted synchronous reluctance machines (PMASynrel). A typical difference between the IPM and SynRels is the number of barriers in the rotor, with SynRels typically having more than one barrier.

3.3 Comparison of PM Topologies

In order to decide which PM topology is to be selected for this dissertation, a comparison between the two most suitable topologies, the SPM and IPM, was conducted. The SynRel machine is not common in HS applications and was therefore not considered as a possible option.

The SPM is easier to manufacture and has shorter end connections in comparison to the IPM [60], [53]. Furthermore, it experiences a higher efficiency when compared to the IPM for a machine of equal size [61]. Cooling techniques are also easier to be implemented in the SPM rather than the IPM due to the magnets being on the surface of the rotor, where most of the heat is generated. On the other hand, SPMs have poor field weakening capabilities due to their inherently low inductance. Furthermore, SPMs have very low or no overload capacity, which may be required in some HS applications [60]. Lastly, when SPMs are operated at HS, a retaining sleeve must be placed over the rotor to add a layer of protection against the magnets flying off during HS. The sleeve also generates additional losses and also increases the cost of production.

The IPM has very good field weakening capabilities over a wide constant power speed range. Since the magnets are embedded inside the rotor, there is no risk of them flying off when operated at HS, and thus no need of having a retaining sleeve. IPMs also have very good overload capacities [60]. However, IPMs are generally larger than SPMs of similar ratings as the magnets embedded in the rotor mean the rotor must be larger [59]. Furthermore, there is a higher chance of irreversible demagnetization in IPMs than in SPM and these machines are also generally less robust [61].

Direct comparisons between SPMs and IPMs revolve around highlighting the wider operating range of the IPM. This advantage is specifically useful for electric vehicle applications, where the IPM has become increasingly used [53], [54]. The overload capability of an electric motor is one of the main advantages over the combustion engine and the IPM provides one of the best topologies to take advantage of this. Another application where the IPM is preferred compared to the SPM is in high-temperature and thermal applications. At HS, significant heat is generated in the magnets and in SPMs the magnets are on the surface which results in the risks of demagnetisation. Lastly, machine tools and traction motor applications prefer to use IPMs over SPMs because less magnet volume is needed for an IPM as there is also a component of reluctance torque that is produced, unlike in SPMs [59].

3.4 Selected Topology

Based on the information in the above section, the IPM topology was selected for design and prototyping for this project. The IPM is well suited to HS applications and has several advantages over the SPM such as a larger field weakening range and since the magnets are embedded inside the rotor, there is no need for a retention sleeve. Furthermore, there are various layouts within the IPM family that can be investigated, compared to limited SPM layouts, which give a larger scope for the IPM machine. In particular, this dissertation will compare the circumferential and radial IPM topologies which are shown in figure 3.4a and 3.4d respectively.

4. Design of Permanent Magnet Machines

There are various factors that need to be considered during the design of PM machines. This chapter will discuss the general design of PM machines including the factors to consider when selecting the stator and rotor configuration, number of poles and slots, details on some mechanical aspects, materials used for the rotor and stator laminations, and finally the windings. Lastly, the design equations will be presented to analytically calculate machine parameters which will be compared to the results obtained from simulations at a later stage.

There are a large number of factors that influence the performance of a PM machine and each of these factors have a large subset of possible values that could be used. As a result, the basic sizing equations are carried out manually using analytical equations while the more complicated detailed design is conducted via a computer-based simulation tool. Finite element analysis (FEA) is also used to further understand the performance of the machine at design variations. Due to the overall design process being intensive, and the existence of large subsets of values for each factor that influences the design, a trade-off needs to be made where some of the requirements and objectives may have to be compromised in order to achieve an optimal design. Extensive research has been presented on the design parameters and influence these have on the machine in [62], [63].

The design and selection of parameters and materials specifically related to this project will be discussed in the next chapter, however, some key fundamentals and understandings of these design parameters will be discussed in this chapter.

4.1 Number of Rotor Poles and Stator Slots

The number of poles in an electrical machine is inversely proportional to the maximum speed of the rotor as shown in equation 4.1.

$$n = \frac{120f}{p} \tag{4.1}$$

Where n is the rotational speed, f is the frequency, and p is the number of pole pairs.

For high-speed machines, two and four pole motors are preferred so as to limit the commutation frequency to avoid high switching losses. However, two pole motors have large diameters and are highly prone to magnetic unbalance which can lead to shaft flux and induced currents in the bearings [59]. Therefore, four pole motors are the most common designs in HS machines.

A critical factor that determines the number of stator slots is the slot/pole/phase ratio defined in equation 4.2. The slot/pole/phase ratio is used to determine the relationship between the rotor poles and the stator windings as well as the shape of the generated back emf.

$$q = \frac{N_s}{2p \cdot m} \quad 4.2$$

Where N is the number of slots, p the number of pole pairs, and m the number of phases.

Achieving a high fundamental winding factor is also important and table 4.1 lists out various slot pole combinations and their fundamental winding factors.

Another factor that determines the slot pole combination is the least common multiple (LCM). The lower the LCM between the slot and pole combination, the lower the cogging torque will be. Cogging torque is an undesirable aspect in many machines and it is important to have a minimum cogging torque value. Table 4.2 shows various slot pole combinations and their LCM values. From tables 4.1 and 4.2, the number of slots were selected as 36, and together with three phases and four poles, this combination gives a high fundamental winding factor and low LCM.

Table 4.1 Winding factors for different slot-pole combinations

Slot/Pole	2	4	6	8	10	12	14
6	1	0.866	-	0.866	0.5	-	0.5
12	0.966	1	-	0.866	0.966	-	0.966
18	0.96	0.945	1	0.617	0.735	0.866	0.902
24	0.958	0.966	-	1	0.588	-	0.766
30	0.957	0.951	-	0.951	1	-	0.64
36	0.956	0.96	-	0.945	0.942	1	0.551
42	0.956	0.953	-	0.953	0.953	-	1

Table 4.2 LCM values for different slot-pole combinations

	0.75								**1.125**			**1.5**							
Slots	3	6	9	12	15	18	21	24	9	18	36	3	6	9	12	15	18	21	24
Poles	4	8	12	16	20	24	28	32	8	16	32	2	4	8	12	10	12	14	16
	2.25								**3**						**3.75**				
Slots	9			18			27		6	12	18	24	30	36	15			30			45
Poles	4			8			12		2	4	6	8	10	12	4			8			12
	4.5								**5.25**						**6**				
Slots	9		18		27		36		21		42				12		24		36		48
Poles	2		4		6		8		4		8				2		4		6		8

4.2 Stator Mechanical Design

The stator is a critical component of a machine as it is the main structural component that holds the windings and completes flux paths from the rotor. There are two types of stator configurations typically used

in electrical machines, slotted or slotless, as shown in figure 4.2. The windings on the slotless stator are placed in the air gap of the machine. Since there are no teeth on the stator, the available space for armature windings is larger and this produces lower conductor losses since less current flows in each winding. A drawback with this design is the lower flux density due to the larger effective airgap which has to accommodate the windings. Further, slotless designs have lower current densities and output power capabilities due to the lack of conduction paths to remove the heat generated from the windings. Eddy current losses are also generally high in slotless designs since the windings are directly exposed to the rotating flux [59].

Slotted stators are the more common stator configuration used in electrical machines. These consist of openings around the stator for the armature windings as shown in figure 4.1 [64]. The slots can take up various shapes but the most common are rectangular, round, and trapezoidal as shown in figure 4.2. The slots provide a good path of low thermal resistance for good heat transfer and therefore keep the windings and magnets cool. The use of slots also allows for a narrower air gap length which increases the permeance and thus the air gap flux density of the machine. However, the slots need to be designed carefully to make sure that the teeth are able to carry the air gap flux without saturating and the slots must be large enough to accommodate the required current density in the windings. Another major disadvantage of using slots is cogging torque, which is highly undesirable in electrical machines.

Overall, a slotted stator, compared to a slotless stator, produces a much better performance and is almost always the preferred option in high power applications [58].

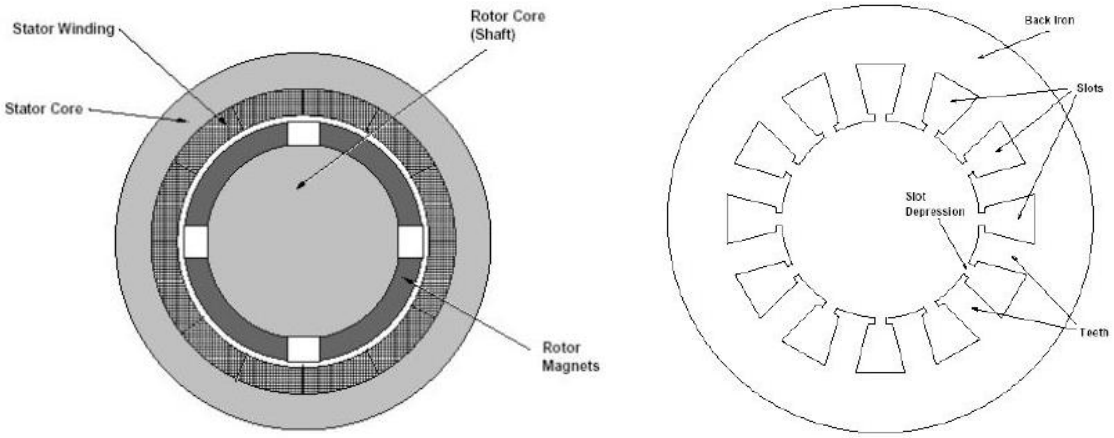

Fig. 4.1 Stator configurations (left: Slotless, right: Slotted) [64]

4.3 Rotor Mechanical Design

One of the most important parameters in the design of the rotor of a PM machine is the aspect ratio. This is defined as the length-to-diameter ratio $\left(\frac{L}{D}\right)$ of the machine. The smaller the aspect ratio, the more compact the machine is. PM machines have higher aspect ratios compared to wound rotor machines and are thus more often preferred in HS applications. Typically the $\frac{L}{D}$ ratio for a wound rotor is 0.5 – 1, while for a PM

machine is 1 – 3 [65]. If the PM rotor configuration consists of magnets on the surface of the rotor and the application is of HS, a retaining sleeve is necessary to help keep the magnets in place. Typical sleeve materials include alloy steel and carbon fibre.

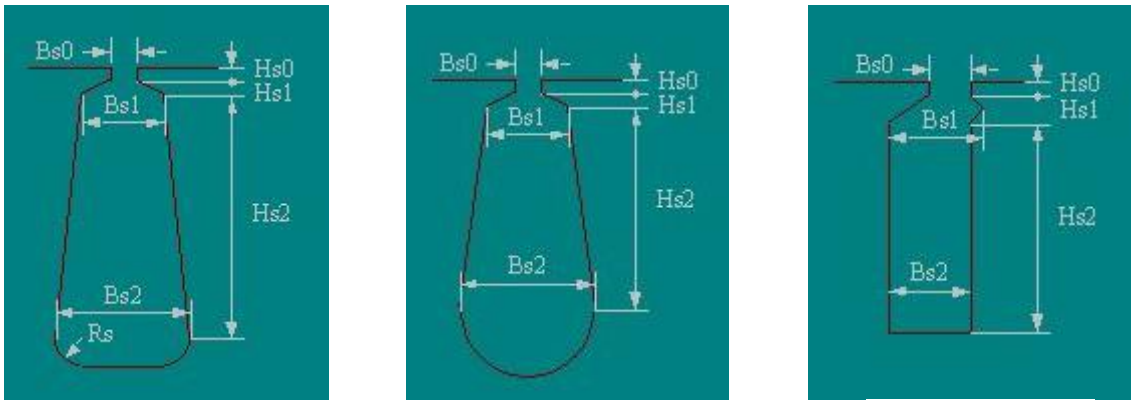

Rectangular Round Trapezoidal

Fig. 4.2 Stator slot shapes

4.4 Material Selection

Another critical consideration in the design of PM machines is the selection of the magnet, rotor, and stator materials [66]. The materials used influence various characteristics of the machines including the output power, temperature, weight and cost. This section will discuss the selection of the magnets, and rotor and stator materials.

4.4.1 Magnet Material

Ferromagnetic materials are the most common magnetic materials used in motor construction. However, due to the nature of these materials (non-linear permeability), it is extremely difficult to effectively analyse them. Further, these materials also have multivalued permeability, meaning that the flux density through the material is not unique for a given field intensity, but rather is a function of the past history of the field intensity [59].

Permanent magnets are available in various types and configurations including alnico, ferrite (ceramic), samarium-cobalt (SmCo), and neodymium-iron-boron (NdFeB). Ferrite magnets are the most popular because they are inexpensive compared to the others. SmCo and NdFeB are known as rear earth magnets and are considerably more expensive than ferrite. They are more common in high-performance applications due to their greater power density, high coercivity, high flux densities, and linearity of demagnetization curves [67]. The B-H loop for a permanent magnet is shown in figure 4.3.

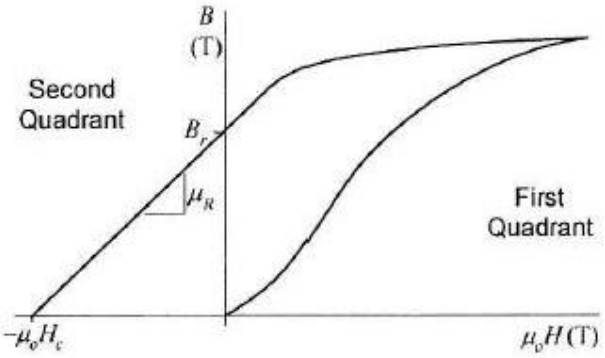

Fig. 4.3 B-H loop for a permanent magnet [58]

Table 4.3 [64] compares the four magnetic materials with respect to some critical magnetic properties. Remnant flux density (B_r) is the remaining flux density after magnetization, and directly influences the air gap flux and magnet dimensions. Coercivity (H_c) is the magnetizing field needed to reduce the flux density in the magnet to zero. This gives an indication of the magnet's resistance to demagnetization. Recoil Permeability (μ_{rec}) is the gradient of the B-H curve and shows the magnet's ability to return to its initial magnetization after being damaged. Energy product (BH_{max}) is the maximum energy product of the magnet and is inversely proportional to the total magnet volume required.

From table 4.3, it is clear that the SmCo and NdFeB materials have superior characteristics than the alnico or ferrite materials, and thus would be better suited for a high power, HS application. Between SmCo and NdFeB, the neodymium magnet is preferred because it is cheaper and more readily available. As a result, NdFeB was selected as the magnet of choice for the PM generator in this project with the assumed values as shown in table 4.4.

Table 4.3 Properties of different magnet materials [64]

Property	**Units**	**Alnico**	**Ferrite**	**SmCo**	**NdFeB**
Remanence	T	0.6 – 1.3	0.35 – 0.43	0.7 – 1.05	1.0 – 1.3
Coercivty	kA/m	40 – 130	180 – 400	800 – 1500	800 – 1900
Recoil Permeability		1.9 – 7	1.05 – 1.15	1.02 – 1.07	1.04 – 1.1
Energy Product	kJ/m^3	20 – 100	24 – 36	140 – 220	180 – 320
Maximum Temperature	^0C	500 – 550	250	250 – 350	100 – 200
B_r Temperature Coefficient	$\%/^0C$	-0.01 to -0.02	-0.2	-0.05	-0.08 to -0.15

4.4.1 Rotor and Stator Material

The type of material selected for the stator and rotor plays an important role in the performance of the machine as the material impacts the machine losses and efficiency. The material selected varies according to the application and requirements of the machine but typically factors to consider are cost, permeability, core losses, and saturation flux [64].

Table 4.4 Properties of the selected magnet (NdFeB)

Property	**Units**	**NdFeB**
Remanence	T	1.23
Coercivty	kA/m	868
Recoil Permeability	-	1.0998
Energy Product	kJ/m^3	263 – 287
Maximum Temperature	^0C	80^0
B_r Temperature Coefficient	$\%/^0C$	-0.11

Typically, high quality, non-oriented steel laminations are used in most machines as these laminations minimize losses. The common materials used include low carbon steels, silicon steels, nickel alloys, and cobalt alloys [64]. Low carbon steels are the cheapest of the materials but have high core losses and are thus used in high volume applications where core loss is not an important factor. Silicon steels, which usually have 3% silicon, are specified based on core loss, with each grade of steel (M19, M27, M36, and M34) having a higher core loss and lower cost [64]. Nickel alloys are either 49% or 80% nickel and have lower losses than silicon steel but are more expensive. They must also be handled with care and have a relatively low saturation flux density of around 0.8 T. For ultra-high-speed motors designed for high power densities, it is recommended to use very thin cobalt-iron laminations. Hard saturation is an important factor in determining the performance of the machine and is typically reached when the differential permeability of the material approaches one at very high field intensities. In common electrical steels, this point is reached between flux densities of 1.7T and 2.3T, while saturation occurs between 1.0T to 1.5T. These values need to be carefully considered when selecting the rotor and stator materials.

Table 4.5 compares the common lamination materials and can be used to select the most suitable material for the PM generator. It is clear that the alloys offer very good properties, but extensive care is required when handling them and they are between 10-50 times more expensive than silicon steel. When comparing silicon steel and alloy properties, the trade-off between the cost of material and properties is too high, and thus would not be justifiable. As a result, based on its relatively good properties and much lower cost, silicon steel was selected as the material of choice for the stator and rotor laminations.

High-performance machines require thinner rotor and stator laminations that have low specific core loses. Typically, the M-19 Silicon steel material is used in such applications with either 29 gauge or 26 gauge used depending on the requirements and applications [59]. Lamination thickness is a trade-off between cost and performance and the most commonly used grades are the 29 gauge (0.355 mm), 26 gauge (0.47 mm), and 24 gauge (0.635 mm).

The M19-29 gauge silicon steel material (0.355 mm thickness) was selected for the rotor and stator laminations for the IPM based on the advantages it has over the other materials as discussed in table 4.5.

Table 4.5 Properties of common lamination materials

Material Type	**Core Loss**	**Saturation Flux Density**	**Permeability**	**Ease of Processing**	**Relative Cost (Si is 1.0)**
Low Carbon Steel	Fair	Good	Good	Best	0.5
Si Steel	Good	Good	Fair	Good	1.0
Thin Si Steel	Better	Good	Fair	Fair	10.0
49% Ni Alloy	Good	Fair	High	Care required	12.0
80% Ni Alloy	Better	Low	Best	Care required	15.0
Co Alloy	Good	Best	Good	Care required	45.0

4.4.2 Stator Windings

The stator windings are where the generator voltage is induced due to the time-varying magnetic flux caused by the permanent magnets on the rotor [64], and the winding arrangement is used to help shape the back voltage to produce a more sinusoidal waveform. There are three parameters that determine the winding configuration: pitch, skew, and distribution.

The pitch of a winding refers to the angular displacement between the sides of a coil. This can be either full-pitched winding, where the displacement between coils is 180°, or short-pitched winding, where the displacement is less than 180°. Short-pitched windings are often used in electrical machines due to their advantages over full-pitched windings. They tend to produce a more sinusoidal waveform when more coils are connected, lower the coil resistance, and make the stator windings more manageable.

Windings can also be skewed axially along the length of the machine. This can be a complicated process and therefore is not used in large, high power machines as it complicates the mechanical construction of the machine. Skewing the stator has advantages such as it lowers the torque ripple produced in the machine and reduces the cogging torque.

Windings can be configured in two ways: distributed windings and concentrated windings. Distributed windings have been used in electrical machines for decades and can achieve high winding factors when the number of slots per pole per phase is high and a full pole pitch is selected. However, distributed windings also have long end windings which are undesirable since this plays a part in the copper losses in the machine. In concentrated windings, the coil turns are concentrated around one tooth and therefore the design benefits from short end windings due to non-overlapping properties [68]. The use of concentrated windings also allows for teeth segmentation, so that the windings can be pre-pressed and the coils can be made with a rectangular shape to have a high slot fill factor and high torque density [69]. Despite the advantages of concentrated windings, one of the major drawbacks is the lower winding factor when compared to distributed windings. To counter this, the use of fractional slot windings are suggested, which uses feasible slot-pole combinations, which allows for higher winding factors with higher torque density. The selection of

slot-pole combinations is a critical parameter and a large amount of research has been conducted to provide suitable guides when selecting these [70].

4.5 Number of conductors per slot

There are geometric constraints which determine how many conductors can be placed in a slot. In smaller machines, coils are formed by placing round, insulated wires in the stator slot along with insulation material [64]. Form-wound windings are typically used in larger machines as they are easy to construct and offer better performance. The coils can be placed in the slots in two ways: single layer windings, with one coil side per slot, or double layer windings, with two coil sides per slot [58], [59]. The double layer arrangement is most commonly used in literature and has been used in this design.

4.6 Slot fill factor

An important variable to consider when designing the windings and slot size is the slot fill factor. This determines how much of the slot cross-sectional area is occupied by the windings and is represented using equation 4.3.

$$\lambda_s = \frac{Winding\ Area}{Total\ Slot\ Area} \tag{4.3}$$

Slot fill factors of between 0.3 and 0.7 have been noted in the literature, depending on the number and size of the conductors. In this design, a minimum slot fill factor of 0.6 was required.

4.7 Proximity and skin effects

Skin effect is the effect caused on the conductor when the current flowing through this conductor is mainly restricted in an area near its outer surface rather than evenly distributed across the conductor. At low frequencies the current is distributed evenly and thus skin effect is negligible. However, as the frequency increases, the tendency is for the current to flow closer to the outer surface of the conductor [71]. Proximity effect is the effect caused when the current flows in loops or concentrated areas due to the presence of magnetic fields generated by nearby conductors.

In HS machines, the windings are typically formed using litz wire. Litz is a specialised multi-strand wire designed to reduce the skin and proximity effect losses in conductors. It is constructed of individually insulated copper wires either twisted or braided into a uniform pattern. The main advantage of using litz wires is the reduction of AC losses. In addition, multi-strand litz wires reduce the power exhibited in solid conductors due to skin effect and since they are twisted together to form a bundle, they ensure that the strand currents are equal hence also reducing the proximity effect.

4.8 Thermal Consideration

Investigating the thermal behaviour of electrical machines is important as increases in temperature can have various undesirable effects on the machine. The performance of the machine would be affected as the power rating typically depends on the thermal load. The lifetime of the machine would also be impacted as temperature affects the insulation, magnetic characteristics, demagnetisation, etc. which would all reduce the lifetime of the machine. To avoid the above effects damaging the machine, a suitable cooling technique is required to be employed in the construction of the machine. The common cooling methods used in literature have been presented in chapter 2.6.3. In this project, a water-based cooling technique was used to ensure the temperature of the machine does not influence the performance and lifetime excessively.

4.9 Bearing Consideration

Bearing consideration is another key design criteria that must be selected very carefully. Bearings suffer from challenges such as mechanical strength, friction loss, and reliability. Typically bearings employed are either ball bearings, air bearings, or magnetic bearings. A detailed comparison of these bearing types and their applications has been presented in chapter 2.6.2. For this project, the ball bearing technology was selected as it provides a simple and robust design, and is readily available.

4.10 Torque Ripple and Cogging Torque

The torque produced by a PM synchronous machine has a pulsating component, which varies as a function of the rotor position, in addition to the dc component [72]. These pulsations are known as torque ripple, which is highly undesirable in an electrical machine. There are several design factors that influence the magnitude and frequency of torque ripple. The addition of PM in the rotor of an electrical machine results in torque pulsations even without any stator excitation. This phenomenon is known as cogging torque. Harmonics in the back EMF also lead to an increase in torque pulsations. Generally, torque ripple is improved by reducing the cogging torque and harmonics in the back EMF, among other techniques.

4.10.1 Torque ripple

Torque ripple consists of three components: reluctance torque, cogging torque and mutual torque. All three components need to be minimised to achieve a reduction in torque ripple. There are various methods that have been investigated to reduce torque ripple, however, these can be grouped into two main categories: design based methods and control based methods. This section will only deal with the design based methods to reduce torque ripple.

The most common methods of reducing torque ripple include rotor/stator skewing, varying slot/pole combinations, using slotted/non-slotted stators, and varying the number of teeth used. Several of these designs have been investigated in [73]–[77] and the results show that they significantly minimise the ripple.

PM rotor shaping has been investigated in [78], the use of fractional slot/pole ratios has been investigated in [79], and spotless motors have been investigated in [78]. Other methods investigated include the elimination of slots, skewed slots, slots and pole combination [62], skewed magnets [73], and varying magnet widths [80].

4.10.2 Cogging Torque

Cogging torque is the pulsating torque produced as a result of the PM aligning with the stator teeth. This tendency to align with the stator slots is due to the presence of varying reluctance, and thus the magnets tend to align themselves with the position of minimum reluctance. Cogging torque can be represented by equation 4.4 [58].

$$T_{Cogging} = -\frac{1}{2}\emptyset_g^2\frac{dR}{d\theta} \tag{4.4}$$

Where $\emptyset_g$ is the magnetic flux crossing the air gap, R is the total reluctance, and θ is the angular position of the rotor. It is clear from equation 4.4 that if the reluctance does not vary with rotor position, the derivative will be zero and thus there will be no cogging torque. In addition, cogging torque is independent of flux direction as the expression (θ_g^2) is squared. Based on the equation, in order to reduce cogging torque, either the reluctance or the amount of flux passing the air gap needs to be minimised.

The most common method to reduce cogging torque is stator slot skewing. The slots are skewed so that each magnet sees a net reluctance that stays the same or nearly the same. This reduces the change of reluctance with angular position, which eventually reduces cogging [72]. Shaping the stator slots can also achieve a similar outcome and some of the techniques of slot shaping include bifurcated slots [73], empty/dummy slots, closed slots, and teeth pairing.

The skew angle, θ_{Skew}, is the mechanical angle required to eliminate the cogging torque and is represented by equations 4.5 and 4.6 [58]. These equations show that the selection of slots and poles play an important role in the reduction of cogging torque, as discussed earlier in this chapter. Despite the advantages that skewing presents, it does have a few drawbacks which must be considered. Skewing makes the construction of the machine more complicated and in cases where the magnet is skewed, the complexity is greatly increased, which increases the overall cost of the machine. Other drawbacks include, reduction in average torque, stray losses, and increase in slot leakage inductance.

$$N_{Period} = \frac{N_p}{HCF\{N_s, N_p\}} \tag{4.5}$$

$$\theta_{skew} = \frac{2\pi}{N_{period}N_s} \tag{4.6}$$

Where N_{period} is the period of the cogging torque waveform, N_s is the number of stator slots, N_p is the number of rotor poles and $HCF\{N_s, N_p\}$ is the highest common factor between N_S and N_p.

In theory, torque ripple cannot be separated from cogging torque and as a result, most of the research conducted is based around reducing the two issues together [79], [81]. Thus, methods used to reduce cogging torque are generally also considered when trying to reduce torque ripple.

4.11 Analytical Design Equations

Once the initial design has been undertaken and the initial output is satisfactory, the design is validated through FEA to review the performance of the machine under operation. The results obtained from the FEA analysis need to be further verified, and one verification stage is to compare the FEA results with analytical results that are obtained by using theoretical equations. As a result, this section will discuss the key equations that would be used to verify the FEA results. This section will discuss general equations for PM machines, and the more detailed equations relating to the IPM machine will be discussed in the next chapter.

4.11.1 Winding resistances

The resistance in the copper phase windings on the stator (R_a) can be represented via equation 4.7 [64].

$$R_a = \frac{l_c}{\sigma \cdot A} \tag{4.7}$$

Where l_c is the length of the conductor, σ is the winding conductivity and A is the cross sectional area of the winding. The cross sectional area of the conductor (A_c) can be obtained via equation 4.8 [64].

$$A_c = \frac{A_S \lambda_S}{2N_c} \tag{4.8}$$

Where A_s is the slot area and N_C is the number of turns per coil.

4.11.2 Winding factors

Windings are typically short-pitched and distributed in some pattern due to the advantages these bring to the machine performance as discussed earlier in this chapter. The winding factor is the ratio of flux linked by an actual winding to the flux linked by a full pitch, concentrated winding having the same number of turns [72]. The winding factor is the product of the pitch factor and distribution factor as described by equation 4.9.

$$k_w = k_p k_d \tag{4.9}$$

Where k_p is the pitch factor and k_d is the distribution factor. The pitch factor is the ratio of the flux produced by short-pitched winding to the flux produced by a full pitched winding, while the distribution factor accounts for the effect of the windings arranged over a range of slots. The pitch and distribution factors $(k_p \; and \; k_d)$ are represented by equations 4.10 and 4.11 as expressed in [64].

$$k_p = \sin\left(\frac{n_h \alpha}{2}\right) \sin\left(\frac{n_h \pi}{2}\right) \quad 4.10$$

$$k_d = \frac{\sin\left(\frac{n_h q \gamma}{2}\right)}{q sin\left(\frac{n_h \gamma}{2}\right)} \quad 4.11$$

Where n_h is the harmonic number, q is the slots per pole per phase, and γ is the coil electrical angle.

4.11.3 Back EMF

The magnetic flux linkage in a machine induces a voltage across the winding whenever the flux varies with time as explained via Faraday's Law. In order to estimate this induced voltage, the air gap flux density needs to be determined first. To account for the leakage flux (K_l), when the flux passes from across the air gap to the stator, and the effect of steel reluctance (K_r) on the air gap flux, a leakage and reluctance factor need to be selected. Typical values for these are $K_l = 0.95$ and $K_r = 1.05$ [64].

The airgap flux density is also affected by the stator slots that cause a difference in permeance as the flux crossing the air gap in the vicinity of a slot needs to travel farther before it reaches the stator core, which has a high permeance than compared to the flux crossing the airgap where there is no slot. Carter's coefficient is used to account for this effect and is represented by equation 4.12 [58].

$$K_c = \left[1 - \frac{1}{\frac{\tau_t}{w_s}\left(5\frac{l_g}{w_S} + 1\right)}\right]^{-1} \quad 4.12$$

Where τ_t is the tooth pitch and, w_s is the average slot width, and l_g is the airgap length .The effective airgap (g_e) is used to account for the slotting effects as shown in equation 4.13, and the permeance coefficient (PC) can be calculated using equation 4.14 as expressed in [58].

$$g_e = K_c l_g \quad 4.13$$

$$PC = \frac{h_m}{g_{\mathrm{e}} \mathrm{C}_{\phi}} \quad 4.14$$

Where C_ϕ is the flux concentration factor relating magnet area to airgap area: $\left(\frac{A_m}{A_g}\right)$ [58]. Thus, the airgap flux density (B_g) is calculated using equations 4.15 and 4.16 as expressed in [58].

$$B_g = \frac{K_l C_\phi}{1 + K_r \frac{\mu_{rec}}{PC}} B_r \quad 4.15$$

Where μ_{rec} is the recoil permeability and B_r is the remnant flux density.

$$B(\theta) = \sum_{n=1}^{\infty} B_n \sin(np\theta) \quad 4.16$$

Where: n is the harmonic number (odd numbers), $B_n = \frac{4}{n\pi} B_g k_{gn} \sin\left(\frac{np\theta_m}{2}\right) \sin\left(\frac{n\pi}{2}\right)$, θ_m is the magnet angle in mechanical radians, k_{gn} is the magnetic gap factor where $k_{gn} \rightarrow \frac{h_m}{g+h_m}$. The flux linkage also needs to be determined in order to calculate the back EMF. Equations 4.17 and 4.18 are used to calculate the flux linkage (λ) as expressed in [64].

$$\lambda(\theta) = \sum_{n=1}^{\infty} \lambda_n \sin(np\theta) \tag{4.17}$$

$$\lambda_n = \frac{2 \cdot R_s \cdot L_{stk} \cdot N_{cph} \cdot B_n \cdot k_w \cdot k_{sn}}{p} \tag{4.18}$$

Where N_{cph} is the number of coils per phase, L_{stk} is the stack length, k_w is the winding factor, and k_{sn} is the skew factor. Finally, the peak back EMF (E) from one phase can be calculated (1 turn/coil) using equations 4.19 and 4.20 [64].

$$E_a = \sum_{n=1}^{\infty} V_n \sin(np\theta) \tag{4.19}$$

$$V_n = \omega_0 \cdot \lambda_n \tag{4.20}$$

Where ω_0 is the angular frequency in rad/sec and V_n is the phase back EMF peak voltage.

4.11.4 Core Losses

The main component of losses in a PM machine is the core loss. Core loss (P_c) is mainly caused by hysteresis of B-H curve (P_h) and induced eddy current (P_e) in the surface [82]. The most common method used to calculate the core loss is the Steinmetz's Two-term model and equations used to calculate the loss are expressed in [82] and in equations 4.21 – 4.27.

The loss density in a material is represented by equations 4.21 and 4.22 [82].

$$P_c = P_h + P_e \tag{4.21}$$

$$P_c = k_h f B^{\beta} + k_e f^2 B^2 \tag{4.22}$$

Where f is the frequency, B is the peak sinusoidal flux density, β is the Steinmetz constant, k_e is the eddy current constant, and k_h is the hysteresis constant. However, flux density in the core of most electrical machines is not purely sinusoidal, and thus core loss is not only caused by the fundamental but also higher harmonics present in the flux density [82]. As a result, loss density calculated by using only the peak value, like in equations 4.19 and 4.20, result in a discrepancy between the estimated and measured values. The harmonic components of the flux density mainly affect the eddy current loss, and so are taken into account by equation 4.23 [82].

$$P_e = \frac{2k_e}{T} \int_0^T \left(\frac{dB}{dT}\right)^2 dt \tag{4.23}$$

In addition to the hysteresis and eddy loss, there is a small component known as excess loss that needs to be to be considered as well. This excess loss (P_a) is calculated using equations 4.24 and 4.25 [82].

$$P_a = k_a f^{1.5} B^{1.5} \tag{4.24}$$

$$P_a = \frac{k_e}{T} \int_0^T \left(\frac{dB}{dT}\right)^{1.5} dt \tag{4.25}$$

Where k_a is the excess loss factor. Thus, the total core loss in an electrical machine is the sum of the hysteresis, eddy current, and excess losses as shown in equations 4.26 and 4.27 [82].

$$P_c = P_h + P_e + P_a \tag{4.26}$$

$$P_c = k_h f B^{\beta} + k_e f^2 B^2 + k_a f^{1.5} B^{1.5} \tag{4.27}$$

5. Sizing of the Interior Permanent Magnet Machine

This chapter presents the design and sizing equations for the IPM machine. The general sizing equations are presented first, which size the machine's length, diameter, etc. followed by equations used to design the stator, which includes yoke height, tooth width, slot height, etc. Lastly, the equations describing the windings are presented. Following that, the magnetic equivalent circuits for the two selected IPM topologies are presented.

Each design is based on the specifications and requirements of the application the machine will be used in, but in general, the design is initially dictated by a combination of the requirements of rated torque, output power, rated speed, supply voltage, or dimensions. To start off the process, the number of phases, the number of stator and rotor poles, and the number of series or parallel paths in each phase are determined or selected. Design parameters such as current density and torque density may also be set at this stage. Following this, the internal and external motor dimensions such as rotor radius, stack length, stator outer radius, etc. are determined through design equations. These parameters are then put through an initial testing phase, usually done via an analytical model, and if the output is satisfactory, then static and dynamic simulations are carried out for verification of overall performance. To avoid repetition of an intensive process, the traditional design starts with an initial realisation which is obtained from past experiences and designs available in the literature. The overall design procedure can be expressed using the flowchart in figure 5.1.

5.1 Requirements and Specifications

The IPM machines are required to satisfy a set criteria of being able to achieve an output power of 10 kW with a rated speed of 30,000 rpm. These parameters were selected to allow the IPM to be used in a gas turbine application that is currently under construction as part of a separate project where the required ratings from the machine would be 10 kW at 30,000 rpm. This speed and power rating determines various design choices made in the following sections and finally in the machine parameters presented at the end of the chapter.

5.2 Machine Sizing

For the preliminary design, the machine was sized on the basis of electromagnetic power produced in the air gap. This depends on the quality of the PMs used as the volume of PMs is proportional to the output power of the synchronous machine.

Equation 5. 1 describes the relationship between the electromagnetic power produced (S_{elm}) in the air gap and the main dimensions of the machine.

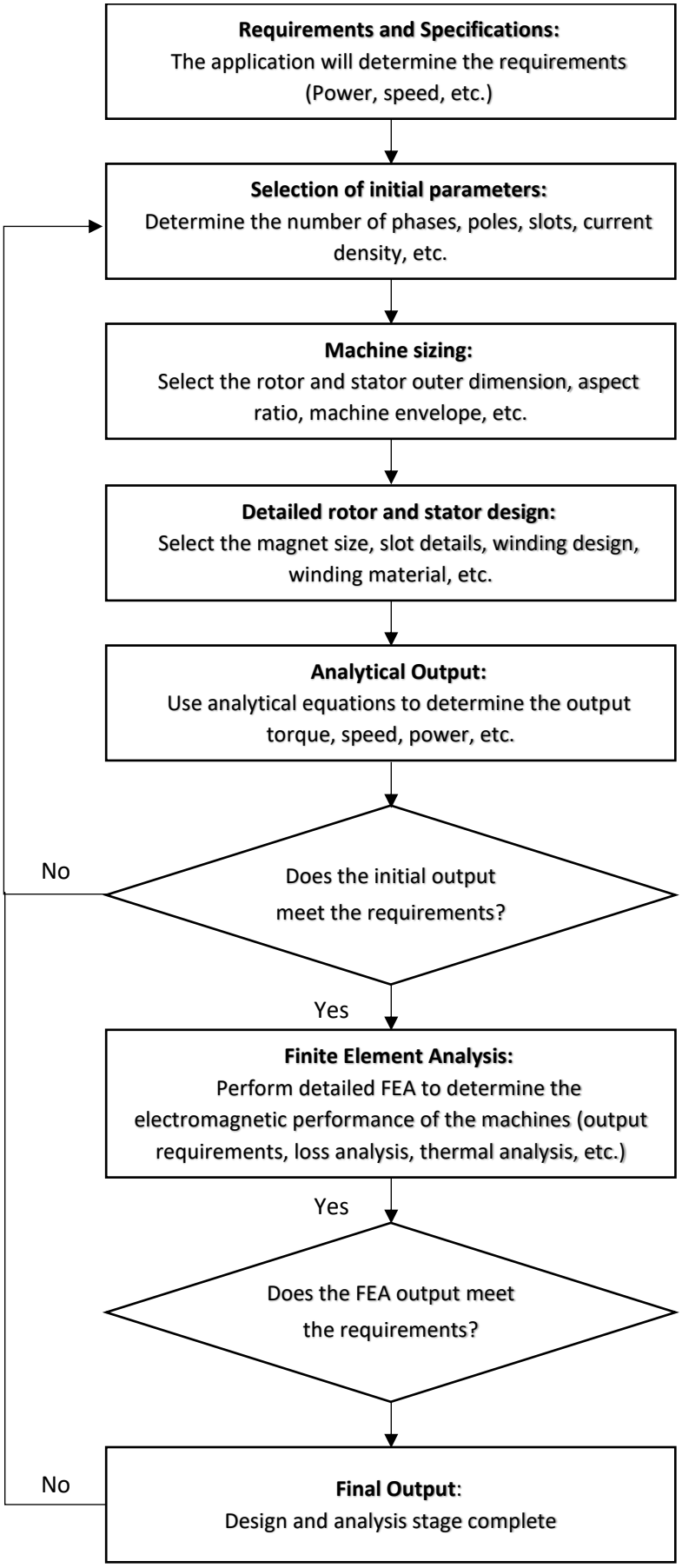

Fig. 5.1 Design Procedure for the interior permanent magnet machine

$$S_{elm} = \frac{\pi^2}{2} k_{w1} D_r^2 L_{stk} n_s B_{mg} A_m \quad 5.1$$

Where k_{w1} is the fundamental winding factor, $D_1$is the rotor diameter (m), L is the stack length of the machine (m), n_s is the synchronous speed (rev/sec), B_{mg} is the magnetic loading (T), and A_m is the electric loading (A/m).

To simplify the equation, the $\frac{L}{\mathrm{D}}$ ratio is introduced. This ratio is a critical parameter for sizing of the machine as it relates the length of the machine to its diameter. The $\frac{L}{D}$ ratio typically ranges from 1-3 for HS PM machines, while the electric loading typically ranges from 10,000 A/m for small motors to 55,000 A/m for medium-power motors.

The output electrical power (P_{gen}) of the machine can be related to its apparent airgap power using equation 5.2.

$$P_{gen} = 3V_a I_a \cos\phi = 3\frac{E_f}{\varepsilon} I_a \cos\phi = \frac{1}{\varepsilon} S_g \cos\phi \quad 5.2$$

Where $\varepsilon = \frac{\mathrm{E_f}}{V_a}$ is the ratio of the excitation voltage to the terminal voltage of the machine, and Ø is the angle of rotation. The product $D_r^2 L$ determines the machine's output torque capability and can be determined using equation 5.3.

$$D_r^2 L = \frac{\varepsilon P_{gen}}{0.5\pi^2 k_{w1} n_s B_{mg} A_m \cos\theta} \quad 5.3$$

Where P_{gen} is the expected output power, ε is the ratio of excitation volage to terminal voltage, n_s is the rotational speed, B_{mg} is the magnetic loading, A_m is the electric loading, and $\cos\theta$ is the designed power factor. Once the $D_1^2 L$ term is determined, the selection of D and L depends on the practical requirements and application of the machine.

5.3 Stator and Rotor Sizing

The stator dimensions are primarily determined by the material selection as this governs the flux density to avoid saturation of the material. The cross-sectional areas of the yokes of the stator and rotor should be adequately designed to avoid saturation of these areas [83].

The design process begins by sizing the yoke height (h_{sy}) using equation 5.4.

$$h_{sy} > \frac{\alpha\pi D_s}{4pK_s} \cdot \frac{B_g}{B_s} \quad 5.4$$

Where D_s is the stator bore diameter, K_s is the stacking factor, p is the number of pole pairs, α is the pole pitch, and B_s is the saturation flux density of the steel. Saturation of the stator teeth is avoided by providing adequate tooth area which is ensured by choosing the tooth width (w_t) based on equation 5.5.

$$w_t > \tau_s \cdot \frac{B_g}{B_s} \quad 5.5$$

Where $\tau_s = \frac{\pi D}{N_s K_s}$ is the stator slot pitch. The required stator slot height (h_s) for the specific electric loading, slot-fill factor and current density chosen can be expressed as shown in equation 5.6.

$$h_s = \frac{A_m}{\sqrt{2} \cdot J \cdot K_s \left(1 - \frac{w_t}{\tau_s}\right)} \quad 5.6$$

Where A_m is the electric loading, J is the current density, and K_{sf} is the stacking factor,

5.4 Winding Design

The number of coils per phase (N_{cph}) is given by:

$$N_{cph} = \frac{N_{coil}}{m} \quad 5.7$$

The frequency (f) is obtained as:

$$f = \frac{n}{60} \times \frac{2 \times p}{2} \quad 5.8$$

The flux per pole (ϕ_{pp}) is obtained using:

$$\emptyset_{pp} = \frac{B_g \times D_r \times L_{stk}}{p} \quad 5.9$$

Where D_r is the rotor diameter, and L_{stk} is the stack length. The induced voltage (E) is taken as:

$$E = 0.9 \times V_{LL} \quad 5.10$$

Where V_{LL} is the line-to-line voltage. The turns per phase (T_{ph}) is thus obtained using:

$$T_{ph} = \frac{E}{4.44 \times k_{w1} \times f \times \emptyset_{pp}} \quad 5.11$$

Where $k_{w1}$is the fundamental winding factor. The turns per coil (N_c) is then obtained as:

$$N_c = \frac{T_{ph}}{N_{cph}} \quad 5.12$$

Based on the above equations and other relevant design equations, the machine dimensions are summarized in table 5.1. The specifications of the machine were set as 10kW, 30,000 rpm and the remaining dimensions were selected in order to achieve this specifications. The number of phases and poles were selected based on the most common values found in literature for HS PM machines. The number of slots was selected based on the high LCM that a 4 pole 36 slot machine has which results in low cogging torque values. The rotor and stator diameters were selected based on the minimum diameter that would be required in order for the laminations to not saturate when in operation and also to effectively fit the magnets within the

rotor. The stack length was selected based on the aspect ratio of 1.5, which is a commonly used ratio in HS machines. The slot dimensions were selected to ensure that there is no saturation during operation. The magnet volume was selected based on the rotor diameter together with the optimum volume of magnet to meet the output design specifications.

Table 5.1 Dimensions of the designed machines

PARAMETER	SYMBOL	VALUE		
Number of phases	m	3		
Number of pole pairs	p	2		
Number of slots	N_s	36		
Power Rating	P	10		kW
Speed	n_s	30,000		rpm
Induced Voltage (RMS)	E_a	219		V
Current (RMS)	I	16.4		A
Frequency	f	1000		Hz
Rotor Diameter	D_r	80		mm
Machine Length	L_{stk}	120		mm
Airgap length	l_g	1.5		mm
Tooth width	w_t	Cir	3.458	mm
		Rad	3.026	
Slot height	h_s	Cir	15.67	mm
		Rad	13.91	
Magnet volume		Cir	18 x 8 x 120	mm^3
		Rad	40 x 3 x 120	
Turns per phase	T_{ph}	24		

5.5 Magnetic Equivalent Circuit Analysis

Using an equivalent circuit is the most common method for designing an electrical machine. The equations presented in this section are obtained from several publications referenced in [58], [84]–[87].

5.5.1 Circumferential IPM

Figure 5.2 shows a simple structure of a circumferential IPM rotor for one pole. By Gauss's law, and neglecting leakage, the total flux from the permanent magnet travels through the path shown.

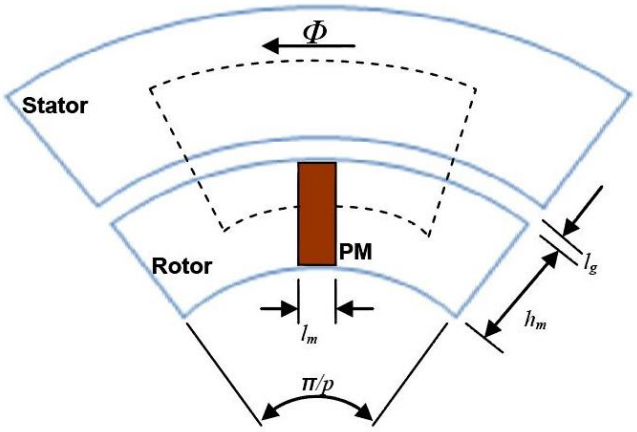

Fig. 5.2 Highlighting one pole of the circumferential IPM [87]

The total flux from the permanent magnet is obtained by:

$$B_m h_m = B_g \frac{\pi R_{rot}}{2p} \tag{5.13}$$

Where B_g is the airgap flux density, R_{rot} is the rotor radius, and p is the number of pole pairs. Using Ampere's law:

$$H_m l_m + 2H_g l_g = 0 \tag{5.14}$$

Where H_m and H_g is the magnetic field strength in the magnet and airgap respectively, and l_m and l_g is the length of the magnet and airgap respectively.

Using: $B_m = B_r + \mu_0 \mu_r H_m$

$$\frac{B_m - B_r}{\mu_0 \mu_r} l_m + 2\frac{B_g}{\mu_0} l_g = 0 \tag{5.15}$$

Where μ_0 is the magnetic permeability of air and μ_r is the relative permeability of the magnet. The air gap flux density is then:

$$B_g = \frac{B_r}{\frac{\pi R_{rot}}{2p} + \frac{2\mu_r l_g}{l_m}} \tag{5.16}$$

The airgap flux density equation can be obtained from the equivalent circuit shown in figure 5.3.

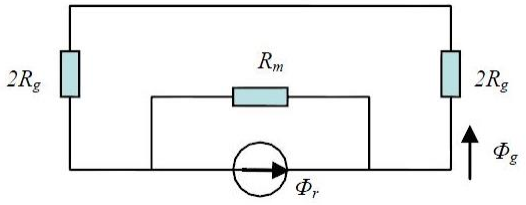

Fig. 5.3 Equivalent circuit for the circumferential IPM [87]

Air gap reluctance (R_g) is expressed as:

$$R_g = \frac{l_g}{\frac{\mu_0 \pi R_{rot} L_{stk}}{p}} \quad 5.17$$

Where l_g is the airgap length, R_{rot} is the rotor radius, L_{stk} is the stack length. The permanent magnet remanence flux (Φ_r) and reluctance (R_m) are:

$$\Phi_r = B_r h_m L_{stk} \quad 5.18$$

$$R_m = \frac{l_m}{\mu_0 \mu_r h_m L_{stk}} \quad 5.19$$

Where h_m is the height of the magnet. Neglecting leakage at the rotor bridges, the air gap flux (Φ_g) is:

$$\Phi_g = \Phi_r \frac{R_m}{R_m + 4R_g} \quad 5.20$$

And the air gap flux density (B_g) is:

$$\mathrm{B}_g = \frac{\Phi_g}{\frac{\pi R_{rot} L_{stk}}{2p}} \quad 5.21$$

The circuit in figure 5.2 and the corresponding equations do not consider leakage at the rotor bridges, which is not negligible. These bridges are necessary to avoid deformation of the rotor due to centrifugal force. In reality, these bridges are fully saturated under operating conditions and behave like air. The equivalent circuit with the leakage at the rotor bridges is shown in figure 5.4.

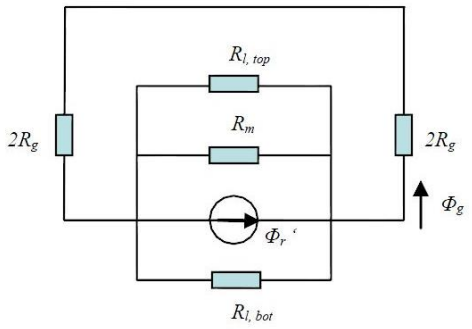

Fig. 5.4 Equivalent circuit for the circumferential IPM with leakage considered [87]

The reluctances at the top $\left(R_{l,top}\right)$ and bottom $(R_{l,bottom})$ of the bridges are:

$$R_{l,top} = \frac{\frac{\pi}{2} l_m}{\mu_o t_{b,top} L_{stk}} \quad 5.22$$

$$R_{l,bot} = \frac{\frac{\pi}{2} l_m}{\mu_o t_{b,bottom} L_{stk}} \quad 5.23$$

Where $\frac{\pi}{2} l_m$ is the approximate distance for traveling leakage flux [33, 34] and $t_{b,top}$ and $t_{b,bottom}$ are the thickness of the top and bottom bridges, respectively. The leakage flux (Φ_l) through each bridge is:

$$\Phi_{l,top} = B_{sat} t_{b,top} L_{stk} \quad 5.24$$

$$\Phi_{l,bot} = B_{sat} t_{b,bottom} L_{stk} \quad 5.25$$

The modified permanent magnet flux (Φ_r') is:

$$\Phi_r' = \Phi_r - \Phi_{l,top} - \Phi_{l,bottom} \quad 5.26$$

By analysis of the equivalent circuit:

$$\frac{1}{R_\sigma} = \frac{1}{R_m} + \frac{1}{R_{l,top}} + \frac{1}{R_{l,bottom}} \quad 5.27$$

Thus, the air gap flux (Φ_g) is:

$$\Phi_g = \Phi_r{}' \cdot \frac{R_\sigma}{R_\sigma + 4R_g} \quad 5.28$$

5.5.2 Radial IPM

Figure 5.5 shows a simple structure of a radial IPM rotor for one pole. In this case, the leakage flux and reluctance at the bridges located at two sides of the permanent magnet have the same value respectively, by symmetry.

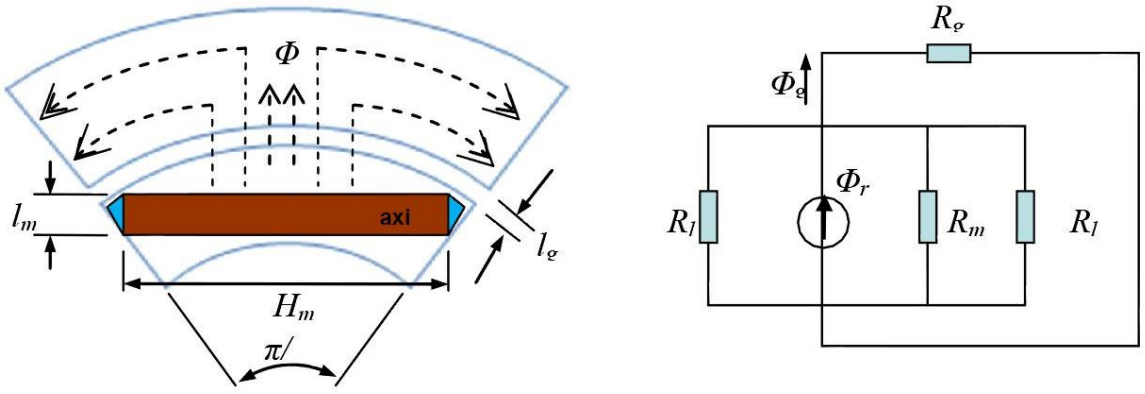

Fig. 5.5 Equivalent circuit for the radial IPM [87]

The equations for the permanent magnet remanence flux and reluctance are the same as those for the circumferential IPM. The reluctance and leakage of the bridges and are:

$$R_{l,top} = \frac{l_b}{\mu_o t_b L_{stk}} \quad 5.29$$

$$\Phi_l = B_{sat} t_b L_{stk} \quad 5.30$$

Where l_b and t_b is the length and thickness of the bridge, respectively. The modified permanent magnet flux is:

$$\Phi_r' = \Phi_r - 2\Phi_l \tag{5.31}$$

By analysis of the equivalent circuit:

$$\frac{1}{R_\sigma} = \frac{1}{R_m} + \frac{2}{R_l} \tag{5.32}$$

The air gap flux is:

$$\Phi_g = \Phi_r' \cdot \frac{R_\sigma}{R_\sigma + R_g} \tag{5.33}$$

Thus, the air gap flux density is:

$$\mathrm{B}_g = \frac{\Phi_g}{\frac{\pi R_{rot} L_{stk}}{p}} \tag{5.34}$$

5.6 Torque Associated with Interior Permanent Magnet Machines

The torque developed by a permanent magnet machine can be described using equation 5.35.

$$T = \frac{3}{2} p\left[\lambda_{PM} + (L_d - L_q) i_d\right] i_q \tag{5.35}$$

Where λ_{PM} is the permanent magnet flux linkage, L_d and L_q are the d-axis and q-axis inductances respectively, and i_d and i_q are the d-axis and q-axis currents respectively. The first term in equation 5.35 represents the permanent magnet torque while the second term represents the reluctance torque. Reluctance torque is related to the difference between the d-axis and q-axis inductances $(L_d - L_q)$ as shown from equation 5.35. For SPMs, $L_d = L_q$ and thus the torque equation only consists of the PM torque. However, in IPMs $L_d \neq L_q$ and therefore the torque consists of a PM component and a reluctance component. The relationship between L_d and L_q is represented in equation 5.36 and is known as the saliency ratio. The larger the saliency ratio, the greater the torque produced by the IPM.

$$\xi = \frac{L_q}{L_d} \tag{5.36}$$

It is clear from equation 5.35 that the inductances are an important factor is the torque produced by the IPM and therefore it is important to calculate these inductances analytically and compare them with the inductances obtained via finite element analysis once the IPMs have been simulated.

5.6.1 Inductance calculations for IPMs

There are several analytical methods reported in literature to determine the d-axis and q-axis inductances for IPMs. Only the final equations for the inductances have been presented here and the detailed derivation can be obtained from [58], [84]–[86].

The d-axis and q-axis inductances ($L_d \; and \; L_q$) and the saliency ratio (ξ) for the circumferential IPM can be expressed as:

$$L_d = \frac{3}{\pi}\frac{\mu_0 D_{si} L_{stk}}{l_g}\left(\frac{k_w T_{ph}}{2p}\right)^2\left[1 - \frac{8D_{si}l_m}{8\pi p l_g \mu_r h_m + \pi^2 l_m D_{si}}\right] \quad 5.37$$

$$L_q = \frac{3}{\pi}\frac{\mu_0 D_{si} L_{stk}}{l_g}\left(\frac{k_w T_{ph}}{2p}\right)^2 \quad 5.38$$

$$\xi = \frac{1}{\left[1 - \frac{8D_{si}l_m}{8\pi p l_g \mu_r h_m + \pi^2 l_m D_{si}}\right]} \quad 5.39$$

Where D_{Si} is the inner diameter of the stator, L_{stk} is the stack length, l_g is the airgap length, k_w is the winding factor, T_{ph} is the number of turns per phase, p is the number of pole pairs, l_m is the length of the magnet, and h_m is the height of the magnet.

The d-axis and q-axis inductances ($L_d \; and \; L_q$) and the saliency ratio (ξ) for the radial IPM can be expressed as:

$$L_d = \frac{3}{\pi}\frac{\mu_0 D_{si} L_{stk}}{l_g}\left(\frac{k_w T_{ph}}{2p}\right)^2\left[1 - \frac{8D_{si}l_m}{2\pi p l_g \mu_r h_m + \pi^2 l_m D_{si}}\right] \quad 5.40$$

$$L_q = \frac{3}{\pi}\frac{\mu_0 D_{si} L_{stk}}{l_g}\left(\frac{k_w T_{ph}}{2p}\right)^2 \quad 5.41$$

$$\xi = \frac{1}{\left[1 - \frac{8D_{si}l_m}{2\pi p l_g \mu_r h_m + \pi^2 l_m D_{si}}\right]} \quad 5.42$$

6. Finite Element Analysis Results

This chapter presents the Finite Element Analysis (FEA) results for the radial and circumferential IPM machines. The results obtained from the FEA analysis are also compared to the analytical results obtained using the equations from the previous chapters.

6.1 Simulation settings and environment

The simulations were conducted on an Intel i7 processor with 3.4GHz speed and 32GB RAM capability. The FEA model for both machines was split into quarters and the simulation and analysis was conducted on one quarter of the machine due to the large computation time and processor requirements a full model would demand. Furthermore, since both IPMs are four pole machines, a quarter represents one pole and thus the results are symmetrical around each pole. The results presented in this chapter are the 3D FEA results as these present a more accurate representation of the machine model compared to the 2D FEA simulations.

6.2 Initial set-up

Ansys Maxwell was used to perform the FEA of the IPM machines and the simulation set up is initiated by defining the current excitation. This involves supplying the machine with a purely sinusoidal signal as shown in equation 6.1.

$$i(t) = \sqrt{2} I_{rms} \, sin(2\pi f t + \gamma + \theta_{ph}) \tag{6.1}$$

Where I_{rms} is the peak phase current, f is the excitation frequency, γ is the current angle, and θ_{ph} is the phase difference.

In order to monitor the rated torque produced by the machines, the current angle was varied from $0°$ to $180°$. When the current angle is $0°$, the machines produce rated torque while when the current angle is $90°$, the machines produce zero torque. Similarly, when the current angle is $180°$, the machines produce a negative rated torque, as expected.

The initial mesh settings were changed to finer values to ensure the critical areas such as the rotor bridges, tooth tips, etc. are accurately measured for saturation. It is important to note that a trade-off must be made between the mesh number and processing time, as the finer the mesh, the longer the processing time.

The simulation stop time and time step were selected to ensure that the machine goes through at least three full cycles to ensure repeatability of results and increased accuracy. Once again, it is important to note that a trade-off must be made between the time step and processing time, as the finer the time step, the longer the processing time.

6.3 3D FEA Results

Ansys Maxwell was used to simulate the machines in 3D and the results obtained are presented in this section. The results show both the circumferential and radial IPM results on the same graph in order to easily compare the performance in the next section.

6.3.1 Airgap flux density

Figure 6.1 shows the airgap flux density for both the IPMs. The circumferential IPM has an average airgap flux density of 0.45T while the radial IPM has an average airgap flux density of 0.35T. The higher airgap flux density for the circumferential IPM can be attributed to the fact that due to the nature of the design and placement of the magnets the per-pole flux of the circumferential IPM is supplied by two magnets at the same time. This phenomenon is known as a flux concentration structure. The typical airgap flux density for PM machines would be around 0.7-0.8T, however due to the relatively large airgap length (1.5mm) in both machines, a low airgap flux density was expected. The airgap flux density curves are similar to a trapezoidal waveform which is caused due to the radial and circumferential components of the flux density plotted together.

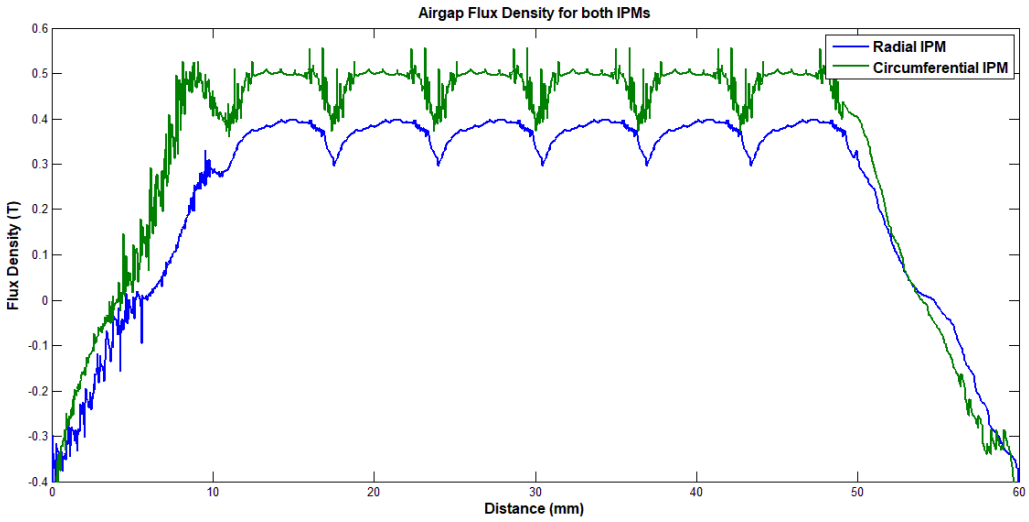

Fig. 6.1 Airgap flux density for both IPM machines

6.3.2 Output torque

Figure 6.2 shows the output torque for both the IPMs and these meet the minimum requirement specified for the project. It can be observed that the circumferential IPM has a higher output torque compared to the radial IPM. Fundamentally, torque capability is decided by flux leakage due to the permanent magnet and the differences between d-axis and q-axis inductances [3]. The air gap flux density of the circumferential IPM is higher than the radial IPM, which means that it has a higher permanent magnet flux leakage and also exhibits a higher permanent magnet torque compared to the radial IPM. There is a large difference in the d-

axis and q-axis inductances and thus the circumferential IPM also produces a larger reluctance torque. The larger permanent and reluctance torque experienced by the circumferential IPM leads it to produce a larger output torque compared to the radial IPM. Furthermore, in the circumferential IPM the magnets are perpendicular to the air gap, rather than facing it as is the case in the radial IPM, and therefore the magnet flux is directed to the air gap via the steel. In addition, the thickness of the magnet in the circumferential IPM is more than in the radial IPM, which results in a larger output torque being produced [88]. However, this higher torque also produces a higher torque ripple as seen in figure 6.3. The ripple in the radial topology is about 11% while the ripple in the circumferential topology is 16%. Even though IPMs generally have a higher torque ripple than other topologies, a 16% torque ripple is considered very high and undesirable. The primary source of torque ripple is as a result of cogging torque and the on-load ripple torque, as mentioned in the previous section. Furthermore, the saliency that the IPMs experience induces a reluctance torque that is at the origin of the increasing ripple torque [89].

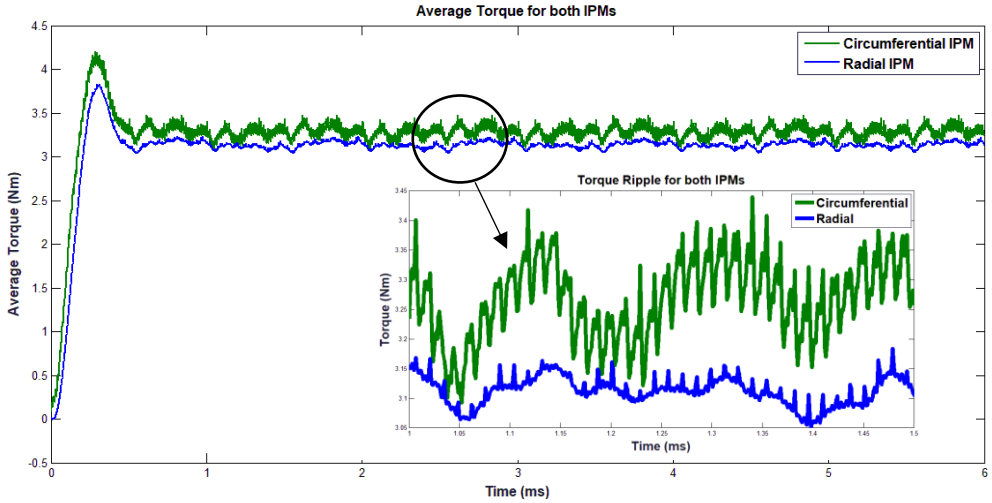

Fig. 6.2 Output torque for both IPM machines

6.3.3 Cogging torque

Figure 6.3 shows the cogging torque for both the machines. Cogging torque is highly undesirable and therefore the lower the cogging torque, the better the performance of the machine. It can be observed from the figure that the radial IPM has a much lower cogging torque than the circumferential IPM (0.5% compared to 2%). Even though both machines are skewed by the same number of slots, the magnet for the circumferential IPM covers only a small section of the rotor adjacent to the air gap and stator teeth and thus, it is constantly having to align with the path of least reluctance as the machine moves, which results in a high cogging torque. This is in contrast to the radial IPM where the magnet covers a large amount of rotor arc and stator teeth, meaning that it is easier for the rotor to align with the path of least reluctance for a longer period, thus the lower cogging torque. Further, the slot openings for the circumferential IPM are wider than

the radial IPM, and this was done due to the winding design in the circumferential IPM in order to find the optimum machine from a torque output view. The wider the slot opening, the higher the cogging torque.

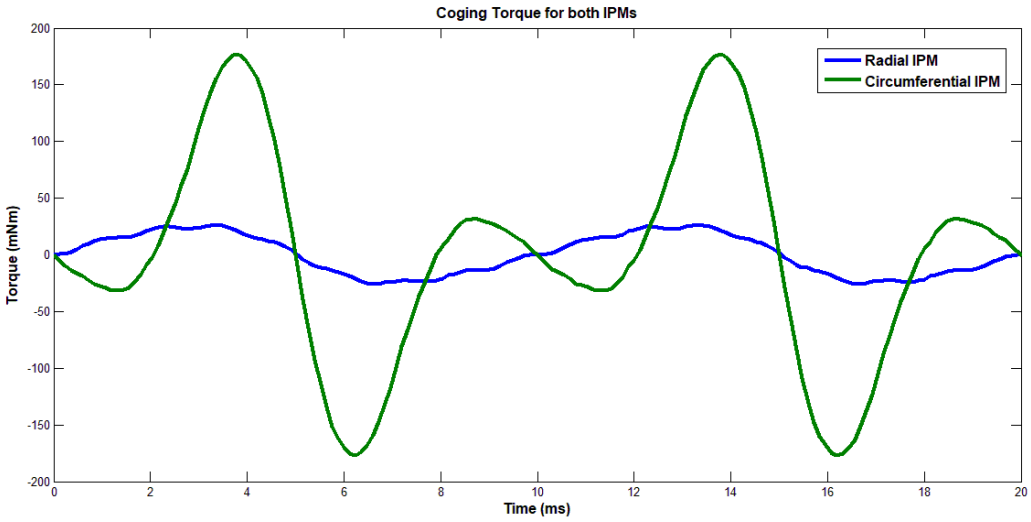

Fig. 6.3 Cogging torque in both IPM machines

6.3.4 Induced voltage and phase current

Figure 6.4 shows the induced voltages in the machines. The induced phase voltage on both the machines is approximately 219 V RMS, which is close to the supply voltage of 220 V RMS which results in lower I^2R winding losses. The winding currents are shown in figure 6.5 and are close to sinusoidal as expected from the induced voltages. The waveforms are distorted due to noise and the voltage waveforms have a THD of 20.7%, while the current waveforms have a THD of 28%, for both machines. The source of the harmonics can be traced back to the winding design used for the machines. The particular winding configuration was selected in order to optimise the performance of the machine and the trade-off with this is the high THD in the waveforms.

6.3.5 Output power

The output power produced by the machines is shown in figure 6.6. Both the machines meet the required output of 10kW at full load operation. The circumferential IPM once again has a higher output power than the radial IPM. This is expected due to the fact that the circumferential IPM generates a larger torque, thus expected to generate a larger output power. Furthermore, the volume of magnet in the circumferential IPM is larger than the radial IPM and thus it is expected to generate a larger output power.

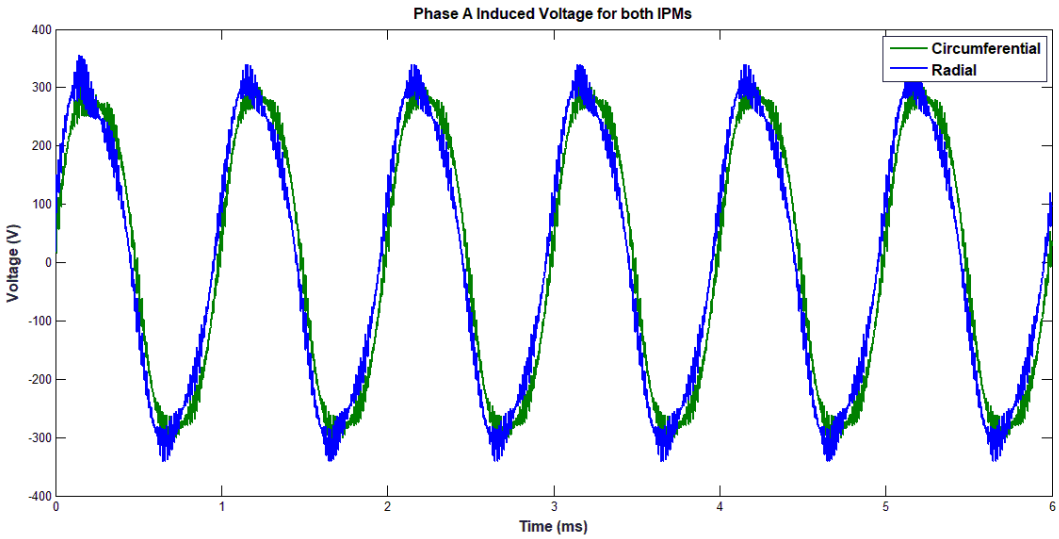

Fig. 6.4 Induced voltage in both IPM machines

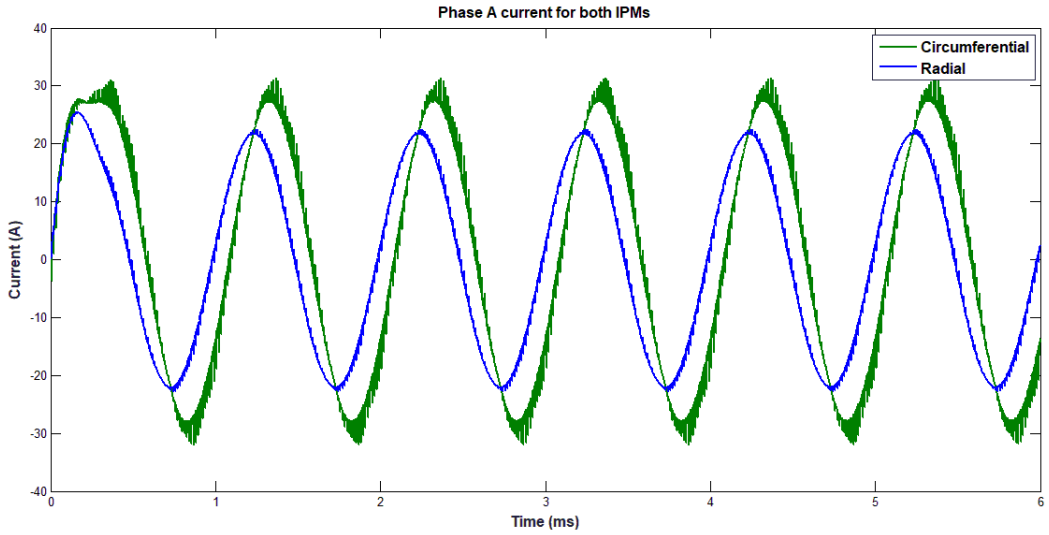

Fig. 6.5 Induced current in both IPM machines

6.3.6 Machine losses

The total machine loss is a sum of the core loss (eddy and hysteresis loss) and the stranded copper loss (winding) loss. Figure 6.7 and figure 6.8 show the eddy and hysteresis loss for both IPMs respectively. Figure 6.9 shows the core loss for both IPMs. It can be observed that the circumferential IPM has a much higher core loss compared to the radial IPM. The primary reason for this is the higher eddy current and hysteresis losses that the circumferential IPM experiences due to the larger volume of magnet in the rotor. In addition, the radial IPM has a lower air gap flux density, which results in lower core loss. The higher core losses also results in the circumferential IPM having a lower efficiency compared to the radial IPM as shown in figure 6.9.

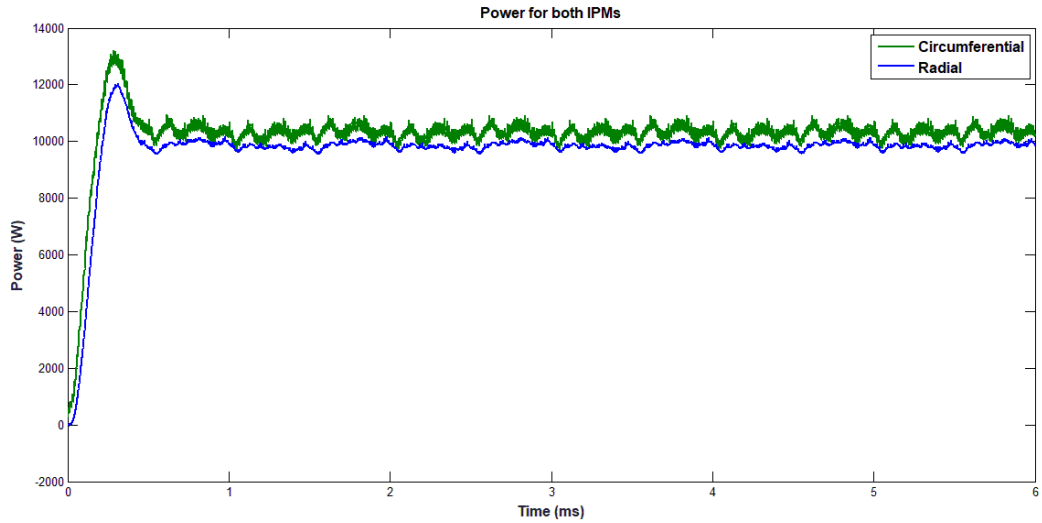

Fig. 6.6 Output power in both IPM machines

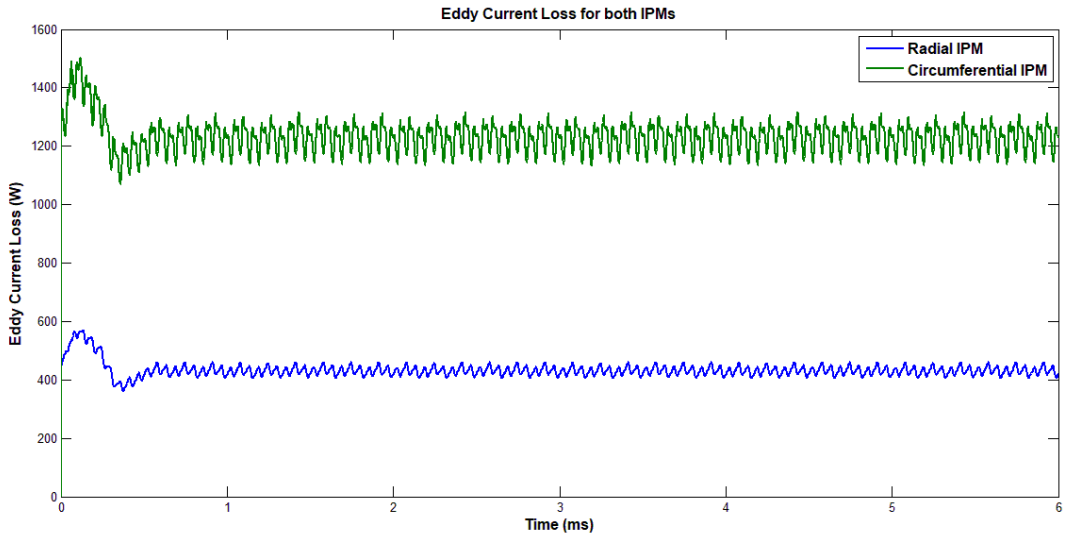

Fig. 6.7 Eddy current loss for both machines

6.3.7 Efficiency

Core losses are highly undesirable and one of the main requirements of this design was to have a high efficiency. Efficiency is negatively impacted by the high core loss, as shown in figure 6.10 where the circumferential IPM efficiency is considerably lower than that of the radial IPM due to the larger core losses. It can be observed from figure 6.10 that at 10kW, the circumferential IPM has an efficiency of 85% compared to the radial IPM efficiency of about 95%. Given that the core loss is the total power lost during operation, this was an expected outcome as the circumferential IPM has considerably higher core losses throughout. There are various factors that contribute to this high core loss and low efficiency such as the higher magnet

volume in the circumferential IPM which results in higher eddy current and hysteresis loss. Furthermore, the larger airgap flux density in the circumferential IPM also factors in to the high losses.

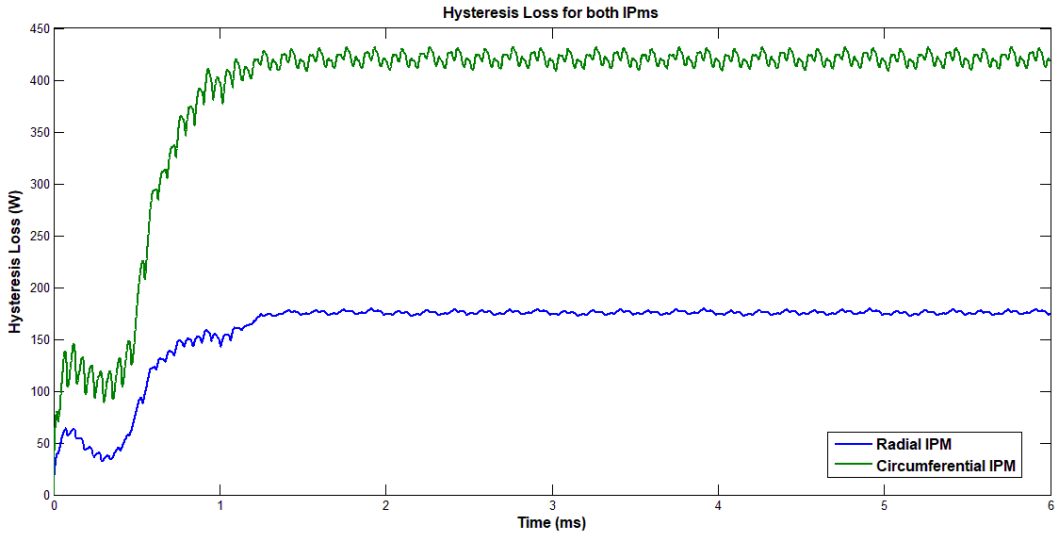

Fig. 6.8 Hysteresis loss for both machines

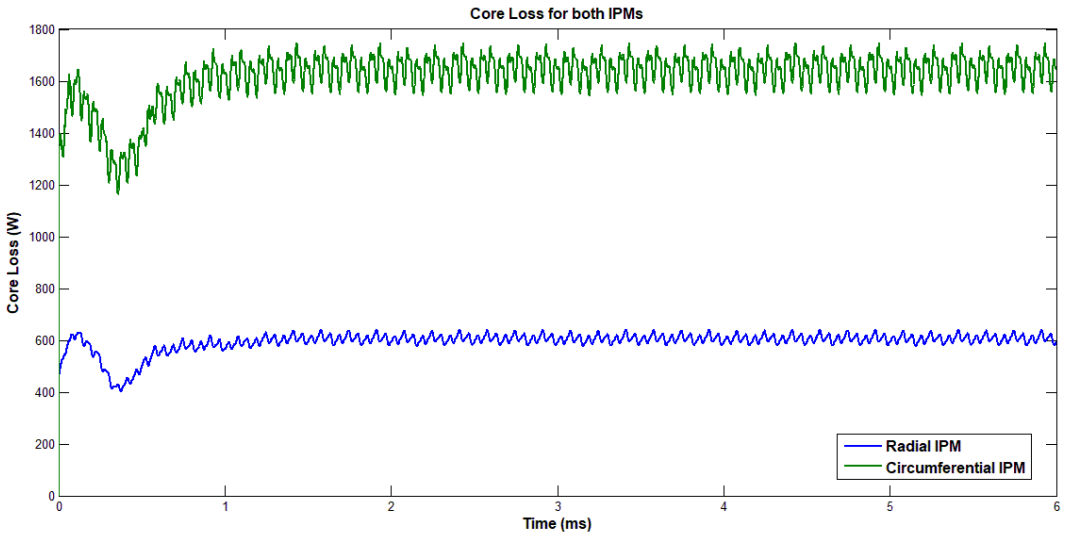

Fig. 6.9 Core loss for both machines

6.3.8 Flux density plots

Figure 6.11 shows the flux density plots for both machines. It can be observed that there is considerable saturation in the flux barriers on the radial IPM, which is expected in this topology. The reason for this is the high number of flux lines that pass through the barrier rather than through the airgap. Careful consideration was taken to ensure that the remaining parts of the machines are not saturated and the flux density throughout was below the saturation level of 1.7T, for the material used.

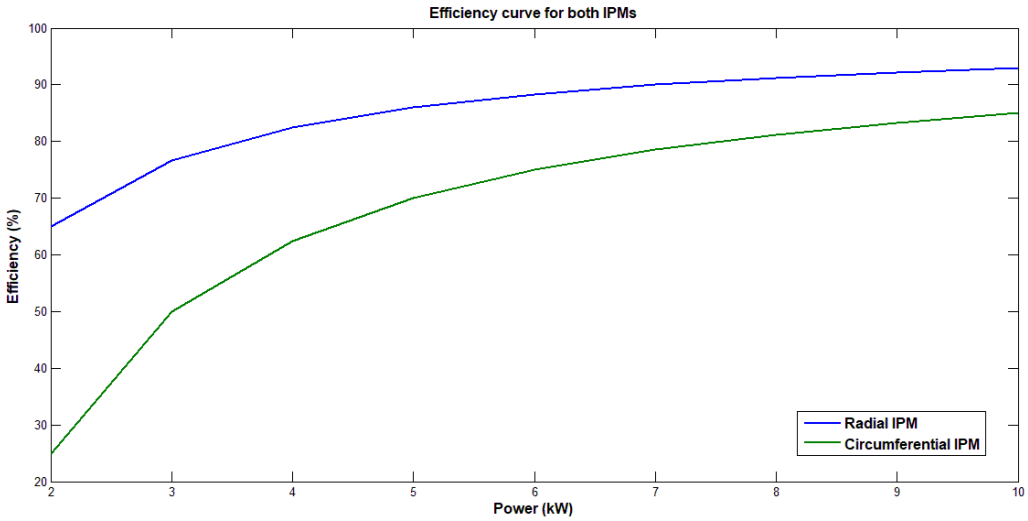

Fig. 6.10 Efficiency in both IPM machines

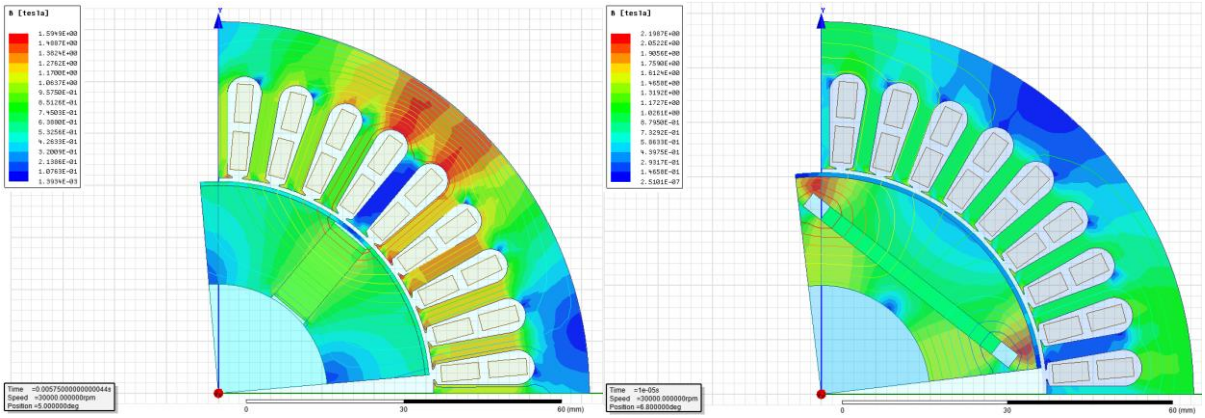

Fig. 6.11 Flux density plots for both machines

Even though no part of the machine is saturated, it is important to check the critical parts by plotting the flux density in these areas. Figures 6.12 – 6.14 show the flux density in the tooth, tooth tip, and the stator yoke, respectively. The tooth has an average flux density of 0.76T for the radial IPM and 1.03T for the circumferential IPM. The tooth tip, where saturation is likely to occur if it is designed to be too small, has an average flux density of 1.1T for the radial IPM and 1.2T for the circumferential IPM. Lastly, the stator yoke has an average flux density of 0.61T for the radial IPM and 0.73T for the circumferential IPM. This means that all these critical areas have flux densities below the saturation limit of the material used. This was expected as these parameters were optimised during the design process to make sure that they do not saturate, while achieving maximum magnetic loading.

6.4 Comparison of Results

The design equations presented in chapter 5 and 6 were used to calculate the theoretical output of the machines. These analytically obtained results can be compared with the results obtained through FEA

simulations for validation purposes. Table 6.1 compares the analytical and FEA results. It can be observed from the table that the results obtained via analytical equations compare well with the FEA simulations thus the obtained results can be considered validated.

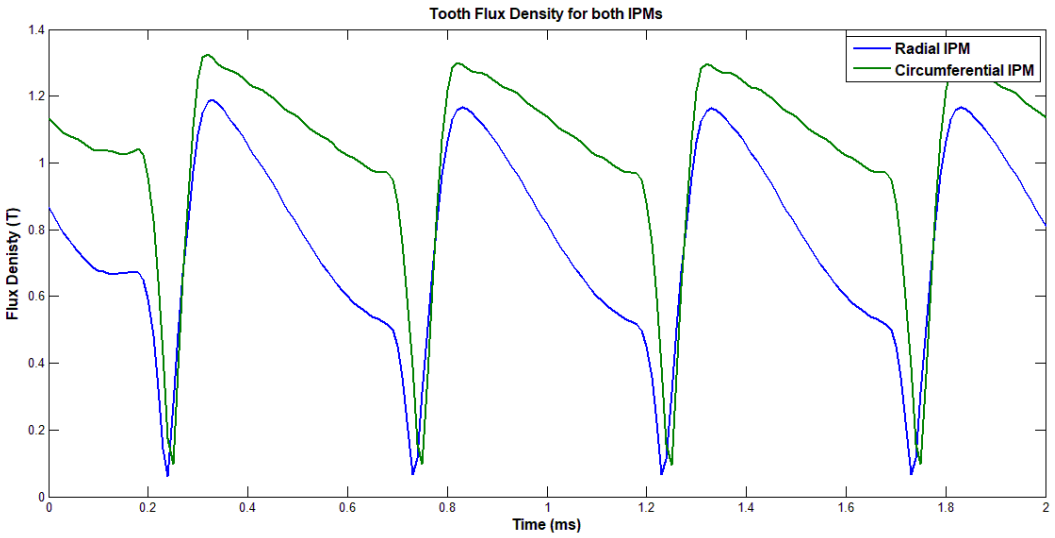

Fig. 6.12 Flux density in the tooth for both machines

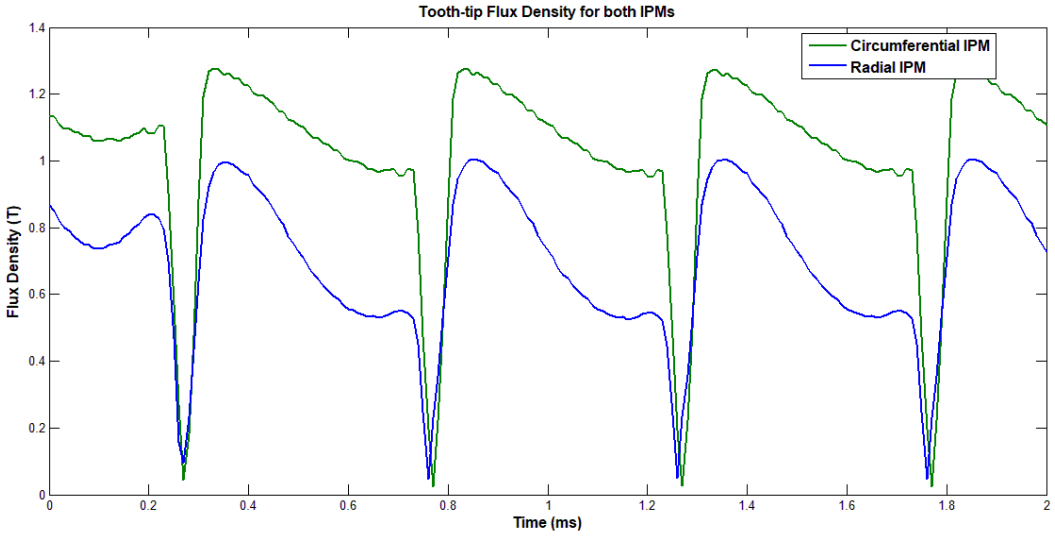

Fig. 6.13 Flux density in the tooth tip for both machines

6.5 Conclusion

From a purely design perspective, the circumferential IPM produces a higher torque and power than the radial IPM. However, it also produces a higher torque ripple and significantly higher core loss, characteristics that are highly undesirable in a HS machine. Furthermore, from a prototyping perspective, the circumferential IPM has a very complex design structure that would require special tools to be manufactured in order to assemble the machine, which would increase the overall cost. On the other hand, the radial IPM

satisfied all the requirements, has a lower core loss, higher efficiency, and is less complex to construct and assemble. Overall, the radial IPM has performed better than the circumferential IPM in most aspects and therefore would be the most likely one to prototype to obtain experimental results.

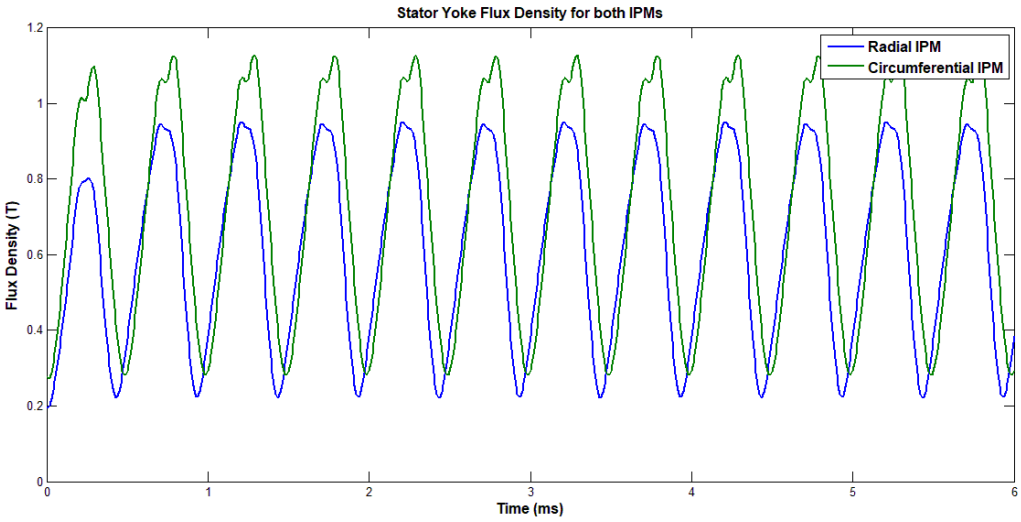

Fig. 6.14 Flux density in the stator yoke in both IPM machines

Table 6.1 Comparison of analytical and FEA results

Parameter	Symbol	Circumferential IPM		Radial IPM	
		Analytical	FEA	Analytical	FEA
Phase Resistance (Ω)	R_a	0.0046	0.0056	0.016	0.019
Airgap Flux Density (T)	B_g	0.50	0.45	0.42	0.35
EMF (V)	E_f	215.5	218.0	214.5	219.0
Core loss (kW)	P_c	1.51	1.6	0.55	0.6
d-axis inductance (μH)	L_d	95.3	100.9	405.5	425.4
q-axis inductance $\mu H)$	L_q	242.5	260.9	810.0	823.8
Saliency	ξ	2.5	2.6	2.0	1.9

7. Development of the High-speed Test Rig

This chapter discusses the process of developing a test rig in order to test the IPM machine. Due to the complexities and mechanical limitations associated with testing a HS machine, as mentioned in Chapter 1, the objective of this thesis was limited to the design, evaluation, and comparison of the two IPM topologies. However, in order to be able to test the performance of the machines experimentally, a suitable test rig is required to be developed. This test rig could then be used in the future as an additional work on this project, to test the IPMs experimentally and compare the results to the analytical and FEA results for validation of the design.

7.1 Requirements of the test rig

As the test rig would be used to experimentally test the machines, there were clear tasks that the test rig needs to be able to achieve, such as:

- Measure the output torque to an accuracy of $\pm 0.05\%$
- Accurately measure the speed and output power produced by the IPM
- Measure the induced voltages and currents
- Measure the alignment and the vibrations produced

7.2 Specifications of the test rig

In order to satisfy the requirements in section 7.1 and measure all the parameters required, the test rig needs to include the following components:

- Servo motor or drive motor to run the IPM up to a desired speed and measure the required parameters
- Torque transducer to accurately measure the output torque
- Encoder to measure the angular position of the IPM
- Lubrication system to lubricate the rotating parts of the machine
- Cooling system to cool the rotating parts of the machine
- Test bench where all the above parts are held in position

Each of these components are discussed individually in the following sections and the reasoning behind the selection of the component is presented. Finally, the entire set-up is presented and the components are identified.

7.3 Selection of the drive motor

The drive motor is used to rotate the machine up to the desired speed. The motor needs to be able to achieve the desired speed as well as the torque and power ratings of the IPM in order to be able to test the IPM at its rated conditions. Since the IPM is rated at 10kW, 30,000rpm, the drive motor needs to be able to achieve these ratings in either the rated conditions or the field weakening mode. After conducting an exhaustive literature survey and contacting various suppliers, locally and abroad, the motor and drive combination described in table 7.1 and figure 7.1 was deemed suitable for this set up. The specifications of the motor and drive, which is a HS brushless motor with an electronic drive supplied by Parker [90], satisfies the speed and power ratings required and the machine can be operated below rated conditions when running the IPM. At a speed of 30,000rpm the maximum torque of the motor is 5Nm and the power is about 15.8Nm, both of which are above the IPM torque and power of 3.2Nm and 10kW respectively.

Table 7.1 Specifications for motor drive combination – Parker product

S1 power	16	kW
S6 power	16	kW
Low speed torque	6.8	N.m
Low speed S6 torque	6.9	N.m
Base speed (S1)	22000	rpm
Max speed	45000	rpm
DC voltage supply when motor is loaded	540	V
Permanent current at low speed	35	Arms
S6 current at low speed	35.4	Arms
Winding resistance(25°C)	0.205	W
Rotor inertia	0.00089	$kg.m^2$
Thermal time constant	1	min
Motor mass	35	kg
Cooling water flow (Tmax = 25 °C)	3	l/min

Even though the test rig could be designed to handle the mechanical vibrations, safety concerns, etc. that would arise when the machine is operated at its rated speed of 30000 rpm, there are several other mechanical parts that must be added to the exterior housing and test rig in order to completely eliminate the safety concerns. Firstly, a complex mechanical process is involved to ensure that the test rig structure would be stable at 30,000rpm. This would include the use of capacitive sensors to ensure alignment, complex balancing equipment, additional protection cases for the torque transducer, installing a speed sensor to ensure that the speed does not exceed 30000 rpm, etc. These additional items were going to increase the overall cost of the project, and as such, it was decided to conduct the tests up to a reasonable speed that would be considered ‘high-speed’. Furthermore, the cost associated with purchasing and installing the drive

motor described in table 7.1 is very high and it would require further planning before an investment of this level could be committed to. As a result, it was decided that the test rig will be designed for a lower speed of 10,000rpm while keeping the power rating at 10kW. Therefore, the new specifications for the test rig were decided as 10kW, 10,000rpm. This will allow the IPM to be tested up to a maximum speed of 10,000 rpm, which is still considered HS according to literature. Lastly, since the original scope of this project did not involve the testing of the IPM, the development of the test rig is seen as an additional item out of the scope and thus it can be justified to design the test rig for 10,000 rpm at the current time and use it as a proof of concept to test the machines. As future work related to the project, the development of a full specification test rig could be undertaken.

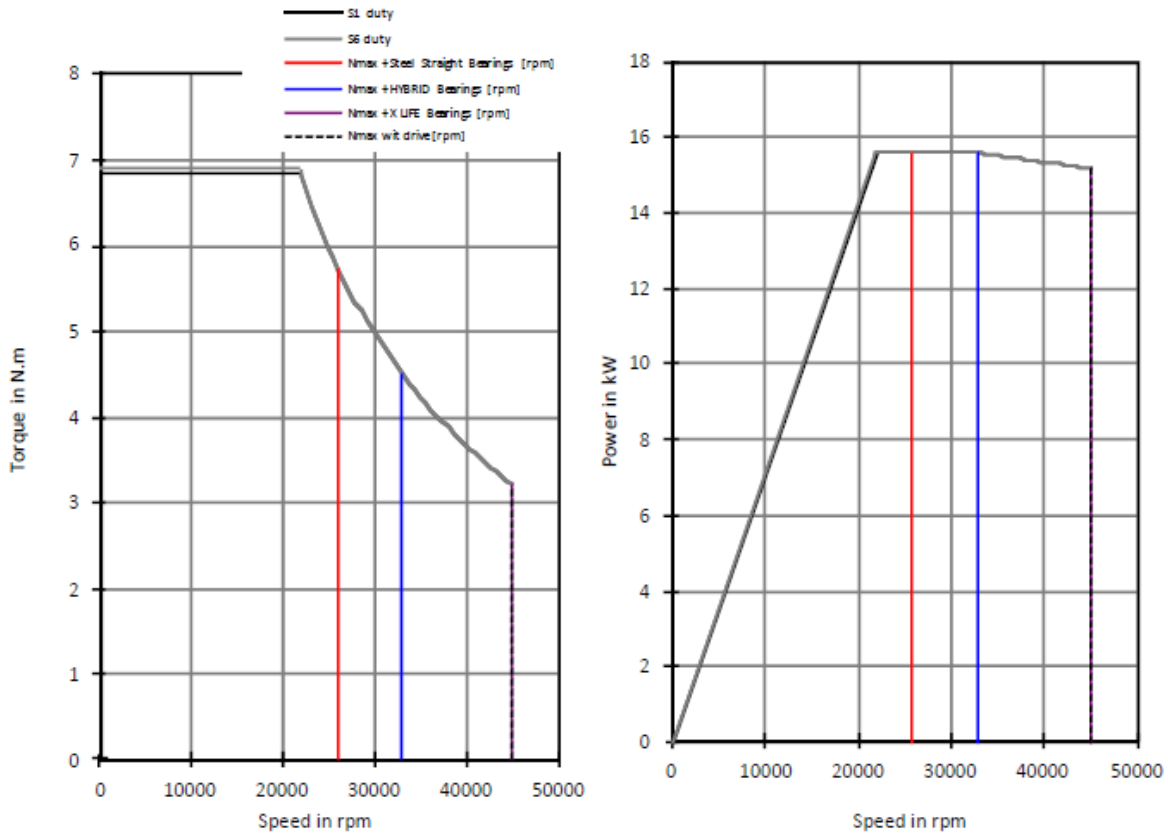

Fig. 7.1 Torque-speed curve (left) and power-speed curve (right) [90]

An aircraft generator rated at 10kW, 2800rpm was then substituted for the motor above to act as the drive motor. Even though the generator is only rated at 2800rpm, it can achieve a speed greater than 10,000rpm in its field weakening mode. Calculations were undertaken to ensure the power and torque achieved in the field weakening mode is above the required levels.

7.4 Selection of the torque transducer

A torque transducer is a device that is used to measure the torque between the drive motor and test motor. The torque transducer for this test rig needs to measure the torque and position with a very high accuracy. In order to be able to test the IPM at maximum speed, the torque transducer must also have a rating of at

least 30,000 rpm. After extensive literature surveying and contacting various suppliers, a contactless torque sensor from Lorenz [91] was selected. This sensor can achieve an accuracy of 0.05% of the measured value within the rated torque specified. Furthermore, it can achieve a maximum speed of 30,000 rpm which means that even though the tests will only be done up to 10,000 rpm due to the drive motor specifications, in future the same sensor can be used to test the IPM to 30,000 rpm. Figure 7.2 shows the specifications of the transducer while the detailed information is available in appendix A.

7.5 Selection of the encoder

An encoder is a device that converts the position of the shaft when in rotation into an analogue or digital signal. There are two main types of encoders: absolute and incremental. Absolute encoders can provide unique position values at all times once they are switched on i.e. even if the system is without power, the absolute encoder can convert the positions accurately once the system is turned on. Incremental encoders generate a signal each time the shaft rotates a certain amount. Each time the encoder is powered on, it takes the start position as the zero position and therefore cannot process the position when it is off, unlike the absolute encoder. For this test rig, a non-contact rotary encoder from RLS was selected and the specifications of the encoder are shown in appendix A. The encoder has a measuring accuracy of $\pm 0.7\%$ with an absolute – to 13 bit conversion capability at 30,000 rpm.

Nominal Torque (Nm)	10
Limit Speed (rpm)	30,000
Accuracy class	0.05% f.scale

Fig. 7.2 Selected torque transducer [91]

7.6 Selection of the lubrication system

The rotating parts in a HS machine are critical to the operation of the machine and when they rotate at these speeds, they need to be constantly lubricated to avoid corrosion and decrease in performance. Given that the IPM is designed for 30,000 rpm, it is important to ensure that all the areas are well lubricated during the operation. For this test rig, an oil-mist lubrication system was used where the lubrication system would pump oil into the IPM in order to effectively lubricate the bearings. The oil-mist system is shown in figure 7.3.

Fig. 7.3 Selected lubrication system

7.7 Selection of the cooling system

One of the main challenges associated with HS machines is the heating in the machine due to the HS and small volume. A sufficient cooling system needs to be designed to ensure that the internal structure of the machine and the magnets do not overheat. Overheating of magnets could lead to demagnetisation or decrease in performance. There are various cooling techniques used in literature such as jacket cooling, water cooling, air cooling, etc., as discussed in previous chapters. For this project, using a conventional cowl and fan system would significantly decrease the efficiency of the IPM and operating the fan based cooling system at HS would cause additional wear on the bearings. A water based cooling system was implemented where the IPM would be cooled using water supplied via a chiller. The cooling set up is shown in figure 7.4.

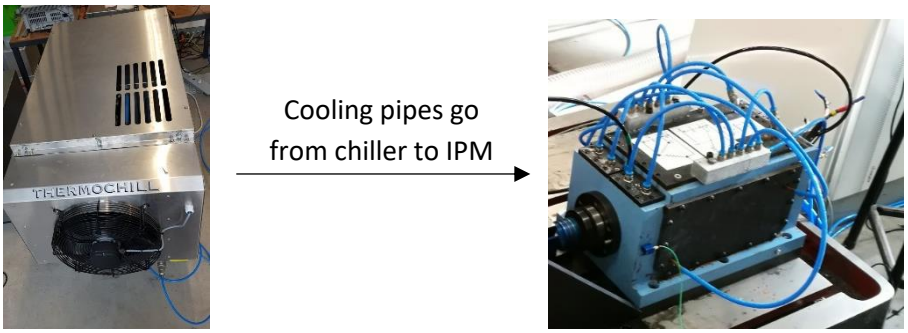

Fig. 7.4 Selected cooling system

7.8 Final design of the test rig

The complete test rig is shown in figure 7.5. The IPM machine is connected to an aircraft motor which represents the drive motor for the set-up. The shaft torque is measured via a torque transducer and a power analyser (Yokogawa WT3000) is used to measure the voltage, current, and power of the prototype IPM.

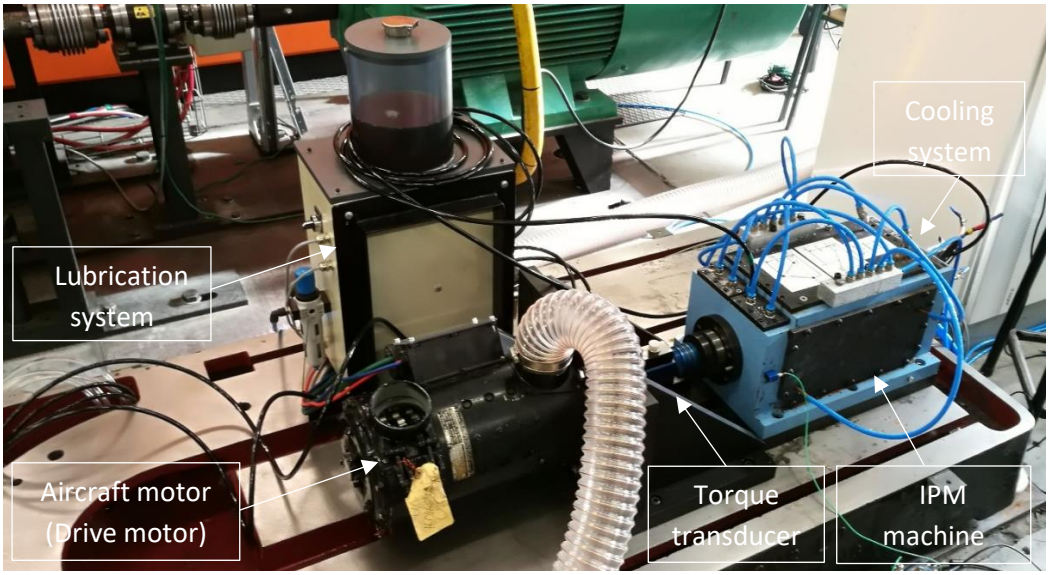

Fig. 7.5 Assembled test rig

7.9 Challenges experienced during the development of the test rig

Even though the test rig has been successfully developed and implemented, there were numerous challenges and limitations experienced during the development phase. As mentioned in the previous sections, the cost of a 30,000 rpm drive motor was too high for this project considering that the testing of the machine was not an objective of the project. As such, the test rig has been set up to test the IPM to a maximum speed of 10,000 rpm. The selection of the lubrication and cooling system involved an exhaustive and detailed design process with various parameters to consider such as cost, availability, how it fits in the test rig system, etc. Furthermore, when the IPM is operating at HS, there is a safety concern for the machine operators and therefore a high quality thick Perspex casing was designed to place over the machine when in operation. This was to ensure that there is no risk of any parts flying off and injuring the operators. One of the major challenges encountered during the development of the test rig was the alignment of the components. Due to the HS of the machines, the tolerance of misalignment is minimal at 0.02mm for 30,000 rpm. Most of the measuring tools do not have the accuracy to align the set up to this precision and additional high precision tools are required before the machine can be operated at 30,000 rpm.

8. Prototyping of the Radial IPM

This chapter will present the prototyping process of the radial IPM. Thereafter, no-load experimental results obtained during the testing process for the radial IPM are also presented. It must be noted that the testing of the IPM was not part of the scope of the project as mentioned in chapter 1. However, since the test rig was developed and the IPM prototyped, no-load experiments were conducted to verify the machine and set up future work that can be undertaken with this project. As mentioned in chapter 6, only the radial IPM was prototyped due to it being the better performing design, as well as cost and design complexity related matters. Lastly, the experimental, FEA, and theoretical results are summarised and compared in the final part of the chapter to ensure the project demands are satisfied.

8.1 The prototyping process

The IPM consists of various parts such as the shaft, rotor laminations, stator laminations, bearing, slip rings, couplings, etc. that are all assembled and cased into a machine housing. The detailed mechanical drawings for the rotor and stator laminations, shaft, and machine housing are presented in appendix B.

Figure 8.1 and 8.2 show the prototyped shaft and rotor for the radial IPM respectively. For the rotor, the barriers were first made on each lamination, then the laminations were stacked together, and finally the magnets inserted into the rotor. Figure 8.3 shows the machine housing that encases the entire assembled IPM. All the detailed drawings for these parts are available in appendix B. The winding details for the radial IPM are presented in figure 8.4 and the final assembled machine is shown in figure 8.5.

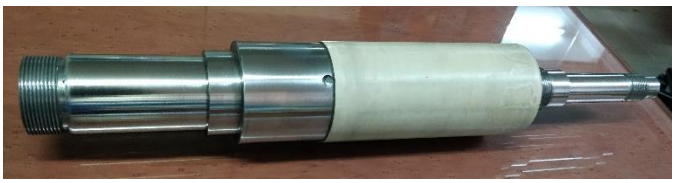

Fig. 8.1 Radial IPM shaft

Fig. 8.2 Radial IPM rotor

Fig. 8.3 Machine housing

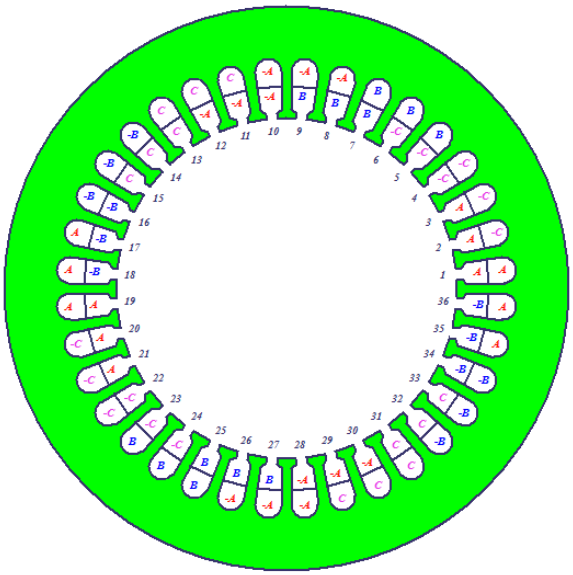

	Phase	Turns	In Slot	Out Slot
Coil_1	A	2	1T	8B
Coil_2	A	2	2T	9B
Coil_3	A	2	3T	10B
Coil_4	-C	2	4T	11B
Coil_5	-C	2	5T	12B
Coil_6	-C	2	6T	13B
Coil_7	B	2	7T	14B
Coil_8	B	2	8T	15B
Coil_9	B	2	9T	16B

Fig. 8.4 Winding layout for the radial IPM

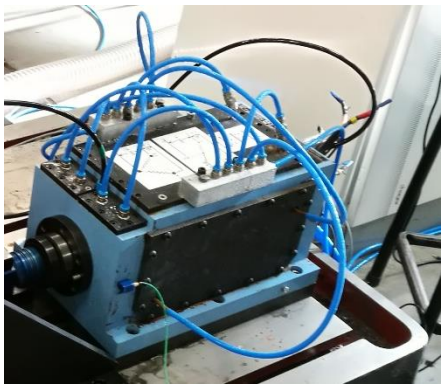

Fig. 8.5 Complete assembled radial IPM

8.2 Experimental Set-up

The radial IPM machine has been experimentally evaluated using the test rig detailed in chapter 7 and shown in figure 7.6. The IPM machine is connected to an aircraft motor which represents the drive motor for the set-up. The shaft torque is measured via a torque transducer. The experimental tests were only conducted up to a maximum speed of 10,000 rpm, which is a third of the design speed of 30,000 rpm due to the concerns raised in chapter 7.

8.3 Open Circuit Voltage

The stator phase windings were connected in series to form the phases of the IPM machine. The open circuit phase voltages are shown in figure 8.6. The sinusoidal shape of the waveform reveals the low harmonic content in the phases. This is as a result of the coil connections and hence the low harmonic winding factors associated with the windings. Furthermore, it can be seen that the phases are equally displaced by 120°. The output is an rms voltage of 72V, which is the expected voltage at one third of the original speed since at one third of the speed (10,000rpm), the voltage should be one third as well due to the linear relationship between speed and voltage.

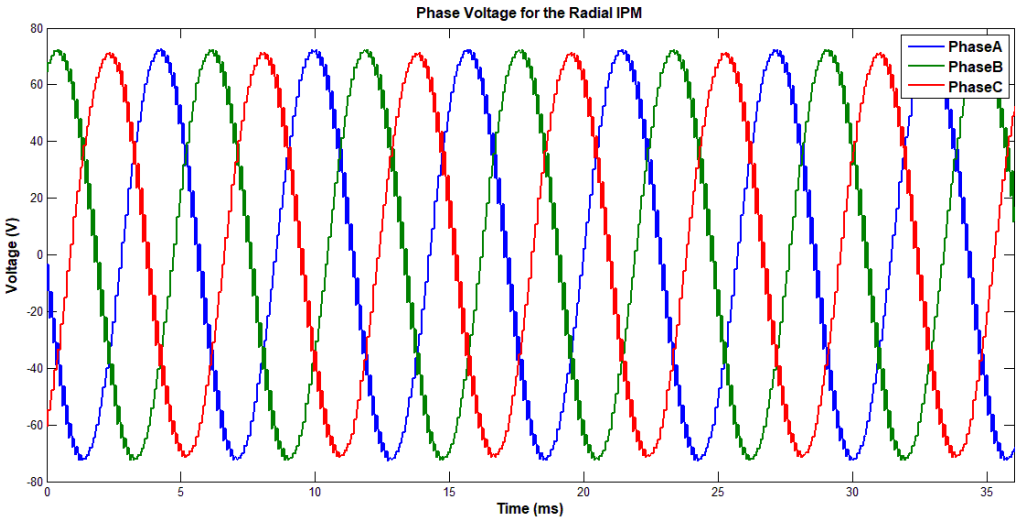

Fig. 8.6 Phase Voltages

The open circuit line to line voltages are shown in figure 8.7. Once again the voltage is an rms voltage of 125V, which is the expected voltage at one third of the original speed since at one third of the speed (10,000rpm), the voltage should be one third as well due to the linear relationship between speed and voltage.

The PM flux linkage (λ_{PM}) can be estimated from the slope of the graph for the open circuit phase voltage against shaft speed as shown in figure 8.3. The value obtained from the graph (0.0042 Wb-turns) compares satisfactorily with the value estimated from the analytical design procedure (0.0058 Wb-turns).

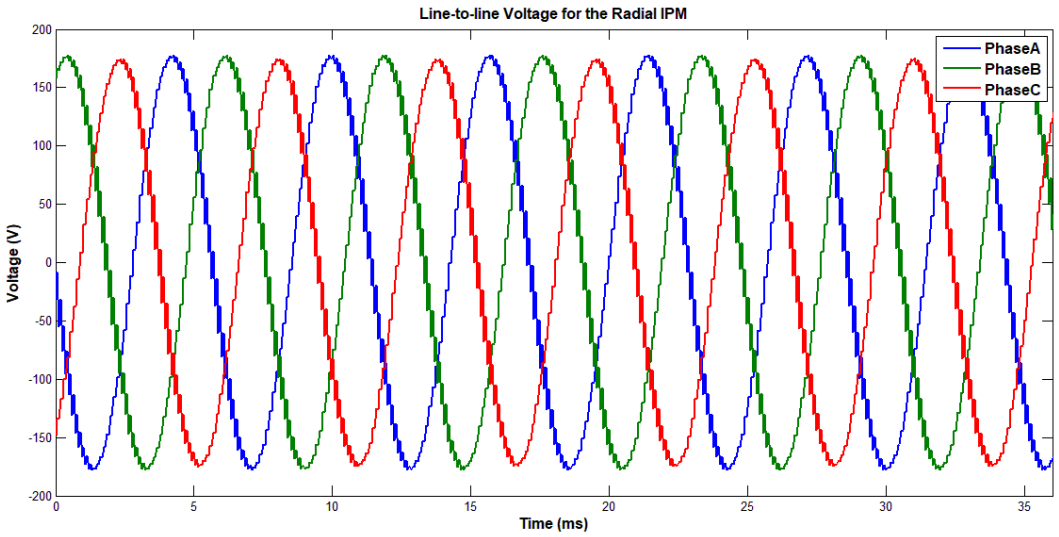

Fig. 8.7 Line Voltages

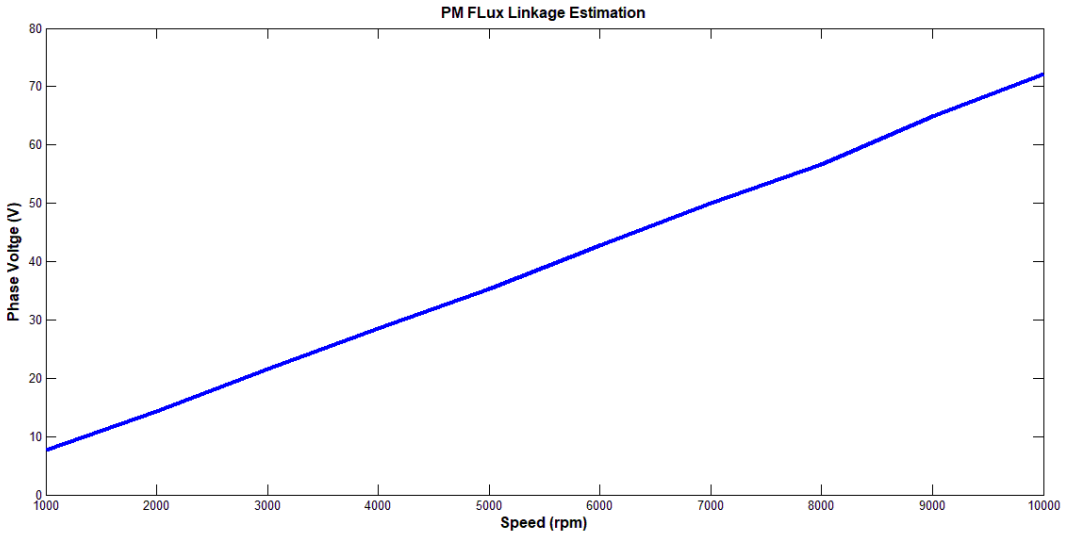

Fig. 8.8 PM flux linkage estimation

9. Conclusions

This dissertation has reviewed and discussed the use and applications of HS machines in the literature and discussed the analytical design of HS PM machines in particular. There are four machine topologies commonly used for HS applications: the PM machine, IM, SRM, and synchronous homopolar machine. Among these four, the PM machine has been extensively used for HS applications in various industries such as automotive, aerospace, etc. and is therefore the best-suited topology for the HS application relating to this project. PM machines have various advantages over the other HS topologies such as their compact structure, lightweight, high efficiency, and reliability. These advantages mean that PM machines are now increasingly used in various HS applications as discussed in chapter 2.

The two most common PM topologies that are used in HS machines are the surface permanent magnet (SPM) and the interior permanent magnet (IPM) machines. These have been designed and used extensively in the literature in varying speeds and applications. Due to its widespread use and advantages over the SPM such as better field weakening and a more reliable structure, the IPM topology was selected for further investigation in this project.

Two IPM topologies, a radial IPM and a circumferential IPM, were designed, simulated, and compared against each other. The general sizing and design equations for PM machines were first used to obtain a general realisation of the machines. These equations were developed from first principles and have been extensively used in the literature. Once the overall machine was sized, detailed analytical design equations were used to obtain a more complete design for the IPM machines. FEA was then used to fine-tune these designs and make subtle changes in order to obtain as close to optimal designs as possible. There were some design constraints that the two machines had to adhere to, such as the rotor diameter, stack length, air gap length, and stator outer diameter. These parameters were kept identical for both machines while other parameters like the magnet volume and winding design were different for the machines so as to maximise their potential by choosing the most optimum design for each machine.

From the FEA results, the circumferential IPM produced a better output torque compared to the radial IPM, but also produced a much larger torque ripple. The circumferential IPM also produced a larger output power compared to the radial IPM. The circumferential IPM has a larger saliency ratio which means it produces a larger reluctance torque which results in a larger output torque compared to the radial IPM. However, the circumferential IPM also produced a much higher core loss compared to the radial IPM, which also meant that it had a lower efficiency. Furthermore, the manufacturing process of the circumferential IPM is quite complex and thus also expensive when compared to the radial IPM process and cost. Therefore, considering all the results and factors, the radial IPM performed better than the circumferential IPM and would be the better suited machine for a HS application.

A HS test rig was also developed to test the IPM experimentally and compare the results with the analytical and FEA results. Since the scope of the dissertation did not include testing the IPMs experimentally, the development of the test rig and subsequent testing of the IPMs was considered as an additional item out of the scope of the dissertation. There were many challenges experienced during the development of the test rig such as selection of an appropriate drive motor, torque transducer, encoder, lubrication system, and cooling system. The cost of developing the test rig to the full specifications of 30,000 rpm were seen as too high, given that this was out of the scope in the first place, as there were various mechanical considerations that needed to be made and extra protection and equipment purchased before the test rig could run up to the full specifications. As a result, it was decided to develop the test rig for operation up to a maximum speed of 10,000 rpm which is still considered as HS in literature.

Given that one of the design requirements was that the machines should have a low torque ripple and core loss, it was decided to prototype the radial IPM which produced better results overall and was also less expensive to manufacture. The machine was tested under no-load conditions in order to confirm the basic operation and characteristics of the machine. The no-load results produced showed that the overall design is valid and successfully meets the design requirements. The theoretical, FEA, and no-load experimental results are also compared and it is shown that these results correlate to each other, thus confirming that the design is valid.

10. Recommendations

Based on the conclusions presented in chapter 10, the following recommendations can be made to improve on the work conducted in this dissertation and areas of potential work for the future:

1. The v-shaped IPM possesses various advantages over the radial and circumferential IPMs, and investigating this topology as an additional possibility for a similar output requirement would open up further areas and possibilities for comparison between the three main IPM topologies
2. Some of the design parameters were kept identical for both machines due to design constraints. Varying these parameters would further result in possibly a more optimum design for both machines. Varying parameters such as the rotor and stator diameter will allow for more designs that may not have been considered under the current restrictions
3. Additional components could be added to the test-rig to increase its capabilities to operate at 30,000 rpm. This would require a new drive motor and additional mechanical equipment which could be part of a new project. It is important as a final check to operate the IPM at full speed and analyse the results obtained and compare them with the FEA results. Furthermore, there may be some interesting observations made when running the machine at this speed that would result in further possibilities for future investigations
4. The circumferential IPM could be prototyped and experimentally tested. This will allow for a more direct comparison between the radial and circumferential IPM and will allow for further comparisons to be made
5. As potential future work, investigating the core losses for the machines in detail would result in a thorough piece of research. Core losses are a critical aspect for HS machines, and they have been monitored and only basic methodologies have been used to minimise these losses in this dissertation. There are various other methods mentioned in this thesis that if implemented would result in lower core losses

11. List of References

[1] R. R. Moghaddam, “High speed operation of electrical machines, a review on technology, benefits and challenges,” in *2014 IEEE Energy Conversion Congress and Exposition, ECCE 2014*, 2014, no. mm, pp. 5539–5546.

[2] Z. Kolondzovski, “Thermal and Mechanical Analysis of High-Speed Permanent-Magnet Electrical Machines,” Aalto University, School of Science and Technology, 2010.

[3] S. Wu, L. Tian, and S. Cui, “A comparative study of the interior permanent magnet electrical machine’s rotor configurations for a single shaft hybrid electric bus,” *2008 IEEE Veh. Power Propuls. Conf. VPPC 2008*, pp. 3–6, 2008.

[4] S. Safi, C. Eng, C. Specialist, and S. D. T. D. Technology, “High Speed Machines Drive Technology Forward,” no. March, 2014.

[5] Y. Hu, T. Wu, L. Chow, Y. Bai, and W. Wu, “Design of a 3kW 150k RPM super high-speed permanent magnet synchronous motor,” in *Proceedings - 2014 International Conference on Electrical Machines, ICEM 2014*, 2014, pp. 2543–2548.

[6] D. Gerada *et al.*, “High-Speed Electrical Machines: Technologies , Trends , and Developments,” *IEEE Trans. Ind. Electron.*, vol. 61, no. 6, pp. 2946–2959, 2014.

[7] R. D. Van Millingen, C. Eng, and J. D. Van Millingen, “Phase Shift Torquemeters for Gas Turbine Development and Monitoring,” in *International Gas Turbine and Aeroengine Congress and Exposition*, 1991, pp. 1–10.

[8] H. Drive, P. Tsao, M. Senesky, S. Member, and S. R. Sanders, “An Integrated Flywheel Energy Storage System With Homopolar Inductor Motor / Generator,” *IEEE Trans. Ind. Appl.*, vol. 39, no. 6, pp. 1710–1725, 2003.

[9] K. Y. Bell and S. Abel, “Optimization of WWTP aeration process upgrades for energy efficiency,” *Water Pract. Technol.*, vol. 6, no. 2, 2011.

[10] M. J. Provost, “The More Electric Aero-engine: a general overview from an engine manufacturer,” *Int. Conf. Power Electron. Mach. Drives*, vol. 2002, pp. 246–251, 2002.

[11] J. B. Bartolo, D. Gerada, L. De Lillo, and C. Gerada, “High speed electrical generators, application, materials and design,” *2013 IEEE Work. Electr. Mach. Des. Control Diagnosis*, pp. 47–59, Mar. 2013.

[12] S. Z. Vijlee, A. Ouroua, L. N. Domaschk, J. H. Beno, and A. Ouroua, “Directly-coupled gas turbine permanent magnet generator sets for prime power generation on board electric ships,” in *IEEE Electric Ship Technologies Symposium, ESTS 2007*, 2007, pp. 340–347.

[13] K. Senda, M. Namikawa, and Y. Hayakawa, “Electrical Steels for Advanced Automobiles — Core Materials for Motors , Generators , and High-Frequency Reactors,” *JFE Tech. Rep.*, vol. 4, no. 4, pp. 67–73, 2004.

[14] S. Consantinides, “Rare Earth Elements in Transportation,” Montreal, Canada, 2013.

[15] “Cuponal™: Co-Extruded Copper-Clad Aluminium Conductors.” [Online]. Available: https://www.bruker.com/products/superconductors-and-metal-composite-materials/cuponal.html.

[16] P. H. Mellor, S. G. Burrow, T. Sawata, and M. Holme, “A wide-speed-range hybrid variable-reluctance/permanent-magnet generator for future embedded aircraft generation systems,” *IEEE Trans. Ind. Appl.*, vol. 41, no. 2, pp. 551–556, 2005.

[17] A. Binder and T. Schneider, “High-speed inverter-fed AC drives,” *2007 Int. Aegean Conf. Electr. Mach. Power Electron.*, pp. 9–16, Sep. 2007.

[18] M. a. Rahman, a. Chiba, and T. Fukao, “Super high speed electrical machines - summary,” *IEEE Power Eng. Soc. Gen. Meet. 2004.*, vol. 1, no. iii, pp. 1–4, 2004.

[19] J. Driesen and R. Belmans, “Specific problems of high-speed electrical drives,” *RTO/AVT/VKI Lect. Ser. Micro Gasturnes*, pp. 1–16, 2005.

[20] A. Boglietti, P. Ferraris, M. Lazzari, and F. Profumo, “About the design of very high frequency induction motors for spindle applications,” *Conf. Rec. - IAS Annu. Meet. (IEEE Ind. Appl. Soc.*, vol. 1992–Janua, pp. 25–32, 1992.

[21] A. Looser and J. W. Kolar, “A hybrid bearing concept for high-speed applications employing aerodynamic gas-bearings and a self-sensing active magnetic damper,” in *IECON Proceedings (Industrial Electronics Conference)*, 2011, pp. 1686–1691.

[22] S. Li, Y. Li, W. Choi, S. Members, and B. Sarlioglu, “High Speed Electric Machines – Challenges and Design Considerations,” *Int. Conf. Electr. Mach.*, pp. 2537–2543, 2014.

[23] A. Borisavljević and A. Borisavljevi, *Limits, Modeling and Design of High-Speed Permanent Magnet Machines*. 2011.

[24] H. Mitterhofer, D. Andessner, and W. Amrhein, “Analytical and experimental loss examination of a high speed bearingless drive,” in *SPEEDAM 2012 - 21st International Symposium on Power Electronics, Electrical Drives, Automation and Motion*, 2012, pp. 146–151.

[25] K. V. Rodrigues, J. F. Pradurat, N. Barras, and E. Thibaut, “Design of high-speed induction motors and associate inverter for direct drive of centrifugal machines,” *Proc. 2008 Int. Conf. Electr. Mach. ICEM’08*, pp. 1–5, 2008.

[26] N. Bianchi, S. Bolognani, and F. Luise, “High speed drive using a slotless PM motor,” *PESC Rec. - IEEE Annu. Power Electron. Spec. Conf.*, vol. 1, no. 4, pp. 458–463, 2004.

[27] G. Munteanu, a. Binder, and T. Schneider, “Development and test of high-speed bearingless PM synchronous machines,” *e i Elektrotechnik und Informationstechnik*, vol. 128, no. 3, pp. 75–80, Mar. 2011.

[28] K. Bennion, “Electric Motor Thermal Management R & D,” 2016.

[29] J. F. Gieras, *Advancements in Electric Machines*, 1st ed. Dordrecht: Springer Netherlands, 2008.

[30] P. B. Reddy, T. M. Jahns, and T. P. Bohn, “Modeling and analysis of proximity losses in high-speed

surface permanent magnet machines with concentrated windings," *2010 IEEE Energy Convers. Congr. Expo. ECCE 2010 - Proc.*, pp. 996–1003, 2010.

[31] P. B. Reddy, T. M. Jahns, and T. P. Bohn, "Transposition effects on bundle proximity losses in high-speed PM machines," *2009 IEEE Energy Convers. Congr. Expo. ECCE 2009*, no. 1, pp. 1919–1926, 2009.

[32] P. B. Reddy and T. M. Jahns, "Scalability investigation of proximity losses in fractional-slot concentrated winding surface PM machines during high-speed operation," *IEEE Energy Convers. Congr. Expo. Energy Convers. Innov. a Clean Energy Futur. ECCE 2011, Proc.*, no. 1, pp. 1670–1675, 2011.

[33] M. Etemadrezaei, J. J. Wolmarans, H. Polinder, and J. A. Ferreira, "Precise calculation and optimization of rotor eddy current losses in high speed permanent magnet machine," *Proc. - 2012 20th Int. Conf. Electr. Mach. ICEM 2012*, pp. 1399–1404, 2012.

[34] M. Dems and K. Komeza, "Performance Characteristics of a High-Speed Energy-Saving Induction Motor with an Amorphous Stator Core," *IEEE Trans. Ind. Electron.*, vol. 61, no. 6, pp. 3046–3055, 2014.

[35] W. Li, H. Qiu, X. Zhang, J. Cao, and R. Yi, "Analyses on electromagnetic and temperature fields of superhigh-speed permanent-magnet generator with different sleeve materials," *IEEE Trans. Ind. Electron.*, vol. 61, no. 6, pp. 3056–3063, 2014.

[36] J. Lähteenmäki, "Design and Voltage Supply of High-Speed Induction Machines," Helsinki University of Technology, 2002.

[37] R. Bumby, E. Spooner, and M. Jagiela, "Solid Rotor Induction Machines for use in Electrically-Assisted Turbochargers," in *Power Electronics, Machines and Drives, 2006. The 3rd IET International Conference*, 2006, pp. 341–345.

[38] J. Pyrhonen, J. Nerg, P. Kurronen, and U. Lauber, "High-Speed High-Output Solid-Rotor Induction-Motor Technology for Gas Compression," *IEEE Trans. Ind. Electron.*, vol. 57, no. 1, pp. 272–280, 2010.

[39] N. D. Sharma, R. Anbarasu, J. Nataraj, A. Y. Dangore, and B. Bhattacharjee, "Experimental investigations on high speed solid and composite rotor induction motor," *Proc. Int. Conf. Power Electron. Drives Energy Syst. Ind. Growth*, vol. 2, pp. 913–919, 1996.

[40] M. Centner and U. Schäfer, "Optimized design of high-speed induction motors in respect of the electrical steel grade," *IEEE Trans. Ind. Electron.*, vol. 57, no. 1, pp. 288–295, 2010.

[41] D. Gerada, A. Mebarki, N. L. Brown, H. Zhang, and C. Gerada, "Design , Modelling and Testing of a High Speed Induction Machine Drive," *Energy Convers. Congr. Expo.*, pp. 4649–4655, 2012.

[42] K. Wang, M. J. Jin, J. X. Shen, and H. Hao, "Study on rotor structure with different magnet assembly in high-speed sensorless brushless DC motors," *IET Electr. Power Appl.*, vol. 4, no. 4, p. 241, 2010.

[43] C. Zwyssig, J. W. Kolar, W. Thaler, and M. Vohrer, "Design of a 100 W, 500000 rpm permanent-magnet generator for mesoscale gas turbines," in *Fourtieth IAS Annual Meeting. Conference Record of the 2005 Industry Applications Conference, 2005.*, 2005, vol. 1, no. Im, pp. 253–260.

[44] I. Takahashi, G. Su, T. Koganezawa, and K. Ohyama, "Super high speed PM motor drive system by a

quasi-current source inverter," *IEEE Trans. Ind. Appl.*, vol. 30, no. 3, pp. 683–690, 1994.

[45] A. Binder, T. Schneider, and M. Klohr, "Fixation of buried and surface-mounted magnets in high-speed permanent-magnet synchronous machines," *IEEE Trans. Ind. Appl.*, vol. 42, no. 4, pp. 1031–1037, Jul. 2006.

[46] C. Zwyssig, J. W. Kolar, and S. D. Round, "Megaspeed drive systems: Pushing beyond 1 million r/min," *IEEE/ASME Trans. Mechatronics*, vol. 14, no. 5, pp. 564–574, 2009.

[47] A. Boglietti, A. Cavagnino, A. Tenconi, and S. Vaschetto, "Key design aspects of electrical machines for high-speed spindle applications," *IECON Proc. (Industrial Electron. Conf.*, pp. 1735–1740, 2010.

[48] D. Gerada, D. Borg-Bartolo, A. Mebarki, C. Micallef, N. L. Brown, and C. Gerada, "Electrical machines for high speed applications with a wide constant-power region requirement," in *2011 International Conference on Electrical Machines and Systems*, 2011, pp. 1–6.

[49] S.-M. Jang, H.-W. Cho, S.-H. Lee, H.-S. Yang, and Y.-H. Jeong, "The Influence of Magnetization Pattern on the Rotor Losses of Permanent Magnet High-Speed Machines," *IEEE Trans. Magn.*, vol. 40, no. 4, pp. 2062–2064, Jul. 2004.

[50] Z. Q. Zhu, K. Ng, and D. Howe, "Design and Analysis of High Speed Brushless Permanent maget Motors," *EMD97 Conf. Publ.*, no. 444, pp. 381–385, 1997.

[51] W. Kakihara, "Rotor Structure in 50 kW Spoke-Type Interior Permanent Magnet Synchronous Motor with Ferrite Permanent Magnets for Automotive Applications," vol. 2, 2013.

[52] R. Dutta and M. F. Rahman, "Design and analysis of an Interior Permanent Magnet (IPM) machine with very wide constant power operation range," *IECON Proc. (Industrial Electron. Conf.*, vol. 23, no. 1, pp. 1375–1380, 2006.

[53] G. Pellegrino, A. Vagati, P. Guglielmi, and B. Boazzo, "Performance comparison between surface-mounted and interior PM motor drives for electric vehicle application," *IEEE Trans. Ind. Electron.*, vol. 59, no. 2, pp. 803–811, 2012.

[54] A. M. El-Refaie and T. M. Jahns, "Comparison of synchronous PM machine types for wide constant-power speed range operation," *Conf. Rec. - IAS Annu. Meet. (IEEE Ind. Appl. Soc.*, vol. 2, pp. 1015–1022, 2005.

[55] A. M. EL-Refaie, "Fractional-slot concentrated-windings synchronous permanent magnet machines: Opportunities and challenges," *IEEE Trans. Ind. Electron.*, vol. 57, no. 1, pp. 107–121, 2010.

[56] A. Wang, Y. Jia, and W. L. Soong, "Comparison of five topologies for an interior permanent-magnet machine for a hybrid electric vehicle," *IEEE Trans. Magn.*, vol. 47, no. 10, pp. 3606–3609, 2011.

[57] E. Spooner and A. C. Williamson, "Direct coupled, permanent magnet generators for wind turbine applications," *IEE Proc. - Electr. Power Appl.*, vol. 143, no. 1, p. 1, 1996.

[58] D. C. Hanselman, *Brushless permanent magnet motor design*. 2006.

[59] J. R. Hendershot and T. J. E. Miller, *Design of Brushless Permanent- Magnet Motors*. Ohio: Magna Physics, 1994.

[60] A. Vagati, G. Pellegrino, and P. Guglielmi, “Comparison between SPM and IPM motor drives for EV application,” in *The XIX International Conference on Electrical Machines - ICEM 2010*, 2010, pp. 1–6.

[61] J. Dong, Y. Huang, L. Jin, and H. Lin, “Comparative Study of Surface-Mounted and Interior Permanent-Magnet Motors for High-Speed Applications,” *IEEE Trans. Appl. Supercond.*, vol. 26, no. 4, pp. 4–7, 2016.

[62] Y. . Chin, W. . Arshad, T. Backstrom, and C. Sadarangani, “Design of a compact BLDC motor for transient applications,” in *IEEE Electric Machines and Drive Conference, IEMDC,* 2001, pp. 743–747.

[63] Y. Kano and N. Matsui, “A Design Approach for Direct-Drive Permanent-Magnet Motors,” *IEEE Trans. Ind. Appl.*, vol. 44, no. 2, pp. 543–554, 2008.

[64] J. E. Rucker, “Design and Analysis of a Permanent Magnet Generator for Naval Applications,” Massachusetts Institute of Technology, 2005.

[65] N. Bianchi, “Permanent magnet generators for wind power industry: an overall comparison with traditional generators,” in *International Conference on Opportunities and Advances in International Power Generation*, 1996, vol. 1996, pp. 49–54.

[66] J. J. H. Paulides, G. W. Jewell, and D. Howe, “An Evaluation of Alternative Stator Lamination Materials for a High-Speed, 1.5 MW, Permanent Magnet Generator,” *IEEE Trans. Magn.*, vol. 40, no. 4, pp. 2041–2043, Jul. 2004.

[67] P. Curiac, D. H. Kang, Y. H. Jeong, and S. J. Jung, “Prospects for magnetization of large PM rotors: conclusions from a development case study,” in *2003 IEEE Power Engineering Society General Meeting (IEEE Cat. No.03CH37491)*, pp. 1901–1901.

[68] N. Madani, “Design of a Permanent Magnet Synchronous Generator for a Vertical Axis Wind Turbine,” Royal Institute of Technology, Sweden, 2011.

[69] F. Magnussen, “Performance evaluation of permanent magnet synchronous machines with concentrated and distributed windings including the effect of field-weakening,” in *Second IEE International Conference on Power Electronics, Machines and Drives*, 2004, vol. 2004, pp. v2-679-v2-679.

[70] F. Magnussen, “On design and analysis of synchronous permanent magnet machines for field weakening operation in hybrid electric vehicles,” Royal Institute of technology, Sweden, 2004.

[71] “Litz Wire Applications and Specifications.” [Online]. Available: http://www.litz-wire.com/applications.php.

[72] M. R. Islam, “Cogging torque, torque ripple and radial force analysis of permanent magnet synchronous machines,” The University of Akron, 2009.

[73] N. Bianchi and S. Bolognani, “Design techniques for reducing the cogging torque in surface-mounted PM motors,” *IEEE Trans. Ind. Appl.*, vol. 38, no. 5, pp. 1259–1265, Sep. 2002.

[74] S. M. Hwang and D. K. Lieu, “Reduction of torque ripple in brushless DC motors,” *IEEE Trans. Magn.*, vol. 31, no. 6, pp. 3737–3739, 1995.

[75] Sang-Moon Hwang, Jae-Boo Eom, Yoong-Ho Jung, Deug-Woo Lee, and Beom-Soo Kang, "Various design techniques to reduce cogging torque by controlling energy variation in permanent magnet motors," *IEEE Trans. Magn.*, vol. 37, no. 4, pp. 2806–2809, Jul. 2001.

[76] V. Petrovic, R. Ortega, A. M. Stankovic, and G. Tadmor, "Design and implementation of an adaptive controller for torque ripple minimization in PM synchronous motors," *IEEE Trans. Power Electron.*, vol. 15, no. 5, pp. 871–880, 2000.

[77] C. Breton *et al.*, "Influence of machine symmetry on reduction of cogging torque in permanent-magnet brushless motors," *IEEE Trans. Magn.*, vol. 36, no. 5, pp. 3819–3823, 2000.

[78] S. Huang, M. Aydin, and T. A. Lipo, "Electromagnetic vibration and noise assessment for surface mounted PM machines," in *2001 Power Engineering Society Summer Meeting. Conference Proceedings (Cat. No.01CH37262)*, 2001, pp. 1417–1426 vol.3.

[79] Z. Q. Zhu, D. Ishak, D. Howe, and J. Chen, "Unbalanced Magnetic Forces in Permanent-Magnet Brushless Machines With Diametrically Asymmetric Phase Windings," *IEEE Trans. Ind. Appl.*, vol. 43, no. 6, pp. 1544–1553, 2007.

[80] G.-D. Lee, G.-T. Kim, H.-K. Shin, and C.-J. Kim, "The optimum design of interior permanent magnet synchronous motor for the vibration reduction," in *2015 18th International Conference on Electrical Machines and Systems (ICEMS)*, 2015, pp. 227–231.

[81] J. F. Gieras, C. Wang, and J. C. Lai, *Noise of Polyphase Electric Motors*, 1st Editio. Boca Raton: CRC Press, 2005.

[82] R. Dutta and M. F. Rahman, "Comparison of Core Loss Prediction Methods for the Interior Permanent Magnet Machine," *2005 Int. Conf. Power Electron. Drives Syst.*, vol. 2, pp. 1396–1401, 2005.

[83] M. Kalyan and M. A. Khan, "Review of High Speed Machines: Topologies, Materials, and Challenges," in *25th Southern African Universities Power Engineering Conference*, 2017.

[84] T. J. E. Miller, *Brushless Permanent-Magnet and Reluctance Motor Drives (Monographs in Electrical and Electronic Engineering 21)*, no. 21. 1989.

[85] L. Marino, "Design and Analysis of a PM-Assisted Reluctance Motor," 2015.

[86] S. Lee, "Development and Analysis of Interior Permanent Magnet Synchronous Motor with Field Excitation Structure_Thesis," *Dr. Diss.*, 2009.

[87] S. Lee, "Development and Analysis of Interior Permanent Magnet Synchronous Motor with Field Excitation Structure," *Dr. Diss.*, 2009.

[88] S. F. Rabbi, P. Zhou, and M. A. Rahman, "Design and Performance Analysis of a Self-Start Radial Flux-Hysteresis Interior Permanent Magnet Motor," *IEEE Trans. Magn.*, vol. 53, no. 11, pp. 1–4, Nov. 2017.

[89] F. Charih, F. Dubas, C. Espanet, and D. Chamagne, "Performances comparison of PM machines with different rotor topologies and similar slot and pole numbers," in *International Symposium on Power Electronics Power Electronics, Electrical Drives, Automation and Motion*, 2012, pp. 56–59.

[90] "Parker Homepage." [Online]. Available:

http://www.parker.com/portal/site/PARKER/menuitem.223a4a3cce02eb6315731910237ad1ca/?vgnextoid=4746ce74fa65e210VgnVCM10000048021dacRCRD&vgnextfmt=EN.

[91] “Elexsys Homepage.” [Online]. Available: https://www.elexsys.co.za/.

12. Appendices

12.1 Appendix A – Test rig details

Figures 12.1 – 12.4 show some detailed mechanical drawings for the radial IPM which were developed for the prototyping process.

LORENZ MESSTECHNIK GmbH
Obere Schloßstr.131
73553 Alfdorf
☎ 07172 /93730-0
Fax 07172 /93730-22

Technische Daten - *Specifications*

Artikel-Nr. *Article-No.* DR-2643	Artikel-Nr. *Article-No.* DR-2643-P[1]	Nenndrehmoment *Nominal Torque* [N·m]	Grenzdrehzahl *Limit Speed* [min^{-1}]	Federkonstante *Springrate* [N·m/rad]	Massen-trägheits-moment *Mass Moment of Inertia* [kg·m^2][2]		Grenzlängskraft *Limit Thrust Load* [N][3]	Grenzquerkraft *Limit Shear Force* [N][4]
					Antriebsseite *Drive Side*	Messseite *Test Side*		
114347	115669	0,1	30000	1,8E+01	9,2E-06	2,5E-07	43	1,5
114348	115670	0,2	30000	1,8E+01	9,2E-06	2,5E-07	58	2
112805	115671	0,5	30000	9,4E+01	9,2E-06	2,5E-07	240	3
112804	115672	1	30000	9,4E+01	9,2E-06	2,5E-07	240	3
112593	115673	2	30000	3,7E+02	9,2E-06	2,5E-07	480	7
112381	115674	5	30000	7,7E+02	9,2E-06	2,6E-07	900	16,5
112806	115675	10	30000	8,8E+02	9,3E-06	3,4E-07	1050	21
112447	115676	20	20000	5,1E+03	1,2E-04	6,8E-06	2300	44
107403	115677	30	20000	5,1E+03	1,2E-04	6,8E-06	2300	44
112807	115678	50	20000	9,6E+03	1,2E-04	7,4E-06	5000	142
112808	115679	100	20000	9,6E+03	1,2E-04	7,4E-06	5000	142
112810	114085	200	15000	8,9E+04	5,4E-04	4,4E-04	10000	275
112811	114538	500	15000	1,3E+05	5,4E-04	4,4E-04	13000	400
112812	115680	1000	15000	1,7E+05	6,4E-04	5,3E-04	20000	920
112814	115681	2000	12000	6,3E+05	5,7E-03	5,1E-03	34000	1250
112816	115682	5000	12000	9,6E+05	5,8E-03	5,2E-03	64000	2900

		DR-2643, DR-2643-P
Genauigkeitsklasse - *Accuracy class*	% v. E. - *f. s.*	0,1
Reproduzierbarkeit - *Repeatability* (DIN 1319)	%	±0,02
Versorgung - *Supply voltage*	VDC	12 ... 28
Stromaufnahme - *Current consumption*	mA	≤60
Ausgangssignal - *Output signal*		±5V
Kontrollsignalaufschaltung - *Control signal excitation*	V	L <2,0; H >3,5
Messrate - *Sample rate*	kSample/s	10
Referenztemperatur - *Reference temperature*	°C	23
Nenntemperaturbereich - *Nominal temperature range*	°C	5 ... 45
Gebrauchstemperaturbereich - *Service temperature range*	°C	0 ... 60
Lagerungstemperaturbereich - *Storage temperature range*	°C	-10 ... 70
Temp. koeff. des Kennwertes - *Temp. coeff. of sensitivity*	% v. E./K - *f. s./K*	±0,01
Temp. koeff. des Nullsignals - *Temp. coeff. of zero signal*	% v. E./K - *f. s./K*	±0,02
Gebrauchsdrehmoment (statisch) - *Service torque (static)*	% v. E. - *f. s.*	150
Grenzdrehmoment (statisch) - *Limit torque (static)*	% v. E. - *f. s.*	200
Bruchdrehmoment (statisch) - *Ultimate torque (static)*	% v. E. - *f. s.*	>300
Schwingbreite - *Bandwidth* (DIN 50100)	%	70 (Spitze - Spitze) - *(peak - peak)*
Schutzart - *Level of protection* (DIN EN 60529)		IP50
Elektrischer Anschluss - *Electrical connection*		12-polig Serie 581 – *12-pin series 581*[5]

Fig. 12.1 Torque transducer data sheet (1/2)

LORENZ MESSTECHNIK GmbH
Obere Schloßstr.131 ☎ 07172 /93730-0
73553 Alfdorf Fax 07172 /93730-22

Anschlussbelegung - *Pin Connection*

12-polig - *12-pin*	DR-2643, DR-2643-P		
Pin A	NC	-	
Pin B	Opt. Signal Winkel B - *Opt. Signal angle B*	5V TTL	
Pin C	Signal (+) - *Signal (+)*	±5V (±10V)	
Pin D	Signal (GND) - *Signal (GND)*	0V	
Pin E	Vers. (GND) - *Supply (GND)*	0V	
Pin F	Vers. (+) - *Supply (+)*	12 ... 28VDC	
Pin G	Opt. Signal Winkel A - *Opt. Signal angle A*	5V TTL	
Pin H	NC	-	
Pin J	NC	-	
Pin K	Kontrollsignal - *Control signal*	L <2,0V; H >3,5V	
Pin L	NC	-	
Pin M	Schirm - *Shield*		

Serie - Series 581

Draufsicht - *Top view*

Optionen/ Zubehör - *Options/ Accessories*

Artikel-Nr. - *Article-No.*	Bezeichnung - *Description*		
101695	Genauigkeitsklasse - *Accuracy class*	% v. E - *f. s.*	0,05
103562	Ausgangssignal - *Output signal*	V	±10
101560	Drehzahl-/Drehwinkelmessung, 2 x 360 Impulse, 90° versetzt, 5V TTL - *Speed/angle measurement, 2 x 360 impulses, 90° displaced, 5V TTL*		Rechtsdrehung - CW-turn 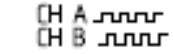
41382	Kabeldose 12-polig Serie 581 - *Female cable connector 12-pin series 581*		
45598	Winkeldose 12-polig Serie 682 - *Female angled connector 12-pin series 682*		
10270	Anschlusskabel, 3 m, mit 12-pol. Kabeldose Serie 581 und freien Lötenden - *Connection cable, 3 m, with 12-pin female cable connector series 581 and free soldered ends*		
10345	Anschlusskabel winklig, 3 m, mit 12-pol. Kabeldose Serie 682 und freien Lötenden - *Connection cable angled, 3 m, with 12-pin female cable connector series 682 and free soldered ends*		

Option Kalibrierungen - *Option Calibrations*

Artikel-Nr. - *Article-No.*	Bezeichnung - *Description*	Stufen - *Steps*	Norm - *Norm*
400676	Linearitätsdiagramm - *Linearity diagram*	25%	Werksnorm - *Factory standard*
400664	Linearitätsdiagramm - *Linearity diagram*	10%	
400961	Werkskalibrierung - *Proprietary calibration*	3	VDI/VDE 2646
400700	Werkskalibrierung - *Proprietary calibration*	5	
400688	Werkskalibrierung - *Proprietary calibration*	8	
	DAkkS-Kalibrierung - *DAkkS-Calibration*		auf Anfrage - *on request*

Fig. 12.2 Torque transducer data sheet (2/2)

RM22I – Incremental outputs

Square wave differential line driver to RS422A

Power supply	V_{dd} = 5 V ± 5%
Power consumption	23 mA for 9 bit resolution 35 mA for all other resolutions
Output signals	A, B, Z, A-, B-, Z- (RS422A)
Max. cable length	50 m
Connector options	9 pin 'D' type plug (standard) Flying lead
Temperature	Operating -25 °C to +85 °C (-40 °C to +125 °C option 08)*
	Storage -40 °C to +125 °C
Edge separation	Min. 1 µs

* Only available with IP68 sealing

Resolution options (counts per rev)	Maximum speed (rpm)	Accuracy*	Hysteresis
200, 400, 500	30,000	±0.7°	0.18°
512	30,000	±0.7°	0.45°
800, 1,000, 1,024	20,000	±0.5°	0.18°
1,600, 2,000, 2,048	10,000	±0.5°	0.18°
4,096	5,000	±0.5°	0.18°
8,192	2,500	±0.5°	0.18°

* Worst case within operational parameters including magnet position and temperature

Timing diagram

(complementary signals not shown)

Recommended signal termination

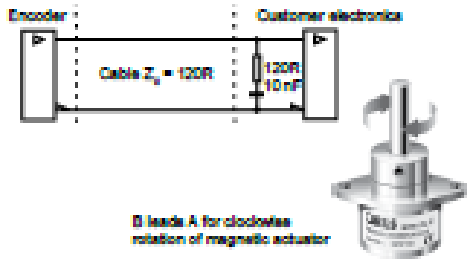

RM22S – Absolute binary synchro-serial interface (SSI)

Serial encoded absolute position measurement

Output code	Natural binary
Power supply	V_{dd} = 5 V ± 5%
Power consumption	23 mA for 9 bit resolution 35 mA for all other resolutions
Repeatability	≤ 0.07°
Data outputs	Serial data (RS422A)
Data inputs	Clock (RS422A)
Max. cable length	100 m (at 1 MHz)
Connector options	9 pin 'D' type plug (standard) Flying lead
Temperature	Operating -40 °C to +125 °C (IP64) -40 °C to +85 °C (IP68)
	Storage -40 °C to +85 °C

Resolution options (positions per rev)	Maximum speed (rpm)	Accuracy*	Hysteresis
200, 400, 500	30,000	±0.7°	0.18°
512	30,000	±0.7°	0.45°
800, 1,000, 1,024	20,000	±0.5°	0.18°
1,600, 2,000, 2,048	10,000	±0.5°	0.18°
4,096	5,000	±0.5°	0.18°
8,192	2,500	±0.5°	0.18°

* Worst case within operational parameters including magnet position and temperature

Timing diagram

Clock ≤ 900 kHz: 16 µs ≤ t_m ≤ 22 µs (for 9 bit resolution)
Clock ≤ 4 MHz: 12.5 µs ≤ t_m ≤ 20.5 µs (for all other resolutions)

Recommended signal termination

(For data output lines only)

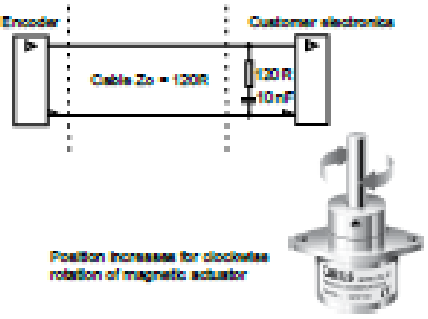

A RENISHAW associate company

Fig. 12.3 Encoder data sheet (1/2)

RM22P – Absolute binary parallel interface

Parallel absolute position measurement

Output code	Natural binary	
Power supply	V_{dd} = 5 V ± 5%	
Power consumption	20 mA without load	
Output voltage	$V_o \geq 4$ V at $-I_o \leq 3$ mA $V_o \leq 1$ V at $I_o \leq 3$ mA	
Resolution	9 bit (512 positions per revolution)	
Hysteresis	0.45°	
Accuracy	±0.7°	
Repeatability	≤ 0.07°	
Data outputs	D0 (LSB) - D8 (MSB)	
Data inputs	LE - latch enable input signal, active high Maximum sampling rate 500 kHz	
Max. cable length	30 m	
Connector options	15 pin 'D' type plug (standard) Flying lead	
Temperature	Operating	-40 °C to +125 °C (IP64)
		-40 °C to +85 °C (IP68)
	Storage	-40 °C to +85 °C
Maximum speed	30,000 rpm	

Timing diagram

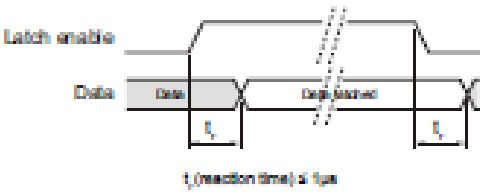

t_r (reaction time) ≤ 1µs

Position increases for clockwise rotation of magnetic actuator

RM22V – Linear voltage output

Power supply	V_{dd} = 5 V ± 5%	
Power consumption	20 mA typical	
Output voltage	0 V to V_{dd}	
Output loading	Max. 10 mA	
Nonlinearity	1 %	
Max. cable length	20 m	
Connector options	9 pin 'D' type plug (standard) Flying lead	
Temperature	Operating	-40 °C to +125 °C (IP64)
		-40 °C to +85 °C (IP68)
	Storage	-40 °C to +85 °C
Maximum speed	30,000 rpm	

Electrical output/shaft position

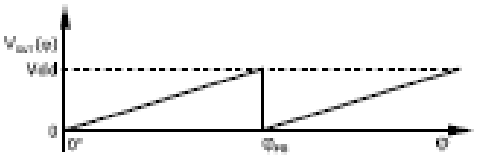

Output type and electrical variant

Φ_{FS}	360°	180°	90°	45°
CW	VA	VB	VC	VD
CCW	VE	VF	VG	VH

Image shows clockwise rotation of magnetic actuator

A RENISHAW associate company

Fig. 12.4 Encoder data sheet (2/2)

12.2 Appendix B – Detailed mechanical drawings

Figures 12.1 – 12.4 show some detailed mechanical drawings for the radial IPM which were developed for the prototyping process.

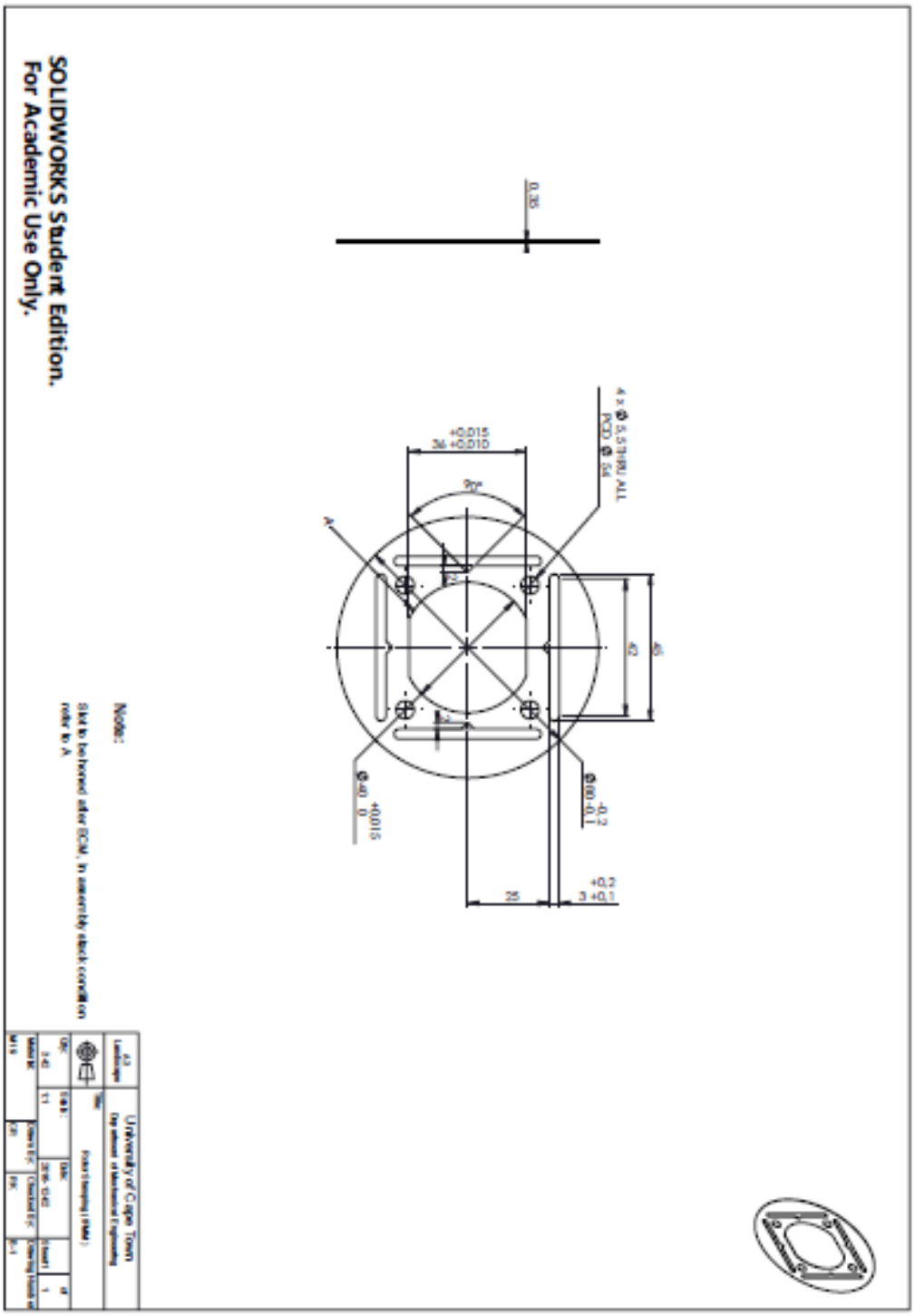

Fig. 12.5 Rotor lamination

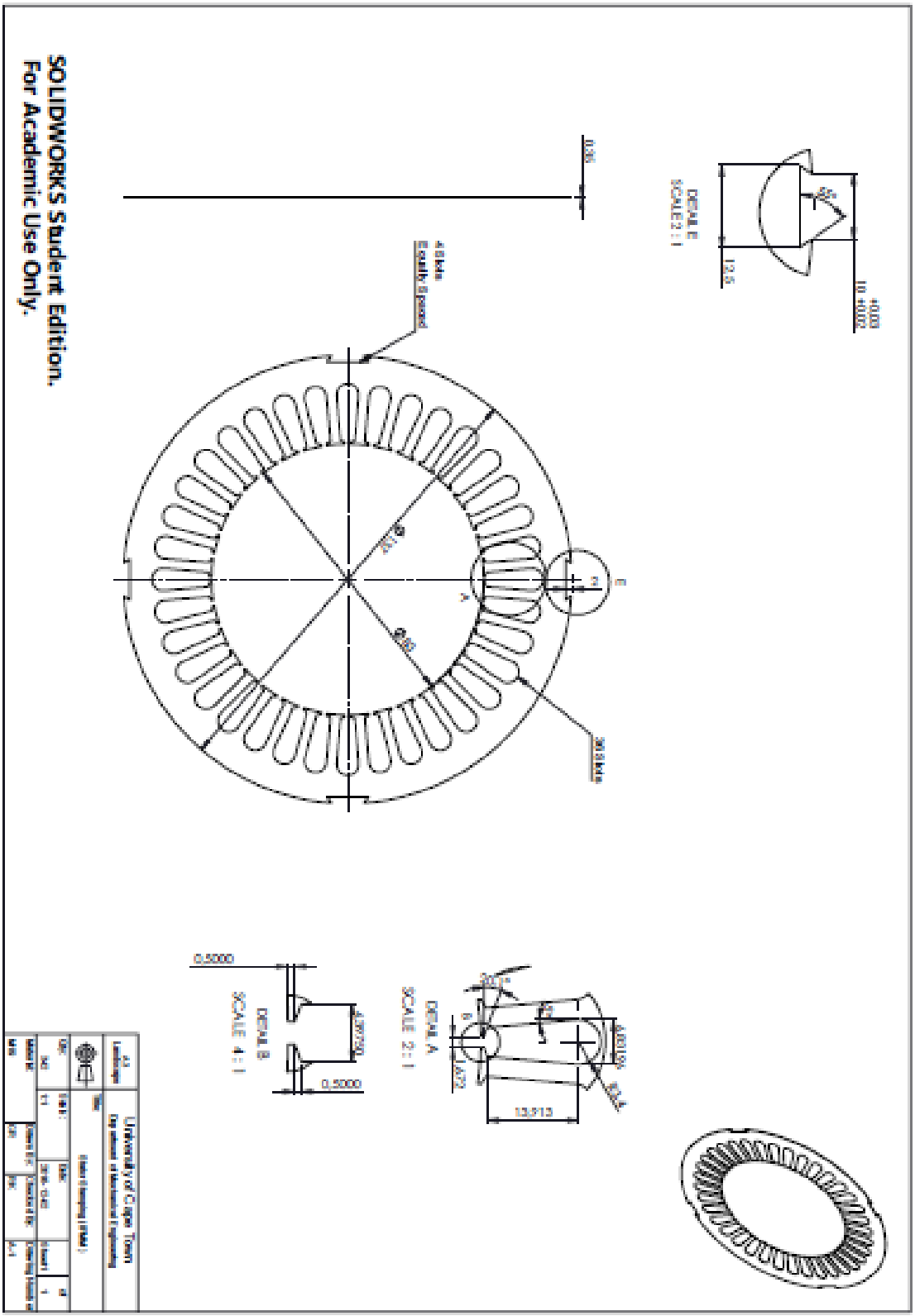

Fig. 12.6 Stator lamination

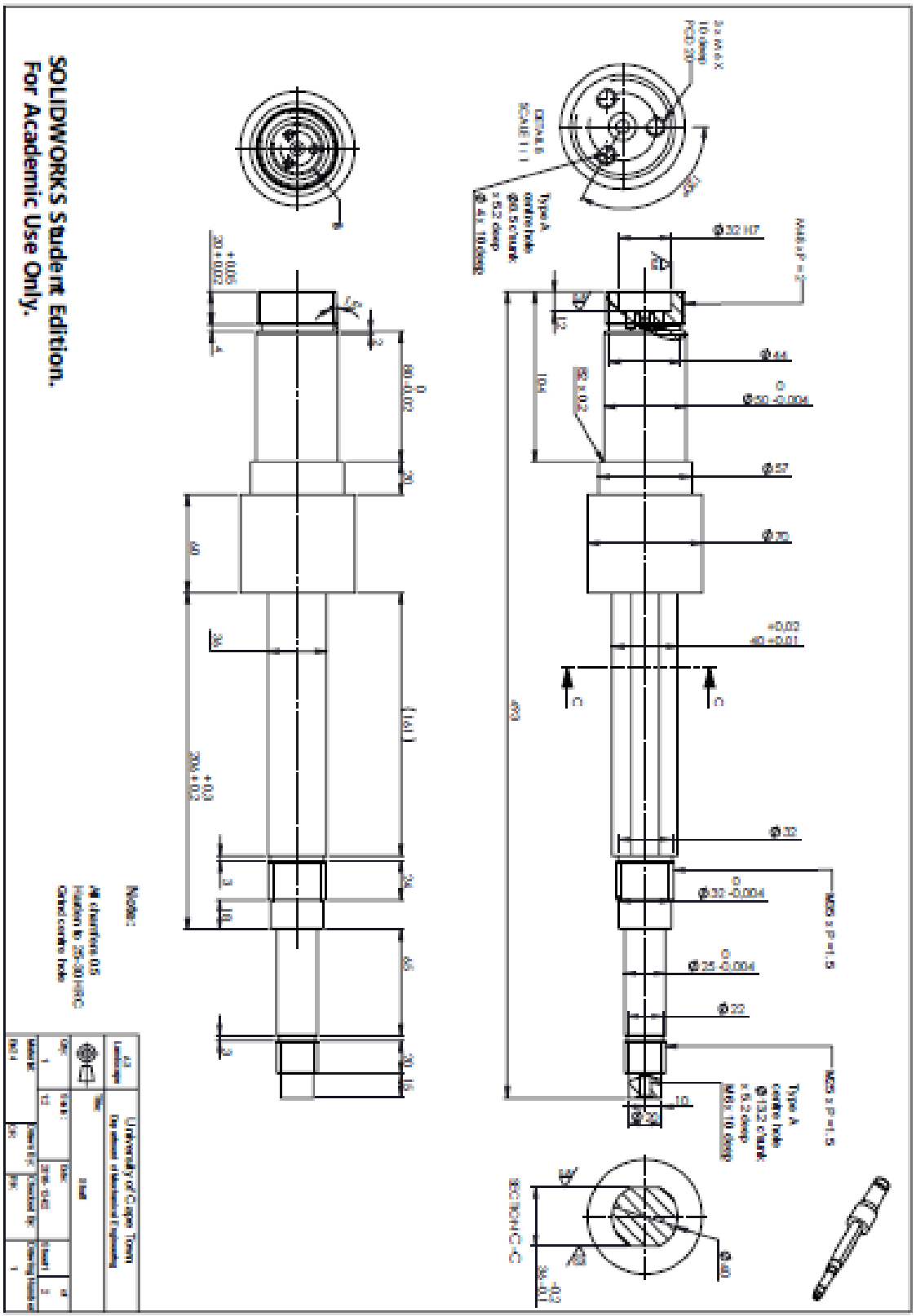

Fig. 12.7 Shaft design

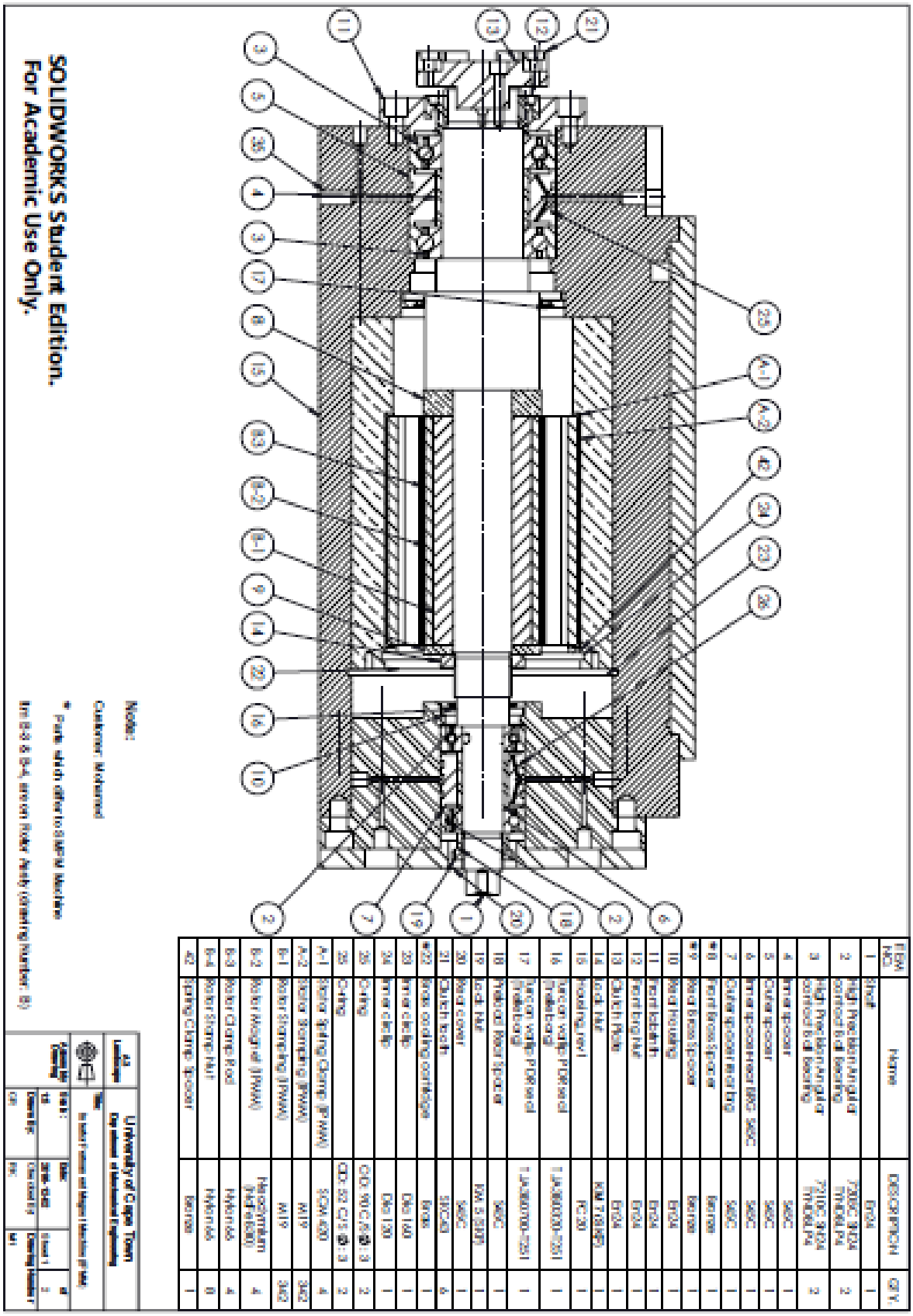

Fig. 12.8 Machine housing

12.3 Appendix C - Manufacturing process

Figures 12.9 and 12.10 show the rotor and stator lamination for the radial IPM.

Fig. 12.9 Radial IPM rotor lamination

Fig. 12.10 Radial IPM stator lamination

13. EBE Faculty: Assessment of Ethics in Research Projects

Any person planning to undertake research in the Faculty of Engineering and the Built Environment at the University of Cape Town is required to complete this form before collecting or analysing data. When completed it should be submitted to the supervisor (where applicable) and from there to the Head of Department. If any of the questions below have been answered YES, and the applicant is NOT a fourth year student, the Head should forward this form for approval by the Faculty EIR committee: submit to Ms Zulpha Geyer (Zulpha.Geyer@uct.ac.za; Chem Eng Building, Ph 021 650 4791).Students must include a copy of the completed form with the final year project when it is submitted for examination.

Name of Principal Researcher/Student:	MOHAMEDREZA KALYAN			**Department:**	ELECTRICAL ENGINEERING
If a Student:	YES	**Degree:**	MSc. ELEC ENG	**Supervisor:**	AZEEM KHAN
If a Research Contract indicate source of funding/sponsorship:				N/A	
Research Project Title:	Comparison of Interior Permanent Magnet Synchronous Machines for a High-Speed Application				

Overview of ethics issues in your research project:

Question 1: Is there a possibility that your research could cause harm to a third party (i.e. a person not involved in your project)?	YES	✗NO
Question 2: Is your research making use of human subjects as sources of data? If your answer is YES, please complete Addendum 2.	YES	✗NO
Question 3: Does your research involve the participation of or provision of services to communities? If your answer is YES, please complete Addendum 3.	YES	✗NO
Question 4: If your research is sponsored, is there any potential for conflicts of interest? If your answer is YES, please complete Addendum 4.	YES	✗NO

If you have answered YES to any of the above questions, please append a copy of your research proposal, as well as any interview schedules or questionnaires (Addendum 1) and please complete further addenda as appropriate.